

# bradscholars

## Development of geochemical identification and discrimination by Raman spectroscopy. The development of Raman spectroscopic methods for application to whole soil analysis and the separation of volcanic ashes for tephrochronology

Item Type	Thesis
Authors	Surtees, Alexander
Rights	<p><a href="http://creativecommons.org/licenses/by-nc-nd/3.0/">http://creativecommons.org/licenses/by-nc-nd/3.0/</a>&lt;img alt="Creative Commons License" style="border-width:0" src="http://i.creativecommons.org/l/by-nc-nd/3.0/88x31.png" /&gt;&lt;/a&gt;&lt;br /&gt;The University of Bradford theses are licenced under a <a href="http://creativecommons.org/licenses/by-nc-nd/3.0/">http://creativecommons.org/licenses/by-nc-nd/3.0/</a>&gt;Creative Commons Licence&lt;/a&gt;.</p>
Download date	2026-06-08 17:43:18
Link to Item	<a href="http://hdl.handle.net/10454/14409">http://hdl.handle.net/10454/14409</a>



## **University of Bradford eThesis**

This thesis is hosted in [Bradford Scholars](#) – The University of Bradford Open Access repository. Visit the repository for full metadata or to contact the repository team



© University of Bradford. This work is licenced for reuse under a [Creative Commons Licence](#).

**Development of geochemical  
identification and discrimination by  
Raman spectroscopy**

A.P.H.Surtees

PhD

University of Bradford

2015

# **Development of geochemical identification and discrimination by Raman spectroscopy**

The development of Raman spectroscopic methods for  
application to whole soil analysis and the separation of  
volcanic ashes for tephrochronology

Alexander Peter Harrison SURTEES

BSc (Hons)

Submitted for the degree of Doctor of Philosophy

Chemical and Forensic Sciences

Faculty of Life Sciences

University of Bradford

2015

## **Abstract:**

### **Raman spectroscopy, PCA, Soil, Tephra, Forensic, Discrimination, Hekla**

Geochemistry plays a vital role in our understanding mechanisms behind major geological systems such as the Earth's crust and its oceans (*Albarède, F. 2003*). More recently, geo-chemistry has played a vital role in the field of forensic investigation and in period dating. Forensic soil samples have been traditionally analysed via examinations of colour, texture and mineral content by physical or chemical methods. However, these methods leave any organic or water-soluble fractions unexamined.

Tephrochronology (the dating of sedimentary sequences using volcanic ash layers) is an important tool for the dating and correlation of sedimentary sequences containing archives and proxies of past environmental change. Its importance in this area has increased since the increased free carbon in our atmosphere has made radio-carbon dating unreliable. Tephrochronology requires successful geo-chemical identification of the tephras, a method reliant on electron probe micro-analysis (EPMA) to analyse major element composition. However, it is often impossible to differentiate key tephra layers using EPMA alone.

Raman spectroscopy is commonly used in chemistry, since vibrational information is specific to the chemical bonds and symmetry of molecules, and can provide a fingerprint by which these can be identified. Here, we demonstrate how Raman spectroscopy can be used for the successful

discrimination of mineral species in tephra through the analysis of individual glass shards. We further demonstrate how, with the use of oxidative preparation methods, Raman spectroscopy can be used to successfully discriminate between soil types using mineralogy as well as the organic and water-soluble fractions of soils.

## **Dedication:**

This work is dedicated to my late father,

Professor **Robert Alexander Harrison Surtees** MA, PhD, FRCP (Lond),  
FRCPCH.

His exceptional work in medicine and in academia was my inspiration in venturing into research. His passion and determination to succeed has constantly been my motivation in my research and in writing my thesis. There have been times when the work load has seemed too great, when it seemed that this thesis would never be completed but my memories of my father and his achievements have driven me to complete this thesis.

Also to my mother,

**Diane Lesley Surtees**

Her love and support over the past few years have given me the strength to carry on.

## **Acknowledgements:**

Over the years I have either been a jinx or a lucky charm to my supervisors with the vast majority of them either retiring or moving on to pastures new. However, without all of them I would not be where I am today. Their help and support has always been given freely and sincerely and I cannot thank them enough for all of their help over the years.

### **Professor Howell Edwards**

For sharing with me his encyclopaedic knowledge of Raman spectroscopy.

### **Professor Ian Scowen**

For teaching me that a two pint lunch is acceptable but a three pint lunch ruins any hope of a productive afternoon.

### **Dr Graeme Swindles**

For starting my obsession with tephra and influenced my drive for finding a new way of tephra analysis.

### **Dr Tasnim Munshi**

For teaching me to “tell a story” over endless cups of tea.

### **Dr Colin Seaton**

For not laughing at me too much when England went crashing out of their own world cup.

A big thank you to all the technical staff who have helped over the years, making the instruments work and for providing invaluable advice along the way.

I must also thank all of my friends and family who have supported me over the years. Embarking on a PhD is a huge undertaking and I think everyone who has ever completed one will agree that their friends are a big source of support and inspiration. All of my friends have played a part in the completion of this PhD and for that I thank them all.

A special thanks goes to

### **Michelle Reid**

For putting up with my moods and stress. For providing me constant love and support whilst I have been writing this thesis

## Table of contents:

Abstract:.....	i
Dedication:.....	iii
Acknowledgements:.....	iv
Table of contents: .....	v
List of figures.....	vii
List of Tables.....	ix
Publications.....	x
Introduction.....	xi
Chapter 1.....	1
1.1- Soil.....	1
1.2- Tephra.....	14
1.3- Hekla .....	19
1.4- Mineralogical Identification.....	24
1.4.1- In-field Mineralogical Identification .....	25
1.4.2- Laboratory Mineralogical Identification .....	27
1.4.3- Mineral Identification using Raman Spectroscopy .....	38
1.5- References .....	41
Chapter 2.....	47
2.1- Analytical techniques used in geo-chemistry .....	47
2.2- Methodology.....	58
2.2.1- X-ray Diffraction.....	58
2.2.2- Raman Spectroscopy .....	61
2.3- References .....	73
Chapter 3.....	76
3.1- Introduction.....	76
3.1.1 – Sample Collection .....	77
3.2.2 – Method of Sample Collection .....	81
3.2 – Instrumentation.....	81
3.2.1 - Renishaw InVia Reflex dispersive spectrometer.....	82
3.2.2 – Delta Nu Inspector Raman FSX .....	82
3.2.3 - Bruker AXS D8 Advance X-Ray Diffractometer .....	83
3.3 – Data Analysis .....	83

3.4 – Soil sample analysis .....	83
3.4.1- Preliminary study on the soils collected from the University of Bradford Campus.....	83
3.4.2 – Method development of the oxidative sample preparation to reduce sample fluorescence.....	84
3.4.3 – Sample Preparation .....	89
3.4.4 – Sample Analysis.....	90
3.5- Results and discussion.....	90
3.6.1 – Preliminary Study .....	92
3.6.2 – Secondary Study.....	96
3.6.2.1 – Urban Samples (Bradford) .....	96
3.6.2.2 – Rural Samples (Lincolnshire).....	99
3.6.2.3 – Urban Samples (Bradford) .....	100
3.6.2.4 – Rural Samples (Lincolnshire).....	101
3.6.3 – Final Study (Soil samples from the route A65).....	102
3.7- Conclusions.....	110
3.8- Further Work .....	113
3.9- References .....	116
Chapter 4.....	119
4.1- Introduction.....	119
4.2- Tephra.....	121
4.3- Initial Study.....	123
4.3.1- Tephra.....	123
4.4- Samples.....	129
4.4.1- Initial study .....	129
4.4.2- Method development.....	131
4.4.3- Sample analysis .....	143
4.5- Results .....	145
4.5.1- Hekla 1947 .....	145
4.5.2- Hekla 1510.....	147
4.6- Discussion .....	150
4.7- Conclusions:.....	153
4.8- References .....	155
Conclusions and further work.....	159
Appendix .....	163

## List of figures

Figure Number	Title	Page Number
CHAPTER 1		
1.1.1	Soil horizens	17
1.1.2	Example structure of humic acid	19
1.2.1	Tephra particle size	30
1.2.2	EMPA data from Hekla tephra	32
1.2.3	Visable tephra layers	33
1.3.1	Hekla and its location	36
1.4.1.1	Types of luster	40
1.4.1.2	Munsell colour system	41
CHAPTER 2		
2.1.1	Raman analysis of blue ice tephra	71
2.2.2.3.1	Structure of ethene	76
2.2.2.4.1	Raman energy level diagram	79
CHAPTER 3		
3.1.1.1	Collection points from UoB campus	91
3.1.1.2	Collection points from city of Bradford	93
3.1.1.3	Collection points from the area surrounding Bitchfield, Lincolnshire	94
3.1.1.4	Collection points from the A65 between Bradford and Cumbria	95
3.4.1.1	Flourescence observed in soil samples	98
3.4.2.1	Improved signal to noise ratio with $H_2O_2$	102
3.4.2.2	Spectra of organic content after $H_2O_2$ treatment	103
3.6.1.1	Spectra of soil from UoB campus	107
3.6.1.2	Spectra of soil from UoB campus	108
3.6.1.3	PXRD of soil samples from UoB campus	109
3.6.2.1.1	Spectra of soil samples from city of Bradford	111
3.6.2.1.2	Spectra of heamatite observed in soil samples from the city of Bradford	112
3.6.2.2.1	Spectra of quartz observed in soil samples from Bitchfield	113
3.6.2.2.2	Spectra of calcite observed in soil samples from Bitchfield	114
3.6.2.3.1	PXRD of soil from the city of Bradford	115
3.6.2.4.1	PXRD of soil from around the village of Bitchfield	115
3.6.3.1	Raman spectra of Ireby soil samples	116
3.6.3.2	Raman spectra of Ingleton soil samples (in-organic)	117
3.6.3.3	Raman spectra of Ingleton soil samples (organic)	118

3.6.3.4	Raman spectra of West Barbon soil samples (in-organic)	119
3.6.3.5	Raman spectra of West Barbon soil samples (organic)	120
3.6.3.6	C±C stretch in Skipton soil samples	121
3.6.3.7	Raman spectra of Skipton soil samples (organic)	122
3.6.3.1.1.	PXRD overlay of A65 route soil samples	123
CHAPTER 4		
4.3.1.1	EMPA data from the Hekla volcano	137
4.3.1.2	Tephra layers forming a cronological framework	138
4.3.1.2.1	Hekla and its location	141
4.4.2.1	Effect of laser power on the Raman spectrum of geothite	151
4.4.2.2	Visual effect of laser power on a sample of geothite	152
4.4.3.1	Phenocryst in groundmass	157
4.5.1.1	Magnetite observed in Hekla 1947 samples	158
4.5.1.2	Further spectral features observed in Hekla 1947 samples	159
4.5.2.1	Spectral features observed in Hekla 1510 sample	161
4.6.1	PCA Biplot of 1510 and 1947 Hekla tephtras (Raman)	164
4.6.2	PCA trilot of 1510 and 1947 Hekla tephtras (EMPA)	164

## List of Tables

Table number	Title	Page number
CHAPTER 3		
3.4.2.1	Mass loss of soil sample with increasing reflux temperature	101
3.4.2.2	H <sub>2</sub> O <sub>2</sub> Solutions	101
3.4.2.3	Mass loss after reflux in 25% H <sub>2</sub> O <sub>2</sub>	102
3.6.1.1	PXRD peaks of mineral species found in Bradford soil samples	109
3.6.2.1.1.	Expected Raman peaks in haematite	112
CHAPTER 4		
4.4.2.1	Changes in laser power	152
4.4.2.2	Changes in exposure time	153
4.4.2.3	Changes in accumulation number	154

## **Publications**

Development of oxidative sample preparation for the analysis of forensic soil samples with near-IR Raman spectroscopy.

Edwards, H., Munshi, T., Scowen, I., **Surtees, A.**, & Swindles, G. T.

Journal of Raman Spectroscopy, July 2010.

Raman Spectroscopy for the discrimination of tephras from the Hekla eruptions of 1510 and 1947

**Alexander PH Surtees**, Graeme T Swindles, Tasnim Munshi, Ivan P Savov, Ian J Scowen and Howell G M Edwards.

The Holocene, accepted August 2015

## Introduction

Geo-chemistry currently relies on a range of multi-proxy methods for the identification of geological samples. These methods are only able to identify small fractions of the materials e.g. powder X-ray diffraction (PXRD) for the identification of inorganic minerals in soil samples. These methods often overlooks potential key areas of discrimination such as the organic humic acid fractions of soils or are unable to provide enough discriminatory power such as electron probe microanalysis (EPMA) and its use in tephra analysis.

The aim of this work is to develop Raman spectroscopic techniques to be able to fully identify and distinguish between geological materials. In order to achieve this aim the work comprises of two dominant themes. The first study highlights a method development for the application of Raman spectroscopy to the analysis of soil samples whilst the second study focuses on applying the methodology to the spectroscopic separation of two identical tephra samples. A detailed introduction for both of these themes can be found at the beginnings of chapters three and four.

The first body of work focusses on the application of Raman spectroscopy to the examination of whole soil samples. Soil samples have been traditionally analysed *via* examinations of colour, texture and mineral content by physical or chemical methods. These methods leave any organic or water-soluble fractions unexamined. Through the development of an oxidative sample preparation we aim to show how Raman spectra of the mineralogical and humic fractions of soil can be gained allowing for the successful interrogation of whole soil samples utilising a single methodology can be achieved.

The second body of work focusses on the application of developed Raman spectroscopic methods to the mineralogical characterization of microlites in tephra. Successful tephrochronology is based on the correct geochemical identification of the tephra, which has until now, been based primarily on the analysis of major element oxide composition of glass shards using EPMA. However, it is often impossible to discriminate between key tephra layers using EPMA alone. For example, the Hekla AD 1947 and AD 1510 tephra, which are found in Iceland and also as 'crypto-tephra' microscopic layers in NW Europe are currently indistinguishable using EPMA. In this body of work we demonstrate how Raman spectroscopic techniques can be successfully applied to tephra analysis and provide further discrimination between samples than is currently possible using the accepted multi-proxy techniques.

Tephra and soils are closely linked by virtue that tephra glass shards are often found distributed throughout soil samples e.g. crypto-tephras in peat bogs. Therefore in order to fully analyse soil samples one must also consider tephra analysis. Indeed, in the majority of areas around areas of intense volcanic activity the soils themselves are formed from erupted tephra by a process known as palagonitization (see chapter one for further detail).

These two themes are brought together in the method development and application of Raman spectroscopy. The current methods of analysis for both tephra and soil samples rely on a multi-proxy approach looking for individual characteristics of the samples. Several of these methodologies are subjective and

it is therefore difficult to achieve consistency in their analysis. Raman spectroscopy offers the ability to become the singular required analytical tool for analysis of these samples thus adding objectivity to the analysis.

## **Chapter 1**

### **1.1- Soil**

The Soil Science Glossary presents two definitions for the term soil (Chesworth, 2008). The first is the unconsolidated mineral or organic material on the immediate surface of the Earth that serves as a natural medium for the growth of land plants. Its second definition is the unconsolidated mineral or organic matter on the surface of the Earth that has been subjected to and shows effects of genetic and environmental factors of: climate (including water and temperature effects), and macro- and microorganisms, conditioned by relief, acting on parent material over a period of time. An alternative definition is provided by the second edition of Soil Taxonomy (Staff, 2009), which defines soil as a natural body comprised of solids (minerals and organic matter), liquid, and gases that occurs on the land surface, occupies space, and is characterized by one or both of the following: horizons, or layers, that are distinguishable from the initial material as a result of additions, losses, transfers, and transformations of energy and matter or the ability to support rooted plants in a natural environment.

Soils are a natural body that consist of horizons of mineral constituents that differ from their parent materials in their morphological, physical, chemical, and mineralogical characteristics (Veldkamp, 1999). Figure 1.1.1 demonstrates the typical soil horizons found in un-touched soils. The Laterite is the uppermost layer developed by intense weathering of the underlying rock, the Regolith is a layer of loose heterogeneous material covering solid rock and the Saprolite represents deep weathering of the bedrock. Soil is comprised of particles of

broken bedrock that differ from its parent material due to interactions with the lithosphere, hydrosphere, atmosphere, and the biosphere (Chesworth,2008).

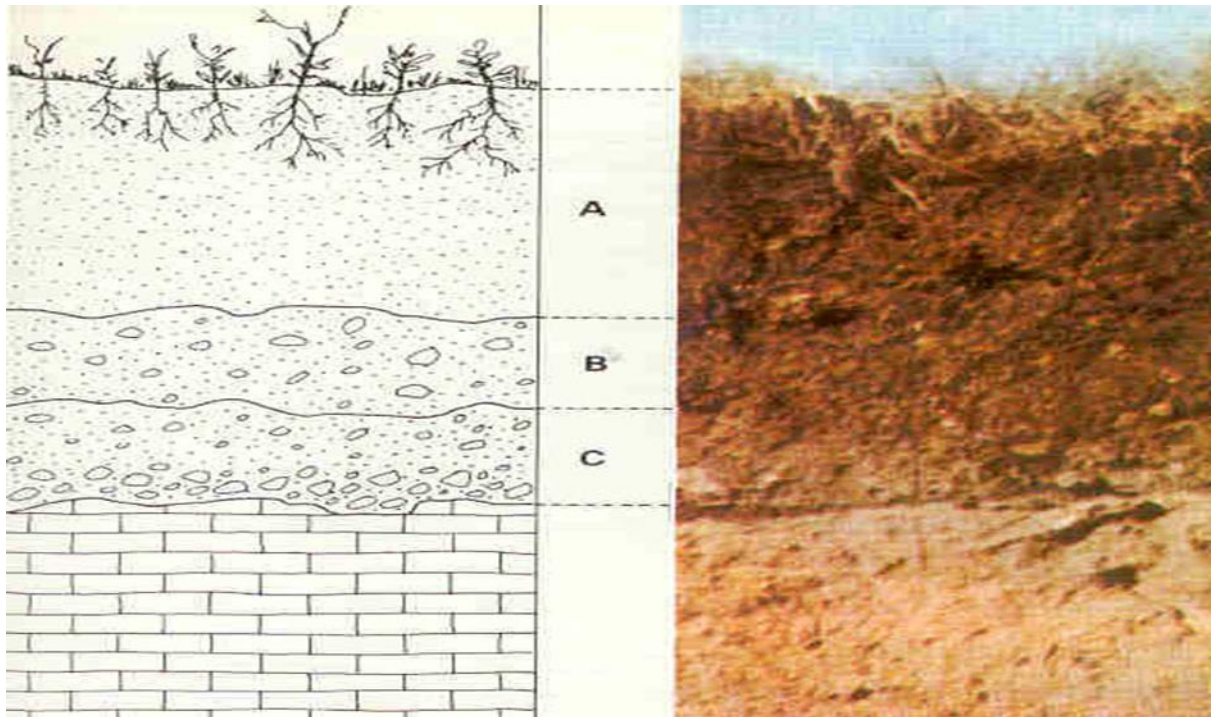


**Figure 1.1.1: Comparison image of the soil horizons with the Laterite (A), the Regolith (B), the Saprolite (C) and underlying all three, the bedrock. (Tardy, 1997)**

Paedogenesis is the combined effect of physical, chemical, biological, and anthropogenic processes on soil parent material. Soil genesis involves processes that develop layers or horizons in the soil profile. These processes involve additions, losses, transformations and translocations of material that compose the soil. Minerals derived from weathered rocks undergo changes that cause the formation of secondary minerals and other compounds that are variably soluble in water, these constituents are translocated from one area of the soil to other areas by water and animal activity. The alteration and movement of materials within soil causes the formation of distinctive soil horizons (Institute,2008).

The weathering of bedrock produces the parent material from which soils form. An example of soil development from bare rock occurs on recent lava flows in warm regions under heavy and very frequent rainfall. In such climates, plants become established very quickly on basaltic lava, even though there is very little organic material. The plants are supported by the porous rock as it is filled with nutrient-bearing water which carries, for example, dissolved minerals and guano. The developing plant roots gradually break up the porous lava and organic matter soon accumulates. Even before it does, the predominantly porous broken lava in which the plant roots grow can be considered a soil (Brevic, 2002).

The purpose of this work is to overcome the fluorescence associated with the organic material in soils in order to record Raman spectra of the whole soil sample. Humic substances are the major organic components of soil and humic acid is the major component of these substances (Schnitzer, 1998). Humic acids are produced by a biodegradation of dead organic matter. Humic acid is not a single acid; rather, it is a complex mixture of many different acids containing carboxyl and phenolate groups so that the mixture behaves functionally as a dibasic acid or, occasionally, as a tribasic acid (Georgia, 2011).

A typical humic substance is a mixture of many molecules, some of which are based on a motif of aromatic nuclei with phenolic and carboxylic substituents, linked together (see fig 1.1.2). The functional groups that contribute most to surface charge and reactivity of humic substances are phenolic and carboxylic groups (Stephenson, 1994) The presence of carboxylate and phenolate groups gives the humic acids the ability to form complexes with ions such as  $Mg^{2+}$ ,  $Ca^{2+}$ ,  $Fe^{2+}$  and  $Fe^{3+}$ . Many humic acids have two or more of these groups arranged so

as to enable the formation of chelate complexes (Tipping,1994). The formation of chelate complexes is an important aspect of the biological role of humic acids in regulating bioavailability of metal ions.

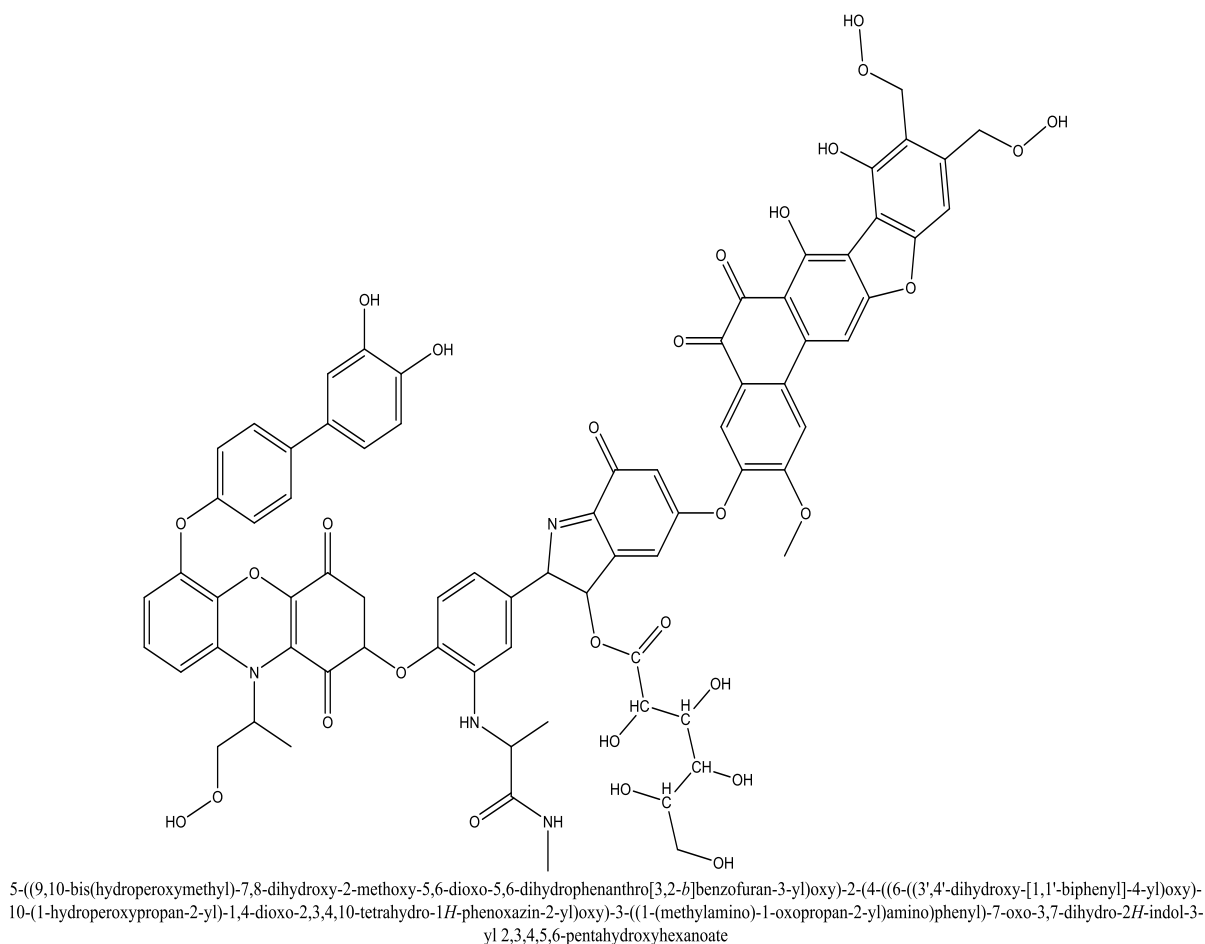


**Figure 1.1.2: An example of a humic acid structure including quinone, phenol, catechol and sugar moieties amongst its components (Tipping, 1994).**

Recently a large body of work has gone into the study of the forensic analysis of soil samples by the “SoilFit” team supported by a research grant awarded by the Engineering and Physical Sciences Research Council (EPSRC). The main aims of this project were to test the potential of advanced soil analysis methods to distinguish different soil types, build a database of analytical data across a variety of soil types common to the UK landscape and develop a prototype ‘soil

comparison' tool capable of determining the most probable origin/landscape characteristics of soil sample of unknown origin (Institute, 2012). Robert Mayes *et al* have focussed their research on the discrimination of garden soils based on the plant wax compounds found within them. Utilising a pilot study in North East Scotland, the team discovered that individual patches of garden planting bed soil could be discriminated from one another based on their plant wax marker profiles. Results indicated that both *n*-alkane and long-chain fatty alcohol profiles in garden soils were generally specific to the individual planting bed (Mayes *et al*, 2009). S Wakelin *et al* have concluded that it may be possible to discern the soil type and therefore soil origin based on the microbial communities found in samples. Following multivariate analysis, soil pH was identified as the key habitat-selective physicochemical soil property associated with variation in biological diversity and profiles of organic substrate utilisation. This work has shown that soil pH is a primary driver of microbial diversity and function in soil (Wakelin *et al*, 2009). Continuing with microbial research in soils comparison, L Macdonald *et al* have focussed on utilising the DNA of microbes found within soils as a tool to discriminate between soil samplers. The team used a M-TRFLP (multiplex-terminal restriction fragment length polymorphism) approach to profile bacterial, archaeal and fungal DNA profiles from five different soil sites. The study concluded that Soil DNA profiling has potential as a forensic tool, but sample condition and the appropriate selection of microbial target taxa must be considered (Macdonald, 2008).

Soil has been demonstrated to be a potentially rich source of information for forensic reconstruction (Morgan, 2007). Significant problems exist in the comparison of trace and bulk samples and there is a clear need for multiple

sample analysis. Multiple soil samples may be taken from the same geographic location but the samples may differ fundamentally in their grain size distribution with the possibility of subsequent interpretation producing a false-negative result (Morgan, 2006). Soil has been characterized for forensic purposes (Cox *et al.*, 2007), but the uniqueness associated with soils has been unappreciated, largely due to the prevalent view that soil is an aggregate of inorganic compounds. Soil could be an important tool within forensic science which has the potential to link suspects and scenes together.

Soil analysis is not only important in the field of forensic science. Soil is very important to our everyday life. We live on it, build on it, grow our crops in it, and allow our livestock to feed on vegetation grown in it. It is for these reasons that we need to know and understand soil and its composition to monitor it for the wellbeing of the planet and the organisms that live off it.

Currently the study of soils requires a whole range of analytical tools to interrogate both the inorganic and the organic fractions of the soils as well as the grain sizes and shapes (Dabas, 2010). The most commonly used tool to study the mineralogical fractions of soil samples is Powder X-Ray Diffraction (PXRD). PXRD has become the gold standard in the interrogation of the mineralogical content of soils (Kempsona *et al*, 2012). Multiple methods are utilised to measure the organic (humic and fulvic acids) fractions of soils. Fourier-Transform Infrared spectroscopy (FTIR) and Carbon-13 Nuclear Magnetic Resonance Spectroscopy (NMR) are the methods favoured by L Celi *et al* for the interrogation of the carboxyl groups in humic acids (Celi, 1997). In addition to NMR and FTIR, Northcott *et al* have utilised High Performance Liquid Chromatography (HPLC), Thin Layer Chromatography (TLC), Ultra Violet Spectroscopy (UV) and Size Exclusion Chromatography (SEC) (Jones, 2000).

Other methods rely on simply measuring the mass of the soils organic content rather than the compounds that form it, with the most commonly used method for this being the Weight Loss on Ignition Method (Heiri, 1999).

The secondary purpose of this study is to demonstrate that Raman spectroscopy is able to become the singular tool required for whole soil sample analysis. Raman spectroscopy has the ability to remove the need for the use of multiple analytical techniques as it has the ability to provide all of the analytical information required for the identification and characterization of all soil components. Raman spectroscopy is routinely used to measure both organic and inorganic materials (Nyquist,1997)( Karr, 1975). Raman instruments can also be coupled with light microscopes thus enabling the study of the micromorphology of soil samples.

Work carried out utilising Raman spectroscopy has typically been very focussed in its desired outcome. Researchers have tended to use Raman spectroscopy as a means to identify specific materials in a soil sample rather than using it to interrogate the sample as a whole. Acta *et al* utilised Raman Spectroscopy to identify a green rust mineral in a sample of reductomorphic soil (Acta *et al*, 1997). In this study the green mineral was identified in the soil sample before being interrogated as an individual mineral by Raman microprobe. Kamnev *et al* have used Fourier transform Raman spectroscopy (FT-Raman) in the study of the bacterium *Azospirillum brasilense* (Kamnev, 2001). *Azospirillum* is a bacterium known to be found in soils that can form an association with various plant species to stimulate the plant growth. In this study the bacterium were extracted from the soil before the structural features of their cells were studied with FT-Raman.

It is widely known that soils are heavily contaminated with a wide range of contaminants, including arsenic (Yarlagadda *et al*, 1995). It is this knowledge and the drive for the remediation of such soils that forms another major branch of soil science research utilising Raman spectroscopy. In these studies Raman spectroscopy is used to identify and characterise the heavy metal contaminants in soil samples. Ray Frost *et al* has used Raman spectroscopy to identify vivianite arsenic materials, Dr Frost later identified a range of arsenate minerals with Raman spectroscopy with implications on soil remediation (Frost *et al*, 2003)

Raman spectroscopy has been regularly used in the identification of minerals of the type found in terrestrial soil samples. Richard Herman *et al* used Raman microprobe analysis to identify individual carbonate minerals (regularly found in the majority of soil samples) such as calcite, dolomite, and aragonite (Herman *et al*, 1987).

Raman spectroscopy has not been used to identify whole soil samples. This is perhaps because of the fluorescence that masks any sample peak signals when whole soil samples are analysed. This fluorescence is thought to be caused by the humic content of the soil samples and to date all Raman data on whole soil samples has been heavily corrected (Ewald *et al*, 1993). There is currently no uncorrected Raman data available for the general organic content of soil samples due to the issues of fluorescence not being resolved. However, there are methods in use that have lessened the effect of fluorescence on the Raman data. Yu-Hui Yang and Ting Wang have successfully characterised some fulvic acid fractions with FT-Raman after chemical treatment. In their study the fulvic acids were broken down into their individual building blocks with hydrochloric

acid and sodium hydroxide treatment and were able to record clear spectra detailing their structures (Wang, 1997). However, it would not be possible to use this method on whole soil samples because the acid treatment would change the nature of some of the soils mineralogical content. Clearly a method needs to be revised that can lessen the fluorescence caused by fulvic acids and yet leave the composition of the soil samples unchanged.

The most recent published papers on soil analysis focus their efforts on the measurement of particular soil components and their effects on plant growth. Calvin Trostle *et al* conducted a study focussing on the nitrogen supplying capacity of soils to rice based on the soils ammonium diffusion. A laboratory procedure using transient-state methods measured the linear movement of soil ammonium ( $\text{NH}_4$ ) in tubes packed with five field soils under aerobic conditions. Ammonium diffusion was measured by sectioning tubes after 48 h of equilibration and then measuring  $\text{NH}_4$  by steam distillation. Effective diffusion coefficients,  $D_e$ , and  $\text{NH}_4$  diffusion distance,  $d$ , per day ranged from  $D_e = 4.6 \times 10^{-5} \text{ cm}^2 \text{ d}^{-1}$  and  $1.5 \text{ cm d}^{-1}$  for Katy sandy loam to  $D_e = 2.9 \times 10^{-7} \text{ cm}^2 \text{ d}^{-1}$  and  $0.11 \text{ cm d}^{-1}$  for League clay. Ammonium diffusion distance  $d$  was strongly related to soil clay content and hence was predicted by  $d = Y \times \{[100/(\% \text{ clay})] - 1\}$ , where  $Y$  is set to 0.1. Predicted  $d$  and measured  $d$  were highly related ( $R^2 = 0.99$ ). Hence sandy soils have a greater capacity for nitrogen transfer to rice plants (Trostle *et al*, 2011). Maria E. Ortiz-Escobar *et al* studied the effects of four different fertilisers to discover their effects on crop growth and the factors most important to their growth in Oxisols (soils containing at all depths no more than 10 percent weatherable minerals, and low cation exchange capacity). Two composts, one urea and one control were applied to a test field in Hawaii and aubergines and Chinese cabbage grown on all four. It was found that soil

quality as measured by hot-water-soluble carbon, dehydrogenase activity, and cation exchange capacity (CEC) increased by compost amendments. Total organic carbon or carbon dioxide (CO<sub>2</sub>) respiration rate did not correlate with the soil amendments. Nitrogen (N) nutrition was the main factor that improved growth and carotenoid content in cabbage. The urea treatment promoted better growth in cabbage, whereas good-quality compost, made of grass clippings/tree trimmings, lime, and rock phosphate yielded better growth in eggplant, suggesting organic N requires time to mineralize and to be available to crops (Hueb, 2011).

Further works on soil samples have been carried out for a range of different applications. Fábio Melquiades *et al* studied the effects of granulometry and moisture on *in situ* EDXRF analysis of soils (Melquiades *et al*, 2011). The soils were analysed for the identification and quantification of metals. They found that, for *in situ* analysis of this soil, it is sufficient to grind the dried sample before measurement. For moisture, concentration values obtained for the samples dried from 30 to 120 minutes at sun are equivalent. On the other hand, the concentration values obtained for the samples dried during 24 h are higher than the values obtained for the same samples dried at sun. Moisture influences the concentrations values in around 20%. Other studies have concentrated on the effects of waste management on soil and more importantly on the species that live on soils. Sewage treatment plants have a huge issue with the destination of sewage sludge with many now favouring turning it out onto degraded soils and using it as fertilisers in agriculture. In this study, animals from the *Rhinocricus padbergi* species were exposed to two sewage sludge samples in the Sao Paulo State, for different periods. The midgut of the animals were removed and histologically processed and subjected to histochemical tests. It

was detected the following tissular responses: clusters of haemocytes through the cells of the fat body layer, increase in the quantity of intracellular granules in the cells of the fat body layer, increase in the release of secretion vesicles of the intestinal epithelium, and intense vacuolization of the cytoplasm of epithelial cells. The results suggest the presence of toxic substances to the studied species in both sludge samples used (Giuliano Perez, 2011).

One of the biggest areas of research into soils and utilising soil samples is forensic geo-chemistry (Johnson, 2011). It has grown as a subject since 1904 when George Popp was believed to be the first person to secure a criminal conviction on the basis of soil evidence (Albarède, 2009). In modern times the use of soil evidence has become widespread due to the useful information it can provide in linking a person or persons to crime scenes. This is due to the nature of soils being unavoidable as transport medium. It is useful here to define the term “soil” and for the purpose of this research the engineers definition of soil as being all disintegrated material lying on the top of solid rock has been used (Johnson, 2011).

The value of soil as evidence is due to the huge variations in its characteristics. When considering soil evidence one encounters extreme difficulty both in the components that make up the soil but also in the physical size of these components. Soil diversity is due to a multitude of factors including parent minerals, topography, climate botanical and microbial functions and human interaction. It is due to this complexity that there is a high degree of diversity between soil samplers. However, it is due to this diversity that as yet there is no set protocol for the examination of forensic soil samples (Pallardy, 2011).

The first thing that one notices about any object is its colour and colour is vital as a tool to determine soil type. For example, geographers are familiar with Red Desert soils in California, Arizona, and Nevada; and Gray Desert soils in Idaho, Utah, and Nevada. We have the White Sands in New Mexico, Green Sands along the Atlantic Coast, and Redbeds in Texas and Oklahoma. Colour development and distribution of colour within a soil profile are part of weathering. As rocks containing iron or manganese weather, the elements oxidize. Iron forms small crystals with a yellow or red colour, manganese black mineral deposits, while organic matter decomposes into black humus. Colour is also affected by the environment: aerobic environments produce sweeping vistas of uniform or subtly changing colour, and anaerobic, wet environments disrupt colour flow with complex, often with intriguing patterns and points of accent. With depth below the soil surface, colours usually become lighter, yellower, or redder. The Munsell System allows for direct comparison of soils anywhere in the world. The system has three components: hue (a specific colour), value (lightness and darkness), and chroma (colour intensity) that are arranged in books of colour chips. Soil is held next to the chips to find a visual match and assigned the corresponding Munsell notation (see page 26, fig 1.4.1.2).

It is a generally accepted view that the most important step in the forensic examination of soil samples is the identification of the primary minerals that make up the sample

(<http://www.interpol.int/Public/Forensic/IFSS/meeting13/Reviews/Soil.pdf>., 2011). Traditionally this would be achieved through optical examination but this relies heavily on the forensic laboratories having a soil expert within the organisation. To overcome this problem McVicar and Graves developed a method for particle search and analysis using an automated scanning electron

microscope coupled with an energy dispersive X-Ray spectrometer (SEM-EDX) (<http://www.interpol.int/Public/Forensic/IFSS/meeting13/Reviews/Soil.pdf>., 2011). This technique allowed for the automated examination of five-thousand particles per soil sample. This allowed for the percentage composition of the elements to be recorded and then the minerals to be classified according to the mineral classification rules (Gerasimowicz *et al*, 1986). Although there are dissimilarities between identification utilising this method over optical examination particles can be identified with the precision of <10% for components more than 5% in soil (<http://www.interpol.int/Public/Forensic/IFSS/meeting13/Reviews/Soil.pdf>., 2011).

The secondary part of forensic soil investigation involves the identification of clay minerals. Due to their minute size optical microscopy identification is not possible. There are several methods in use for the identification of clay minerals including infrared spectroscopy, transmittance electron microscopy (TEM) and X-ray diffraction (XRD) with the latter being the most commonly used technique.

The most important organic material in soil samples is the humic matter. The humic matter is derived from the microbial breakdown of plant material as well as animal debris. Due to the nature of its make up humic substances are a complicated heterogeneous mixture of organic molecules and it is due to this that very little work has been done on identifying these substances. Further adding to the lack of study into the humic content of soils is the fact that the organic fraction does not show as much variation between two samples as the mineralogical content does. The most commonly used technique for humic

analysis is Fourier transform infrared absorption spectroscopy (FTIR) (Gerasimowicz *et al*, 1986) (Filip, 1998).

A further study that may be carried out on soil samples is Palynology, which is the science that studies contemporary and fossil palynomorphs, including pollen, spores, orbicules, dinoflagellate cysts, acritarchs, chitinozoans and scolecodonts, together with particulate organic matter (POM) and kurgan found in sedimentary rocks and sediments (Faegri *et al*, 2000). The geochemical value of Palynology is two-fold. Firstly it may provide an insight into the vegetation of a locality, both past and present. Secondly it allows for a soil sample to be placed in one particular area (particularly useful in forensic investigations) due to the idea that pollen assemblages on surface soils are particular to the local area (Horrocks, 1998). Palynology is by no means a simple study; rather it may involve complex preparations to remove the subject from its surrounding medium. These preparations are not standardised (Lignuma *et al*, 2008). However, once prepared the analysis of the subject becomes relatively simple however expertise is required. Grain size and morphology is compared traditionally using a light microscope at x400 magnification or under oil immersion at x1000 magnification and the species identified through experience by an expert botanist. More recently electron microscopy has started to overtake the use of light microscopy (Lignuma *et al*, 2008).

## **1.2- Tephra**

Tephra is fragmental material produced by a volcanic eruption regardless of composition, fragment size or emplacement mechanism. Volcanologists also refer to airborne fragments as pyroclasts. Once clasts have fallen to the ground

they remain as tephra unless hot enough to fuse together into pyroclastic rock or tuff.

The distribution of tephra following an eruption usually involves the largest boulders falling to the ground quickest and therefore closest to the vent, while smaller fragments travel further—ash can often travel for thousands of miles, even circumglobal, as it can stay in the stratosphere for days to weeks following an eruption. When large amounts of tephra accumulate in the atmosphere from massive volcanic eruptions (or from a multitude of smaller eruptions occurring simultaneously), they can reflect light and heat from the sun back through the atmosphere, in some cases causing the temperature to drop, resulting in a climate change: "volcanic winter". Tephra mixed in with precipitation can also be acidic and cause acid rain and snowfall.

Tephra fragments are classified by size:

- Ash - particles smaller than 2 mm (0.08 inches) in diameter
- Lapilli or volcanic cinders - between 2 and 64 mm (0.08 and 2.5 inches) in diameter
- Volcanic bombs or volcanic blocks - larger than 64 mm (2.5 inches) in diameter.



Figure 1.2.1: Tephra particle sizes ranging from ash (left hand two piles) to Lapilli (right hand two piles). Taken from <http://volcanoes.usgs.gov/about/pglossary/tephra.php>.

The words "tephra" and "pyroclast" both derive from Greek. *Tephra* means "ash". *Pyro* means "fire" and *klastos* means "broken"; thus pyroclasts carry the connotation of "broken by fire".

Tephra vary in chemistry from basaltic (low-silica) through to rhyolitic (high-silica) compositions, reflecting the chemical variation typical of magmas. Due to the geological settings of different volcanic centres differ from one another in detail, even within localised regions, magma and hence tephra compositions produced by different volcanoes have distinct ranges of chemical composition. This chemical distinctiveness may extend to sequences of tephra erupted by an individual volcano.

Geochemical fingerprinting of tephra to match them with source eruptions can be achieved very reliably and rapidly by EPMA (electron probe microanalysis). Discrimination between the majorities of tephra layers is usually achieved easily by analysis of the 10 major and minor elements present in the magma (Na, Mg, Al, Si, P, K, Ca, Ti, Fe, and Mn). Thus geochemical fingerprinting of tephra horizons by EPMA represents a very precise and cost effective dating tool (Albarède, 2009).

In this work tephra from the Hekla volcanic eruptions of 1947 and 1510 AD are being studied and for this reason the following data considers the chemistry of the eruptions only from the Hekla volcano. This EPMA data focuses on the glass chemistry, again the main focus of this investigation.

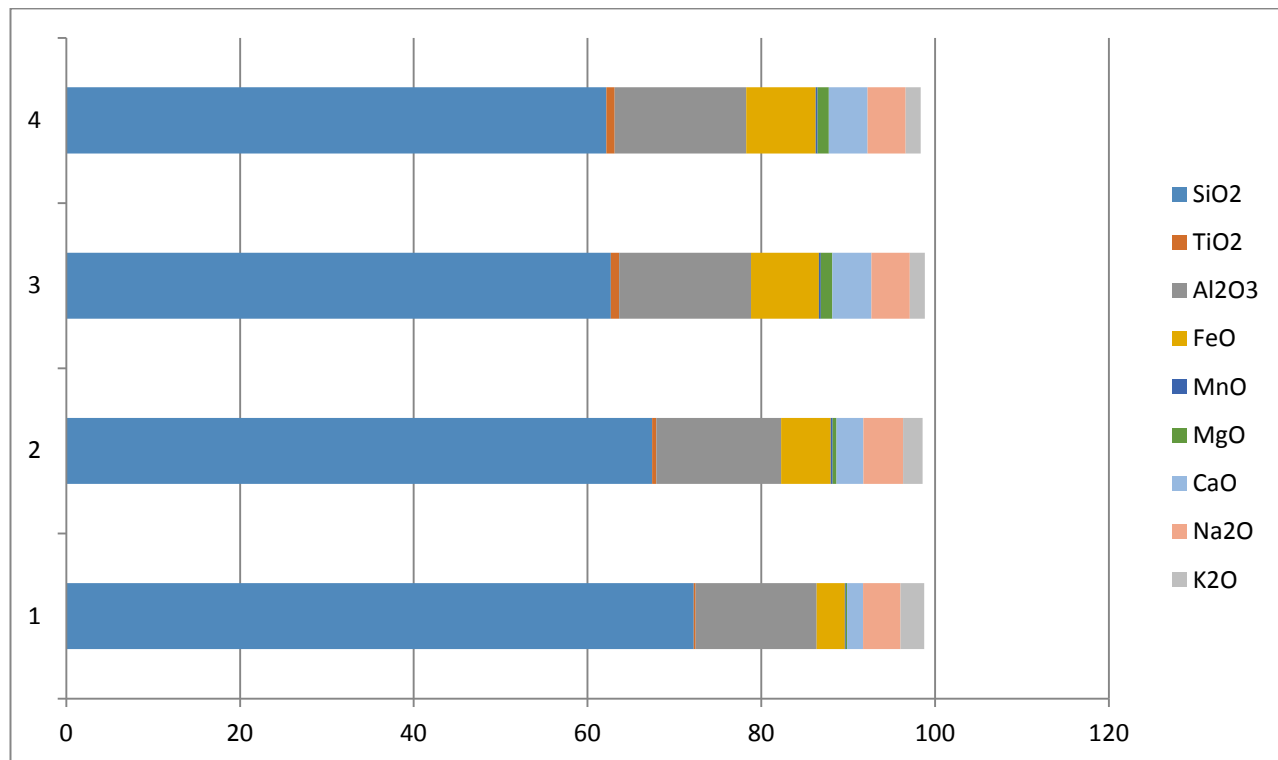


**Figure 1.2.2: Collated EMPA data of glass chemistry from Rea *et al.* Where 1 is Hekla 1104 AD, 2 is Hekla 1158 AD, 3 is Hekla 1510 AD and 4 is 1947 AD.**

The use of tephra layers, which bear their own unique chemistry and character, as temporal marker horizons in archaeological and geological sites is known as tephrochronology. The premise of tephrochronology is that each tephra deposit from a singular volcanic eruption has a unique chemical fingerprint. These tephra deposits form discrete layers and using the chemical fingerprints these layers can be distinguished from one another. These events form a chronological framework in which paleoenvironmental or archaeological records can be placed.



**Figure 1.2.3: Examples of visible tephra layers forming a chronological framework (Alber, 2012).**

The main advantages of the technique are that the volcanic ash layers can be relatively easily identified in many sediments (see fig. 1.2.3) and that the tephra layers are deposited relatively instantaneously over a wide spatial area (Pallardy, 2011). This means they provide accurate temporal marker layers which can be used to verify or corroborate other dating techniques, linking sequences widely separated by location into a unified chronology that correlates climatic sequences and events.

Recently, tephra chronology has been key in the dating of peat sequencing and examining inter-site records across specific isochrones allowing the spatial synchronicity of environmental changes to be scrutinised (Interpol, 2011).

Tephra horizons are sometimes visible to the naked eye (see figure 1.2.3) yet criptotephra samples invisible to the naked eye have been found in many more areas around the world further away from their volcanic source (Gerasimowicz, 1986). In some cases these tephra horizons can be assigned a known calendar date based on historical, documented evidence (Hekla 1947, 1510 and 1104)( Filip, 1998). Other tephra horizons have been aged utilising radiocarbon techniques such as wiggle match dating of the surrounding deposits in which

they are found and Bayesian age modelling (Knut Faegri, 2000). These ageing techniques can only be achieved if accurate, quantitative distributional and geochemical data are obtained from the tephra layer in question.

### **1.3- Hekla**

Hekla ([hɛ<sup>h</sup>kla]) is a stratovolcano located in the south of Iceland with a height of 1,491 metres (4,892 ft). Hekla is one of Iceland's most active volcanoes; over 20 eruptions have occurred in and around the volcano since 874.

Hekla is part of a volcanic ridge, 40 kilometres (25 mi) long. However, the most active part of this ridge, a fissure about 5.5 km (3.4 mi) long named *Heklugjá*, is considered to be the volcano Hekla proper. Hekla looks rather like an overturned boat, with its keel being in fact a series of craters, two of which are generally the most active. The volcano's frequent large eruptions have covered much of Iceland with tephra and these layers can be used to date eruptions of Iceland's other volcanos. 10% of the tephra created in Iceland in the last thousand years has come from Hekla, amounting to 5 km<sup>3</sup>. The volcano has produced one of the largest volumes of lava of any in the world in the last millennium, around 8 km<sup>3</sup>.

Hekla has a morphological type between that of a crater row and stratovolcano sited at a rift-transform junction in the area where the south Iceland seismic zone and eastern volcanic zone meet. The unusual form of Hekla is found on very few volcanoes around the world, notably Callaqui in Chile. Hekla is situated on a long volcanic ridge of which the 5.5 km *Heklugjá* fissure is considered Hekla proper. This fissure opens along its entire length during major eruptions and is fed by a magma reservoir estimated to have a top 4 km below the surface with centroid 2.5 km lower. The tephra produced by its eruptions is

high in SiO<sub>2</sub>. Hekla's basaltic andesite lava generally has a SiO<sub>2</sub> content of over 54%, compared to the 45-50% of other nearby transitional alkaline basalt eruptions. It is the only Icelandic volcano to produce calc-alkaline lavas.

Phenocrysts in Hekla's lava can contain plagioclase, pyroxene, titanomagnetite, olivine & apatite.

When not erupting Hekla is often covered with snow and small glaciers, it is also unusually aseismic with activity only starting 30–80 minutes before an eruption. Hekla is located on the mid-ocean ridge, a diverging plate boundary. Hekla is closely studied today for parameters such as strain, tilt, deformation and other movement and seismic activity.

Hekla (currently 1491m in height) is one of the most active volcanoes in Iceland.

Hekla is a morphological stratovolcano located near the rift-transform fault junction in the area where Iceland's South and Eastern Seismic Zones meet.

Hekla's repeated fissure eruptions result in the formation of a vaulted ridge of about 5 km (*Heklugjá* fissure) that opens along its entire length during major eruptions. The magma reservoir(s) under Hekla appears to be not well constrained but it is generally agreed that it is situated between 4 km (Linde *et al.*, 1993) and 8 km (Kjartansson and Gronvold, 1983).

All known Hekla eruptions have begun with an explosive phase followed by more effusive eruptions. After the eruptions in 1693, 1845 and 1947, tephra fallouts were recorded in contemporary written accounts (Thorarinsson, 1981), and among the most recent eruptions of Hekla only two are accompanied by physical evidence on the ground (Salmi, 1948). This is a common problem in tephrochronology and is due to the fact that tephra blankets can either disappear (often completely after major erosion due to an associated rainfall

event) or have never been deposited at a particular site. During the last 1100 years Hekla has produced 17 wide spread silicic tephra layers (Haflidason *et al*, 2000). All of these tephra layers have been analysed with EMPA and the eruptions responsible for producing these tephras have been well-dated.

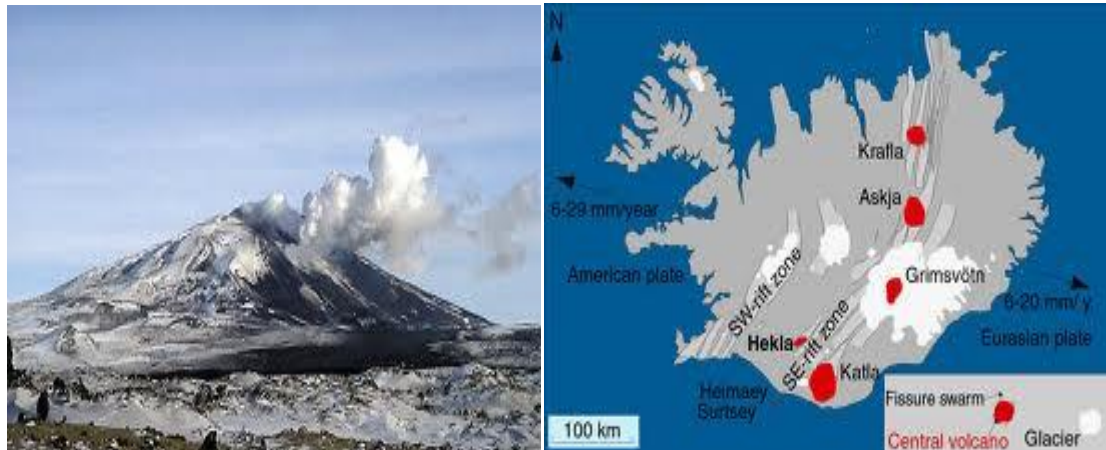


**Figure 1.3.1: Hekla and its location on the map of Iceland (Pfeiffer, T., 2003)**

Details of the 1510 eruption were not recorded until a century later. It started on July 25 and was particularly violent, (VEI 4) firing volcanic bombs as far as Vördufell, 40 km west. Tephra was deposited over Rangárvellir, Holt and Landeyjar,  $0.2 \text{ km}^3$  in total.

The 1947 eruption started on March 29, 1947 and ended on April 21, 1948. At VEI 4 it is likely that this was both the second greatest lava eruption of Hekla whilst Iceland was inhabited and the second greatest lava eruption in the world in the period 1900-1970. A total lava volume  $0.8 \text{ km}^3$  was produced with  $0.21 \text{ km}^3$  of tephra. The height of Hekla was 1447 m before the eruption, increasing to a maximum of 1503 m, before dropping to 1491 m subsequently.

The 1947 eruption occurred over a century since the last eruption of Hekla proper, the longest dormant period since 1104. Before the eruption the volcano had been visible from the surrounding area but nothing remarkable was noticed. The eruption occurred at 6:41 am  $\pm$  3 min with a loud roar, later eruptions could be heard throughout Iceland. An earthquake at 6:50 am measured 6 on the Mercalli intensity scale and increased the eruption intensity until it covered a 4 km fissure on the ridge. For the first hours the eruption was Plinian, after that it became Vesuvian. The cloud from the eruption had ascended to a height of 30 km by 7:08 am, the wind then carried it southwards towards the Eyjafjallajökull glacier, turning it black. Pumice first landed on Fljótshlíð at around 7:10 am and tephra and ash continued falling until it formed a 3–10 cm layer. A lava bomb that landed 32 km from Hekla was 0.5 m across and weighed 20 kg. Between Vatnafjöll and Hekla a layer of tephra up to a metre thick was deposited including bombs with a diameter larger than this. Bombs with areas of 50 m<sup>2</sup> were dropped onto the slopes of Hekla, up to 1 km away, 51 hours after the eruption had started ash fell on Helsinki, Finland having covered 2860 km in this time.

The initial tephra production rate in the first 30 minutes of the eruption was 75,000 m<sup>3</sup>s<sup>-1</sup>, dropping to 22,000 m<sup>3</sup>s<sup>-1</sup> for the next half hour. The initial phase produced 0.18 km<sup>3</sup> of tephra, equating to 4.5×10<sup>7</sup>m<sup>3</sup> of solid rock, covering 3,130 km<sup>2</sup> of land and sea. 98 farms were damaged by the eruption but only 2 were no longer farmed in 1970. A large volunteer effort was mobilized to clear the tephra - around 1000 man-days by the end of July. The eruption produced around 3 Ml of water (snowmelt and directly from the fissure) which caused flooding of the Ytri Rangá river.

In the first 20 hours of the eruption approximately  $3,500 \text{ m}^3\text{s}^{-1}$  of lava was produced from the fissure dividing into various branches and covering 12–15  $\text{km}^2$ . On the second day 8 distinct eruption columns were discernable. A crater formed at 860 m called the Lava Crater (*Hraungígur*) producing a constant flow of lava. Another crater named the Shoulder Crater (*Axlargígur*) produced a column of smoke every 10 s together with loud explosions that created visible compression waves in the smoke. By the fourth, fifth and sixth days the eruption was greatly diminished and only the shoulder and summit craters were erupting explosively.

The explosive eruption increased in strength from 9–12 April and then from April 28 reduced again. On May 3 the volcano stopped throwing out lava in sudden explosions from its craters and changed to continuously ejecting tephra and ash for long periods, until early June when this reduced. On September 2 the Shoulder Crater had a 960 m circumference at its top and the Summit Crater a 700 m circumference at its highest point, 90 m above the ridge. Sandy tephra and ash fell over Iceland in May and June, sometimes making it dark in the daytime near to Hekla. The tephra caused fluorine poisoning of grazing sheep, making them unable to walk. That winter more craters formed, building up cones. Explosive activity had ceased six months after the first eruption. Lava flowed from the Lava Crater continuously during the eruption, starting at a rate of over  $100 \text{ m}^3\text{s}^{-1}$ , dropping to  $5\text{--}10 \text{ m}^3\text{s}^{-1}$  in April and early May at a speed of around  $20 \text{ cm}^{-1}$  before increasing, eventually reaching  $150 \text{ m}^3\text{s}^{-1}$  at the end of June and at similar levels until mid-July with a peak flow speed of  $2\text{--}2.5 \text{ ms}^{-1}$ . From there it gradually decreased to less than  $10 \text{ m}^3\text{s}^{-1}$  in November. Initially the lava comprised 57-58%  $\text{SiO}_2$  and 11%  $\text{Fe}_2\text{O}_3$ ; from the time of peak flow onwards this changed to 54%  $\text{SiO}_2$  and 13.5%  $\text{Fe}_2\text{O}_3$ .

The lava river sometimes ran through tunnels before emerging again. The lava front had a height of up to 15 m. On June 15 and 16 a branch of lava flow to the south of Melfell travelled over 1 km in 30 hours before slowing and stopping by June 21, 7.8 km from the Lava Crater. The longest lava stream produced was 8 km long and stopped in Stóraskógsbotnar. A scientist filming one of the lava streams on November 2 was hit by a block of lava and killed.

The lava flow stopped after 13 months on April 21 having covered 40 km<sup>2</sup> and with a maximum depth of 100 m. In April and May 1948 CO<sub>2</sub> emitted from cracks in the ground pooled in hollows near to Hekla killing 15 sheep and some wild animals and birds. In total 24,000 tonnes of CO<sub>2</sub> was emitted. Ditches were dug by farmers to drain these hollows and the CO<sub>2</sub> emission had stopped by the end of the year.

#### **1.4- Mineralogical Identification**

A key method of geochemical sample identification is through identification of the mineral samples contained within it. As the humic and fulvic acid fractions, along with the chemical compositions, of geochemical samples are often very similar, identification and quantification of key minerals is often the only way to separate samples. Mineral identification also plays a key role in other areas of geochemical investigation, particularly in forensic issues surrounding pollution or contamination as well as in commercial mining.

Mineral identification has long been achieved by the methods mentioned in the rest of this chapter. However, these methods rely on a multi-proxy approach. These methods are often time consuming and subjective. The aim of this work was to evaluate Raman spectroscopy for use in the field of geochemistry. In this work we consider its use in soil science as a means to identify samples through

mineral composition and its organic fractions. We further investigate the use of Raman spectroscopy in tephra analysis and its ability to provide further discrimination of mineralogy within samples than is currently achievable.

#### 1.4.1- In-field Mineralogical Identification

Mineralogical identification has evolved throughout the ages and with the advancement of modern spectroscopic techniques. However, to a field geologist a traditional multi-step semi visual method is still used in the preliminary identification of minerals where laboratory analysis is unavailable based on the luster, hardness and colour of the sample (Yingst *et al*, 2014).

The three major types of luster are metallic, glassy (vitreous) and dull (fig 1.4.1.1). A luster between metallic and glassy is called adamantine, and a luster between glassy and dull is called resinous or waxy (Johnson, 2011). Dull minerals exhibit very little luster due to coarse granulations which scatter light in all directions. Glassy luster occurs because of a large number of microscopic inclusions whilst metallic luster appears as very reflective and polished.



**Figure 1.4.1.1: An example of the three main types of luster. On the left is a dull luster, a glassy luster in the middle and a metallic luster on the right. Taken from GIA Gem Reference Guide, Geological institute of America.**

The hardness of the mineral is measured using the Mohs hardness scale. The Mohs scale is a relative technique whereby common objects are used to test the relative hardness of the mineral through scratching. For example; a fingernail is at 2.5 Mohs, a penny is 3 Mohs, glass is 5.5 Mohs and sandpaper uses artificial corundum and is hardness 9 Mohs (Johnson, 2011).

Due to the fact that colour is perceived differently by individuals the Munsell colour system has been adopted for identification (fig 1.4.1.2). The Munsell colour system is a colour space that specifies colours based on three colour dimensions: hue, value (lightness), and chroma (colour purity). It was created by Professor Albert H. Munsell in the first decade of the 20th century and adopted by the United States Department of Agriculture (USDA) as the official colour system for soil research in the 1930s (Wiley, 1982).

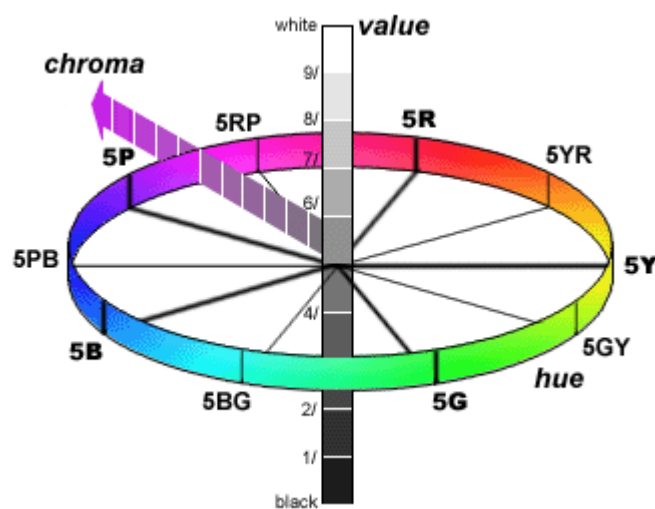


Figure 1.4.1.2: An example of the Munsell Colour System identifying colour through hue, value and chroma (Wiley, 1982).

The streak of the mineral is then identified, also using the Munsell colour system. The streak of a mineral is the colour of that mineral when it is freshly crushed (Road, 1880). This process is normally carried out by scratching the

unknown sample across a streak plate, an unglazed piece of ceramic with a hardness of 7 Mohs where the colour left on the plate is then determined.

The cleavage and fracture of the mineral are then identified, by how the mineral breaks. Many minerals will break along flat planes (cleavages) some in only one direction (like mica), others in two directions (like feldspar), and some in three directions (like calcite) or more (like fluorite) (Tromans & Meech, 2004). Some minerals, like quartz, have no cleavage. Fracture is breakage that is not flat.

The two main kinds of fracture are conchoidal (shell-shaped, as in quartz) and uneven. Metallic minerals may have a hackly (jagged) fracture. A mineral may have good cleavage in one or two directions but fracture in another direction (Tromans & Meech, 2004).

Magnetism is a distinctive property in a few minerals. Magnetite is the prime example, but a few other minerals may be weakly attracted by a magnet, notably chromite and pyrrhotite.

#### **1.4.2- Laboratory Mineralogical Identification**

Traditionally minerals are identified using a combination of complimentary analytical techniques. In the majority of geological investigations X-ray diffraction (XRD), optical light microscopy, electron microprobe microscopy and scanning electron microscopy are all used to confirm mineral identification (Thornalley, McCave *et al*, 2011).

*X-Ray* scattering techniques are a family of non-destructive analytical techniques that reveal information about the crystallographic structure, chemical composition, and physical properties of materials and thin films. These techniques are based on observing the scattered intensity of an X-ray beam

hitting a sample as a function of incident and scattered angle, polarization, and wavelength or energy (Cardell *et al*, 2009). Powder X-ray diffraction (PXRD) is a technique using X-ray diffraction on powder or microcrystalline samples for structural characterization of materials.

XRD is particularly useful for identifying fine-grained minerals and mixtures or intergrowths of minerals, which may not lend themselves to analysis by other techniques (Cardell *et al*, 2009). XRD can provide additional information beyond basic identification. If the sample is a mixture, XRD data can be analyzed to determine the proportion of the different minerals present. Other information obtained can include the degree of crystallinity of the mineral(s) present, possible deviations of the minerals from their ideal compositions (presence of element substitutions and solid solutions), the structural state of the minerals (which can be used to deduce temperatures and (or) pressures of formation), and the degree of hydration for minerals that contain water in their structure. Some mineralogical samples analyzed by XRD are too fine grained to be identified by optical light microscopy. XRD does not, however, provide the quantitative compositional data obtained by the electron microprobe or the textural and qualitative compositional data obtained by the scanning electron microscope.

XRD has been used to identify mineralogy in a wide range of geological applications. In studies of areas affected by acid mine drainage, the identification of secondary minerals and fine-grained precipitates is a critical element (Dinelli & Tateo, 2002). Sulphuric acid is generated when iron sulphide minerals, such as pyrite, weather. Elements derived from the alteration of the sulphide minerals can form secondary minerals or go into solution. Minerals that

are soluble may form mineral precipitates as conditions (temperature, acidity, solution composition) change. Accurate mineralogical characterization of the precipitates and secondary minerals, together with hydro geochemical data, help us to better understand the solubility, transport, and storage of metals (Zhu & Burden, 2001).

In ore genesis studies minerals form under specific ranges of temperature and pressure. Mineralogical identification of ore minerals and associated minerals, including fine-grained hydrothermal alteration minerals, provides evidence used to deduce the conditions under which ore deposits formed and the conditions under which, in many cases, they were subsequently altered (Mehrabi & Yardley, 1999).

XRD is routinely used in Predictive Stratigraphic Analysis where mineralogical characteristics of paleosols (ancient buried soil horizons) and under clays (the fine-grained detrital material lying immediately beneath a coal bed) have been instrumental in correlating coal zones from the Appalachian basin into the Western Interior basin (Rawlins *et al.*, 2006). They have been the key to quantifying the paleolatitudinal climate gradient in North America during the late Middle Pennsylvanian.

Mineralogical analysis by XRD is used in conjunction with remotely sensed data in several research investigations. XRD is used to identify the minerals composing clay-rich, hydrothermally altered rocks that occur on several Cascade volcanoes (Zimbelman *et al.*, 2005). Such rocks are believed to play an important role in the generation of large landslides and mudflows. XRD is used to analyze saline minerals, including borates. Many saline hydrate minerals produce diagnostic spectral bands, and spectral data provide a basis for mineral

exploration using remote-sensing data. Analysis of airborne imaging spectrometer data can directly map mineral occurrences by detecting diagnostic spectral absorption bands, the shape and position of which are determined by individual mineral structures. A detailed knowledge of sample mineralogy, provided at least in part by XRD, is required to understand the observed spectral absorption features.

XRD is one of the primary tools used to evaluate the lateral and vertical variations in mineral matter and major, minor, and trace elements in coal beds. These data are used to help determine the impact of geologic and geochemical processes on coal bed formation in order to understand and predict both inorganic and organic variability within and among minable coal beds (Rawlins *et al*, 2006).

Mineralogical characterization provides part of the data required to determine the particular kind of mineral deposits encountered in mineral-resource assessment studies. XRD allows us to identify fine-grained mixtures of minerals found in associated gangue and alteration assemblages, which cannot be resolved by other methods.

Optical light microscopy is used extensively in the identification of mineralogical species. It is often used to identify lustre, colour, cleavage and fracture as well as aiding in the identification of a minerals crystal structure (Fandrich, Gu *et al*, 2007)(Smith & Clark, 2004). In order to aid these identifications four fields of illumination are used; Cross-polarized light illumination, Bright illumination, Dark illumination and Phase contrast illumination.

Cross-polarized light illumination is most commonly used on birefringent samples where the polarized light interacts strongly with the sample and so

generating contrast with the background. Polarized light microscopy is capable of providing information on absorption colour and optical path boundaries between minerals of differing refractive indices, in a manner similar to bright-field illumination, but the technique can also distinguish between isotropic and anisotropic substances. Furthermore, the contrast-enhancing technique exploits the optical properties specific to anisotropy and reveals detailed information concerning the structure and composition of materials that are invaluable for identification and diagnostic purposes.

Bright-field illumination is arguably the simplest form of optical microscopy. Sample illumination is achieved through white light being passed through it with a transmitted image to an eyepiece. Sample contrast is caused by the absorbance of some of the light in the densest areas of the sample.

An electron probe micro-analyzer (EPMA) is a microbeam instrument used primarily for the *in situ* non-destructive chemical analysis of minute solid samples. The primary importance of an EPMA is the ability to acquire precise, quantitative elemental analyses at very small "spot" sizes (as little as 1-2 microns), primarily by wavelength-dispersive spectroscopy (WDS) (Muralha, Rehren *et al*, 2011). The spatial scale of analysis, combined with the ability to create detailed images of the sample, makes it possible to analyze geological materials *in situ* and to resolve complex chemical variation within single phases (in geology, mostly glasses and minerals). The electron optics of an SEM or EPMA allow much higher resolution images to be obtained than can be seen using visible-light optics, so features that are irresolvable under a light microscope can be readily imaged to study detailed micro textures or provide the fine-scale context of an individual spot analysis (Cardell *et al*, 2009).

This technique is most commonly used by mineralogists and petrologists. Most rocks are aggregates of small mineral grains. These grains may preserve chemical information adopted during their formation and subsequent alteration. This information may illuminate geologic processes, such as crystallization, lithification, volcanism, metamorphism, orogenic events (mountain building), and plate tectonics. This technique is also used for the study of extraterrestrial rocks (i.e. meteorites), and provides chemical data which is vital to understanding the evolution of the planets, asteroids, and comets.

The change in elemental composition from the center (also known as core) to the edge (or rim) of a mineral can yield information about the history of the crystal's formation, including the temperature, pressure, and chemistry of the surrounding medium. Quartz crystals, for example, incorporate a small, but measurable amount of titanium into their structure as a function of temperature, pressure, and the amount of titanium available in their environment. Changes in these parameters are recorded by titanium as the crystal grows.

An electron microscope (EM) has a higher resolving power than a light microscope and can reveal the structure of smaller objects because electrons have wavelengths about 100,000 times shorter than visible light photons. They can achieve better than 50 pm resolution and magnifications of up to about 10,000,000x whereas ordinary, non-confocal light microscopes are limited by diffraction to about 200 nm resolution and useful magnifications below 2000x. The electron microscope uses electrostatic and electromagnetic lenses to control the electron beam and focus it to form an image. These electron optical lenses are analogous to the glass lenses of a light optical microscope.

The electron beam of the scanning electron microscope (SEM) does not at any time carry a complete image of the specimen. The SEM produces images by probing the specimen with a focused electron beam that is scanned across a rectangular area of the specimen (raster scanning). When the electron beam interacts with the specimen, it loses energy by a variety of mechanisms. The lost energy is converted into alternative forms such as heat, emission of low-energy secondary electrons and high-energy backscattered electrons, light emission (cathodoluminescence) or X-ray emission, which provide signals carrying information about the properties of the specimen surface, such as its topography and composition. The image displayed by an SEM maps the varying intensity of any of these signals into the image in a position corresponding to the position of the beam on the specimen when the signal was generated.

Generally, the image resolution of an SEM is about an order of magnitude poorer than that of a TEM. However, because the SEM image relies on surface processes rather than transmission, it is able to image bulk samples up to many centimetres in size and (depending on instrument design and settings) has a great depth of field, and so can produce images that are good representations of the three-dimensional shape of the sample. Environmental scanning electron microscopes (ESEM) can produce images of sufficient quality and resolution without the conductive coatings used in traditional SEM allowing for studies on wet samples or contained in low vacuum or gas. This greatly facilitates imaging biological samples that are unstable in the high vacuum of conventional electron microscopes.

Further analytical techniques are widely used in the geological field, although these techniques are rarely used in the identification of minerals. These

analytical techniques are most often used in soil identification and characterization. A brief overview of these further techniques and their uses are given below.

Gas chromatography is a chromatographic technique used in the separation of volatile compounds. A gas chromatograph consists of a flowing mobile phase, an injection port, a separation column containing the stationary phase, a detector, and a data recording system. The organic compounds are separated due to differences in their partitioning behaviour between the mobile gas phase and the stationary phase in the column. By itself gas chromatography is simply a method of separation but can be coupled with mass spectrometry to provide a means of identification for forensic samples. Gas chromatography is a common tool used in the separation and subsequent identification of the humic fractions of soil through the analysis of its pyrolysis products. G. E. Orzechowska *et al* are currently utilising gas chromatography to study the polycyclic aromatic hydrocarbons (PAH) of soils from the desert areas of Utah (Orzechowska *et al*, 2011). PAHs are molecules believed to be in abundance in extraterrestrial environments based on their inclusions in meteorites found on earth.

Mass spectrometry (MS) is an analytical technique that measures the mass-to-charge ratio of charged particles. It is used for determining masses of particles, for determining the elemental composition of a sample or molecule, and for elucidating the chemical structures of molecules, such as peptides and other chemical compounds. The MS principle consists of ionizing chemical compounds to generate charged molecules or molecule fragments and measuring their mass-to-charge ratios. J Campo *et al* utilised mass spectrometry to determine the quality of Soil Organic Matter (SOM). Samples

were heated under laboratory conditions at different temperatures (220, 380 and 500 °C) to establish their effects on the SOM quality and quantity by comparison with unheated control samples (25 °C). The SOM content in the soil under canopy was higher than in the bare one and in the micro-aggregate fractions than in the macro-aggregate ones. Increasing temperatures caused, in general, the decrease of SOM content in both soils as well as in both aggregate classes. The quality of SOM was determined after extraction with 0.1 M NaOH and analysed by pyrolysis-gas chromatography/mass spectrometry (Py-GC/MS). The composition of the SOM extracted from the soils heated at 220 °C, was quite similar to that obtained from unheated soils. The products derived from polysaccharides and lignin, and some coming from polyphenols, were not detected in the pyrolysates of the soil heated at 380 and 500 °C (Campo *et al* 2001)(Holmkvist *et al.*, 2010).

MS can be combined with many other analytical techniques including HPLC, GC, IR and Raman spectroscopy. Stable isotope ratio mass spectrometry is of particular (SIR-MS) use in the analysis of street drugs. It's development was largely driven by the geochemical scientists who wanted to extract further information contained in fossil biomarkers such as sedimentary long-chain alcohols and sterols( Meier-Augenstein., 1999). The technique requires the sample to be converted into a gas (CO<sub>2</sub>, N<sub>2</sub>, CO, SO<sub>2</sub> or H<sub>2</sub>) and can then be used to distinguish between two different samples of the same drug by determining which carbon and nitrogen isotopes are most abundant in the sample. Pyrolysis Mass Spectrometry has been used forensically in the analysis of synthetic textile fibres and paints. Laser ablation inductively coupled plasma mass spectrometry can be used to simultaneously analyse multiple layers of

paint simultaneously and has been used to compare glass evidence (Gao *et al*, 2002).

Thin Layer Chromatography (TLC) is a simple, quick, and inexpensive procedure that gives the chemist a quick answer as to how many components are in a mixture. TLC is also used to support the identity of a compound in a mixture when the  $R_f$  of a compound is compared with the  $R_f$  of a known compound.

A TLC plate is a sheet of glass, metal, or plastic which is coated with a thin layer of a solid adsorbent (usually silica or alumina). A small amount of the mixture to be analyzed is spotted near the bottom of this plate. The TLC plate is then placed in a shallow pool of a solvent in a developing chamber. This liquid, or the eluent, is the mobile phase, and it slowly rises up the TLC plate by capillary action. As the solvent moves past the spot that was applied, equilibrium is established for each component of the mixture between the molecules of that component which are adsorbed on the solid and the molecules which are in solution. In principle, the components will differ in solubility and in the strength of their adsorption to the adsorbent and some components will be carried farther up the plate than others. In a geochemical context TLC is commonly used in the analysis of pesticide mobility through soil micro structures (Ravanel *et al*, 1999).

High Performance Liquid Chromatography (HPLC) can, unlike TLC, can provide quantitative information. The sample to be analyzed is introduced, in small volumes, into the stream of mobile phase. The solution moved through the column is slowed by specific chemical or physical interactions with the stationary phase present within the column. The velocity of the solution

depends on the nature of the sample and on the compositions of the stationary (column) phase. The time at which a specific sample elutes (comes out of the end of the column) is called the retention time; the retention time under particular conditions is considered an identifying characteristic of a given sample. The use of smaller particle size column packing (which creates higher backpressure) increases the linear velocity giving the components less time to diffuse within the column, improving the chromatogram resolution.

HPLC is perhaps most commonly used in geochemistry in the analysis of herbicide levels and concentrations in soil samples (Mouet *et al*, 2008)(Tran *et al*, 2007). More recently however, it has been used in warzones to measure the amount of trace explosives found in soil samples within a blast region in an attempt to identify the likely long term exposures to the citizens in these areas.

Nuclear Magnetic Resonance Spectroscopy (NMR) is both a qualitative and quantitative analytical technique. Nuclear magnetic resonance (NMR) is an effect whereby magnetic nuclei in a magnetic field absorb and re-emit electromagnetic (EM) energy. This energy is at a specific resonance frequency which depends on the strength of the magnetic field and other factors. This allows the observation of specific quantum mechanical magnetic properties of an atomic nucleus. Many scientific techniques exploit NMR phenomena to study molecular physics, crystals and non-crystalline materials through NMR spectroscopy. NMR is also routinely used in advanced medical imaging techniques, such as in magnetic resonance imaging (MRI) (Filler, 2005).

NMR is widely regarded as an untapped and un-understood tool in the area of geo-chemistry. It has been utilised in looking at soil organic matter and has

increased our understanding of the nature of its decomposition and the effects of cultivation (Ktigel-knabner, 1997).

Work has been carried out to characterise the chemical composition of SOM with Carbon 13 NMR (Ktigel-knabner, 1997). Fractions of SOM were extracted by an integrated physical–chemical procedure and their chemical natures were characterized through  $^{13}\text{C}$  nuclear magnetic resonance (NMR) spectroscopy. Whole SOM was obtained by dissolving the soil mineral component through HF washes. All samples were analyzed by advanced  $^{13}\text{C}$  NMR techniques, including quantitative direct polarization/magic angle spinning, spectral-editing techniques, and two-dimensional  $^1\text{H}$ – $^{13}\text{C}$  heteronuclear correlation NMR. The NMR spectra were comparable for the light fraction and two POM fractions and were dominated by carbohydrates and to a lesser extent lignins or their residues, with appreciable proteins or peptides. By contrast, spectra of the two humic fractions were dominated by aromatic C and COO/N–C=O groups, with smaller proportions of carbohydrates and NCH/OCH<sub>3</sub> groups, indicative of more humified material.

#### **1.4.3- Mineral Identification using Raman Spectroscopy**

Raman spectroscopy is a spectroscopic technique used to study vibrational, rotational, and other low-frequency modes in a system. It relies on inelastic scattering, or Raman scattering, of monochromatic light, usually from a laser in the visible, near infrared, or near ultraviolet range. The laser light interacts with molecular vibrations, phonons or other excitations in the system, resulting in the energy of the laser photons being shifted up or down. The shift in energy gives information about the vibrational modes in the system.

In Geo-chemistry Raman spectroscopy is regularly used to study gemstone and mineral identification, fluid inclusions, mineral and phase distribution in rock sections, phase transitions and mineral behaviour under extreme conditions. Generally speaking, it has largely been used as a means to identify specific materials in a sample rather than using it to interrogate the sample as a whole e.g. Trolard *et al* utilising Raman spectroscopy to identify a green rust mineral in a sample of reductomorphic soil (Acta *et al.*, 1997). Raman spectroscopy has been regularly used in the identification of minerals of the type found in terrestrial soil samples. Richard Herman *et al* used Raman microprobe analysis to identify individual carbonate minerals (regularly found in the majority of soil samples) such as calcite, dolomite, and aragonite (Banerjee *et al.*, 2006).

The methodologies used in the identification of minerals with Raman spectroscopy vary widely due to a number of analytical problems that can be caused by these materials. For example, when analysing the mineral content in soil samples fluorescence regularly masks any sample peak signals. This fluorescence is caused by the humic content of the soil samples and to date all Raman data on whole soil samples has been heavily corrected (Edwards *et al* 2011). Raman spectroscopy can itself be a problem in the analysis of minerals and as such a systematic development is required for the analysis of any new materials. Although laser Raman spectroscopy is a non-destructive technique, samples can undergo localized heating and oxidation if the laser power is too high (what is considered “high” laser power depends on the sample) (Edwards *et al.*, 2011). An example of these spectral changes brought about by sample heating has been described by D.L.A. de Faria *et al.* In their work Hematite ( $\alpha$ - $\text{Fe}_2\text{O}_3$ ), magnetite ( $\text{Fe}_3\text{O}_4$ ), wüstite ( $\text{FeO}$ ), maghemite ( $\gamma$ - $\text{Fe}_2\text{O}_3$ ), goethite ( $\alpha$ - $\text{FeOOH}$ ), lepidocrocite ( $\gamma$ - $\text{FeOOH}$ ) and  $\delta$ - $\text{FeOOH}$  were studied by Raman

microscopy (Faria & Vena, 1997)(Faria & Lopes, 2007). Here, Raman microscopy was employed to investigate the laser power dependence of the spectra of these oxides and oxyhydroxides. Low laser power was used for the reference spectra in order to minimize the risks of spectral changes due to sample degradation. The results obtained show that increasing laser power causes the characteristic bands of hematite to show up in the spectra of most of the compounds studied whereas the hematite spectrum undergoes band broadening and band shifts.

## 1.5- References

- Acta, C., Gi, M. R., Bourrii, G., Ceclex, R., Physique, C., Poincar, C. H. (1997). "SCIENTIFIC COMMENT Identification of a green rust mineral in a reductomorphic soil by Mossbauer and Raman spectroscopies" *61*(5), 1107–1111.
- Albarède, F., *Geochemistry: An Introduction*. 2 ed. 2009: Cambridge University Press. 356.
- Alber, J.S.,. *Volcanism of the Eifel, Germany Region*. (2012)  
<http://academic.emporia.edu/aberjame/tectonic/eifel/eifel.htm>
- Meier-Augenstein, W. "Applied gas chromatography coupled to isotope ratio mass spectrometry." *Journal of Chromatography A* 842.1 (1999): 351-371.
- Banerjee, S., Jia, S., Kim, D. I., Robinson, R. D., Kysar, J. W., Bevk, J., & Herman, I. P. (2006). "Raman Microprobe Analysis of Elastic Strain and Fracture in Electrophoretically Deposited CdSe Nanocrystal Films". *Nano Lett.* 2006 Feb 6(2):175-80.
- Brevik, E. C. 2002. *Soil classification in geology textbooks*. *Journal of Geoscience Education* 50(5): 539-543.
- Campo, J., Maass, M., Jaramillo, V. J., Martínez-yrizar, A., & Sarukhán, J. (2001). Phosphorus cycling in a Mexican tropical dry forest ecosystem. *Biogeochemistry* 161–179.
- Cardell, C., Guerra, I., Romero-pastor, J., Cultrone, G., & Rodriguez-navarro, A. (2009). Micro-X-Ray Diffraction , Scanning Electron Microscopy-Based Mineral Maps , and Diffuse Reflectance Infrared Fourier Transform Spectroscopy to Characterize Archeological Artifacts, *Analytical Chemistry* 81(2), 604–611.
- Celi, L.S., Morris; Nègre, Michèle, Analysis of Carboxyl Groups in Soil Humic Acids By A Wet Chemical Method, Fourier-Transform Infrared Spectrophotometry, and Solution-State Carbon-13 Nuclear Magnetic Resonance. A Comparative Study. *Soil Science*, 1997. **162**(3): p. 7.
- Chesworth, W., ed. *Encyclopedia of Soil Science*. 2008, Springer.
- Cox, R.J., Young, J., Cusik, C., Espinoza, E.O., The forensic analysis of soil organic by FTIR. *Forensic Science International*, 2000. **108**(2): p. 9.
- Dabas, P.C., New and traditional analytical tools for the study of soils and humic acids, in 19th World Congress of Soil Science, *Soil Solutions for a Changing World*. 2010: Australia.
- Dinelli, E., & Tateo, F. (2002). Different types of fine-grained sediments associated with acid mine drainage in the Libiola Fe – Cu mine area ( Ligurian Apennines , Italy ), *Applied Geochemistry* 17, 1081–1092.

- Edwards, H., Munshi, T., Scowen, I., Surtees, A., & Swindles, G. T. (2011). Development of oxidative sample preparation for the analysis of forensic soil samples with near-IR Raman spectroscopy. *Journal of Raman Spectroscopy*, (July 2010). doi:10.1002/jrs.3031
- Ewald, M., Berger, P., Weber, J., Corrected fluorescence spectra of fulvic acids isolated from soil and water. *Environmental Science Technology*, 1983. **17**(8): p. 3.
- Faegri, K., Krzywinski, K., *Textbook of Pollen Analysis*. 2000: The Blackburn Press. 340.
- de Faria, D. L. a., & Lopes, F. N. (2007). Heated goethite and natural hematite: Can Raman spectroscopy be used to differentiate them? *Vibrational Spectroscopy*, *45*(2), 117–121. doi:10.1016/j.vibspec.2007.07.003
- Fandrich, R., Gu, Y., Burrows, D., & Moeller, K. (2007). Modern SEM-based mineral liberation analysis, *84*, 310–320. doi:10.1016/j.minpro.2006.07.018
- Faria, D. L. A. D., & Vena, S. (1997). Raman Microspectroscopy of Some Iron Oxides and Oxyhydroxides, *Journal of Raman Spectroscopy*, *28*(February), 873–878.
- Filip, J.J.A.Z., Metal Binding in Estuarine Humic and Fulvic Acids: FTIR Analysis of Humic Acid-Metal Complexes. *Environmental Technology*, 1998. **19**(9): p. 8.
- Filler, A (2009). "The History, Development and Impact of Computed Imaging in Neurological Diagnosis and Neurosurgery: CT, MRI, and DTI". *Nature Precedings*. doi:10.1038/npre.2009.3267.5.
- Gao, S., Liu, X., Yuan, H., & Hattendorf, B. (2002). Determination of Forty Two Major and Trace Elements in USGS and NIST SRM Glasses by Laser Ablation-Inductively Coupled Plasma-Mass Spectrometry, *American Journal of Analytical Chemistry* *26*, 181–196.
- Georgia, U.o. *The Georgia Oceans and Human Health Initiative*. 2011 [cited 2011 24th September]; Available from: <http://georgiaoceansandhealth.org/research>.
- Gerasimowicz, W.V., D.M.B., and Heino Susi Resolution-Enhanced FT-IR Spectra of Soil Constituents: Humic Acid. *Applied Spectroscopy*, 1986. **40**(4): p. 3.
- Hafliðason, H., Eiriksson, J., & Kreveld, S. V. (2000). The tephrochronology of Iceland and the North Atlantic region during the Middle and Late Quaternary: a review. *Journal of Quaternary Science*, *15*(1), 3–22. doi:10.1002
- Heiri, O., Lemcke, G., Loss on ignition as a method for estimating organic and carbonate content in sediments: reproducibility and comparability of results. *Journal of Paleolimnology*, 1999. **25**(1): p. 9.

- Richard G. Herman, C.E.B., Andre J. Sommer, and Dale R. Simpson  
Discrimination Among Carbonate Minerals by Raman Spectroscopy Using  
the Laser Microprobe. *Applied Spectroscopy*, 1987. **41**(3): p. 3.
- Ray L. Frost, T.K., Matthew L. Weiera, Wayde N. Martensa, Z. Dinga and  
Howell G. H. Edwards, Raman spectroscopy of selected arsenates—  
implications for soil remediation *Spectrochimica Acta Part A: Molecular and  
Biomolecular Spectroscopy*, 2003. **59**(10): p. 5.
- Holmkvist, L., Arning, E. T., Küster-Heins, K., Vandieken, V., Peckmann, J.,  
Zabel, M., & Jørgensen, B. B. (2010). Phosphate geochemistry,  
mineralization processes, and Thioploca distribution in shelf sediments off  
central Chile. *Marine Geology*, 277(1-4), 61–72.
- Horrocks, M., S.A.C.a.K.A.J.W., Forensic Palynology: Variation in the Pollen  
Content of Soil Surface Samples. *Journal of Forensic Science*, 1998. **43**(2):  
p. 3.
- Hueb, M.E.O.-E.N.V., Changes in Soil Properties and Vegetable Growth in  
Preparation for Organic Farming in Hawaii. *Communications in Soil  
Science and Plant Analysis*, 2011. **42**(17): p. 8
- Institute, M.L.U.R. Integration of Soil Fingerprinting Techniques for Forensic  
Application. 2012 10th January 2012 [cited 2012 5th Febuary]; Available  
from: <http://www.macauley.ac.uk/soilfit/>.
- Interpol. *FORENSIC EXAMINATION OF SOIL EVIDENCE*. [PDF] 2011 2011  
[cited 2011 26th June]; Available from:  
<http://www.interpol.int/Public/Forensic/IFSS/meeting13/Reviews/Soil.pdf>.
- Johnson, C., *Geochemistry@BGS: A guide to geochemical data at the British  
Geological Survey*. 2011, British Geological Survey: Nottingham.
- Jones, G.L.N.a.K.C., *Experimental approaches and analytical techniques for  
determining organic compound bound residues in soil and sediment*.  
*Science Direct*, 2000. **108**(1): p. 24.
- A. A. Kamnev, P.A.T., L. P. Antonyuka, L. A. Bespalovaa, M. G. Polissioub, M.  
Colinac, P. H. E. Gardinerc and V. V. Ignatova, Fourier transform Raman  
spectroscopic characterisation of cells of the plant-associated soil  
bacterium *Azospirillum brasilense* Sp7 *Journal of Molecular Structure*, 2001.  
**563-564**(1): p. 8.
- Karr, C.J., *Infrared and Raman spectroscopy of lunar and terrestrial minerals*,  
ed. C.J. Karr. 1975, New York: Academic Press.
- Ivan M. Kempsona, K.P.K., William M. Skinnera and John Coumbarosb,  
Applications of synchrotron radiation in forensic trace evidence analysis.  
*Talanta*, 2005. **67**(2): p. 17.
- Ktigel-knabner, I. (1997). 15N NMR spectroscopy as a tool in soil organic matter  
studies, *Geodenna* 80, 243–270.

- Lignuma, J., I.J., Martin A. Pearce, A critical assessment of standard processing methods for the preparation of palynological samples. *Review of Palaeobotany and Palynology*, 2008. **149**(3-4): p. 16.
- L.M. Macdonald, B.K.S., N. Thomas, M.J. Brewer, C.D. Campbell and L.A. Dawson, Microbial DNA profiling by multiplex terminal restriction fragment length polymorphism for forensic comparison of soil and the influence of sample condition. *Journal of Applied Microbiology*, 2008. **105**(3): p. 9.
- Mayes, R.W., L.M.M., Jasmine M. Ross and Lorna A. Dawson, Discrimination of Domestic Garden Soils Using Plant Wax Compounds as Markers *Criminal and Environmental Soil Forensics*, 2009. **4**: p. 13.
- Mehrabi, B., & Yardley, B. W. D. (1999). Sediment-hosted disseminated gold mineralisation, *Mineralium Deposita*, 673–696.
- Melquiades, F., Biasi, G., Paulo S. Parreira, and Carlos R. Appoloni. Granulometry and Moisture Influence for In Situ Soil Analysis by Portable EDXRF. in *XXXIII BRAZILIAN WORKSHOP ON NUCLEAR PHYSICS*. 2011. Brazil: AIP.
- Morgan, R., P.A.B., The use of grain size distribution analysis of sediments and soils in forensic enquiry. *Science and Justice*, 2007. **47**(3): p. 10.
- Morgan, R., Parker, A., Bull, P., The role of forensic geoscience in wildlife crime detection. *Forensic Science International*, 2006. **162**(1-3): p. 10.
- Mou, R., Chen, M., & Zhi, J. (2008). Simultaneous determination of 15 phenylurea herbicides in rice and corn using HPLC with fluorescence detection combined with UV decomposition and post-column derivatization, *875*, 437–443. doi:10.1016/j.jchromb.2008.09.022
- Muralha, V. S. F., Rehren, T., & Clark, R. J. H. (2011). Characterization of an iron smelting slag from Zimbabwe by Raman microscopy and electron beam analysis. *Journal of Raman Spectroscopy*, *42*(12), 2077–2084. doi:10.1002/jrs.2961
- Nyquist, R.A., ed. Infrared and Raman Spectral Atlas of Inorganic Compounds and Organic Salts. 1 ed., ed. A. Press. 1997, *Academic Press: San Diego*.
- Orzechowska, G. E., Kidd, R. D., Foing, B. H., Kanik, I., & Stoker, C. (2011). Analysis of Mars analogue soil samples using solid-phase microextraction , organic solvent extraction and gas chromatography / mass spectrometry, *Astrobiology*, *10*(3), 209–219. doi:10.1017/S1473550410000443
- Pallardy, R. *Munsell Colour System*. 2011 [cited 2012 17th February]; Available from: <http://www.britannica.com/EBchecked/topic/397642/Munsell-colour-system>.
- Pfeiffer, T., Hekla Volcano, Iceland (2003). Available from: <http://www.decadevolcano.net/volcanoes/iceland/hekla.htm>

- Ravanel, P., Liegeois, M. H., Chevallier, D., & Tissut, M. (1999). Soil thin-layer chromatography and pesticide mobility through soil microstructures *New technical approach*, 864, 145–154.
- Rawlins, B. G., Ph, D., Kemp, S. J., Sc, B., Hodgkinson, E. H., Ph, D., Riding, J. B., *et al.* (2006). Potential and Pitfalls in Establishing the Provenance of Earth-Related Samples in Forensic Investigations, *Geoforensics*, 51(4), 832–845. doi:10.1111/j.1556-4029.2006.00152.
- Road, C. (1880). Embreyite , a new mineral from Berezov , Siberia, *Minerological Magazine*, 38, 790–793.
- Schnitzer, M., Soil Organic Matter-the Next 75 Years. *Soil Science*, 1991. **151**(1): p. 8.
- Smith, G. D., & Clark, R. J. H. (2004). Raman microscopy in archaeological science, 31, 1137–1160. doi:10.1016/j.jas.2004.02.008
- Staff, S.S., Soil Taxonomy; A Basic System of Soil Classification for Making and Interpreting Soil Surveys, *U.S.D.o. Agriculture*, Editor. 1999, Natural Resources Conservation Service.
- Stevenson, F.J., *Humus Chemistry: Genesis, Composition, Reactions*. 2 ed. 1994: John Wiley and Sons.
- Tardy, Yves (1997). *Petrology of Laterites and Tropical Soils*. ISBN 90-5410-678-6. Retrieved April 17, 2010.
- Tipping, E., *WHAM*—a chemical equilibrium model and computer code for waters, sediments, and soils incorporating a discrete site/electrostatic model of ion-binding by humic substances. *Computers and Geosciences*, 1994. **20**(1): p. 50.
- Thornalley, D. J. R., McCave, I. N., & Elderfield, H. (2011). Tephra in deglacial ocean sediments south of Iceland: Stratigraphy, geochemistry and oceanic reservoir ages. *Journal of Quaternary Science*, 26(2), 190–198. doi:10.1002/jqs.1442
- Tran, A. T. K., Hyne, R. V., & Doble, P. (2007). Determination of commonly used polar herbicides in agricultural drainage waters in Australia by HPLC, 67, 944–953. doi:10.1016/j.chemosphere.2006.11.002
- Tromans, D., & Meech, J. A. (2004). Fracture toughness and surface energies of covalent minerals : theoretical estimates, 17, 1–15. doi:10.1016/j.mineng.2003.09.006
- Trostlea, C., Turnerb, F., & Doub, F., Soil Ammonium Diffusion Constraints Contribute to Large Differences in Nitrogen Supply to Rice in the Southern United States. *Communications in Soil Science and Plant Analysis* 2011. **42**(15): p. 6.

- United States Geological Society.  
<http://volcanoes.usgs.gov/about/pglossary/tephra.php>. Updated 2008.
- Veldkamp, T., Soils and Geomorphology, 3rd Edition. *Soil Science*, 1999. **164**(3): p. 1.
- Wakelina, S., Rogersa, S., Gregga, A., Bolgerd, T., Baldocka, J., Habitat selective factors influencing the structural composition and functional capacity of microbial communities in agricultural soils. *Soil Biology and Biochemistry*, 2008. **40**(3): p. 10.
- Wang, Y.-h.Y.a.T., Fourier transform Raman spectroscopic characterization of humic substances *Vibrational Spectroscopy*, 1997. **14**(1): p. 7.
- Wiley, J. (1982). COLOR SCIENCE Concepts and Methods , Quantitative Data and Formulae ,
- Prasad S. Yarlagadda, M.R.M., John E. VanBenschoten and Ajay Kathuria, Characteristics of Heavy Metals in Contaminated Soils *Journal of Environmental Engineering*, 1995. **121**(4): p. 11.
- Yingst, R. A., Cohen, B. A., Hynek, B., Schmidt, M. E., Schrader, C., & Rodriguez, A. (2014). Acta Astronautica Testing Mars Exploration Rover-inspired operational strategies for semi-autonomous rovers on the moon II : The GeoHeuristic operational Strategies Test in Alaska. *Acta Astronautica*, 99, 24–36. doi:10.1016/j.actaastro.2014.01.019
- Zhu, C., & Burden, D. S. (2001). Mineralogical compositions of aquifer matrix as necessary initial conditions in reactive contaminant transport models.
- Zimbelman, D. R., Rye, R. O., & Breit, G. N. (2005). Origin of secondary sulfate minerals on active andesitic stratovolcanoes, 215, 37–60. doi:10.1016/j.chemgeo.2004.06.056

## Chapter 2

### 2.1- Analytical techniques used in geo-chemistry

Thermogravimetric analysis or thermal gravimetric analysis (TGA) is a method of thermal analysis in which changes in physical and chemical properties of materials are measured as a function of increasing temperature (with constant heating rate), or as a function of time (with constant temperature and/or constant mass loss). TGA can provide information about physical phenomena, such as second-order phase transitions, including vaporization, sublimation, absorption, adsorption, and desorption. Likewise, TGA can provide information about chemical phenomena including chemisorptions, desolvation (especially dehydration), decomposition, and solid-gas reactions (e.g., oxidation or reduction). TGA is commonly used to determine selected characteristics of materials that exhibit either mass loss or gain due to decomposition, oxidation, or loss of volatiles (such as moisture).

TGA has not been used in tephra analysis as a tool to identify and separate tephra from different eruptions. Indeed its published use has been as a bulk extraction technique in the analysis of magmatic gasses. Indeed it was in this context that Hugh Tuffen *et al* used TGA in their work to reconstruct paleo-ice thickness (Tuffen & Castro, 2009).

Powder X-ray diffraction is the primary tool used in the characterisation of geological mineralogy, identifying and quantifying the mineralogy of crystalline compounds in rocks, soils and particulates. XRD has been an essential technique for identifying and characterising the nature of clay minerals,

providing information which thus far had not been determined by any other method.

Powder XRD is particularly useful for identifying fine-grained minerals and mixtures or intergrowths of minerals, which may not lend themselves to analysis by other techniques (Cardell *et al*, 2009). Powder XRD can provide additional information beyond basic identification, if the sample is a mixture, PXRD data can be analyzed to determine the proportion of the different minerals present. Other information obtained can include the degree of crystallinity of the mineral(s) present, possible deviations of the minerals from their ideal compositions (presence of element substitutions and solid solutions), the structural state of the minerals (which can be used to deduce temperatures and (or) pressures of formation), and the degree of hydration for minerals that contain water in their structure. For example, in their study of a 14<sup>th</sup> century Moorish brick oven Cardell *et al* were able to quantify the composition of the bricks used to build the oven. They found that XRD quantitative analysis showed that quartz was the main component ( $\text{SiO}_2$ , 28.1%) followed by calcite ( $\text{CaCO}_3$ , 19.9%), anorthite ( $\text{CaAl}_2\text{Si}_2\text{O}_8$ , 16.8%), diopside ( $\text{CaMgSi}_2\text{O}_6$ , 7.1%), and hematite ( $\text{Fe}_2\text{O}_3$ , 4.3%). XRD does not, however, provide the quantitative compositional data obtained by the electron microprobe or the textural and qualitative compositional data obtained by the scanning electron microscope. It was also found that XRD is not an apt technique to detect minerals at very low amounts.

XRD has been used to identify mineralogy in a wide range of geological applications.

In studies of areas affected by acid mine drainage, the identification of secondary minerals and fine-grained precipitates is a critical element. Acid is generated when iron sulfide minerals, such as pyrite, weather. In their study of local drainage waters in Ligurian Apennines, Italy Dinelli *et al* discovered that they were very acidic (with a pH as low as 2.5) and were rich in dissolved metals (Fe, Al, Cu, Zn, Mn, Ni). Sediments associated with low pH water (pH <4.5) were ochreous mixtures of schwertmannite and goethite with traces of jarosite. Their chemistry was dominated by Fe and they had, compared to other sediments investigated, low concentrations of other metals. Elements derived from the alteration of the sulfide minerals can form secondary minerals or go into solution. Elements that go into solution may form mineral precipitates as conditions (temperature, acidity, solution composition) change. Mineralogical identification was carried out using a Siemens D-5000 diffractometer with spinner and secondary monochromator. Powders were pressed in the sample holder using a frosted glass in order to minimize possible preferential orientation. All samples were analysed under natural conditions, after ethylene glycol solvation, and after heating at 120 °c for about 90 min. Accurate mineralogical characterization of the precipitates and secondary minerals, together with hydrogeochemical data, help us to better understand the solubility, transport, and storage of metals (Dinelli & Tateo, 2002).

In ore genesis studies minerals form under specific ranges of temperature and pressure (Faria & Lopes, 2007). Mineralogical identification, through XRD, of ore minerals and associated minerals, including fine-grained hydrothermal alteration minerals, provides evidence used to deduce the conditions under which ore deposits formed and the conditions under which, in many cases, they were subsequently altered (Cardell *et al.*, 2009). XRD is one of the primary tools

used to evaluate the lateral and vertical variations in mineral matter and major, minor, and trace elements in coal beds (Mukhopadhyay *et al* 1998). These data are used to help determine the impact of geologic and geochemical processes on coal bed formation in order to understand and predict both inorganic and organic variability within and among minable coal beds (Henry *et al*, 2005).

XRD is routinely used in Predictive Stratigraphic Analysis where mineralogical characteristics of paleosols (ancient buried soil horizons) and underclays (the fine-grained detrital material lying immediately beneath a coal bed) have been instrumental in correlating coal zones from the Appalachian basin into the Western Interior basin (Varela *et al*, 2012). Palaeosols or fossil soils are the remains of ancient soils that may have been buried by subsequent deposits, or exposed over long time intervals without any pedogenic activity (Retallack, 2001). These soils are generally not in equilibrium with the present soil-forming factors, that is, they are soils which developed under conditions which differ from the ones now prevailing. Soil formation always depends on five 'soil-forming factors', namely, (1) parent material, (2) climate, (3) topographic relief, (4) organisms and (5) time (Jenny, 1941; Leckie *et al.*, 1989; Retallack, 2001) and therefore the precise definition of palaeosol features may provide important information on the conditions prevailing during the accumulation of ancient sequences. The mineralogy of mudstones, mottles, concretions, nodules and rhizoliths was obtained by X-ray diffraction (XRD) analysis. Clay mineralogy was determined from diffraction patterns obtained using samples that were air-dried, ethylene glycol-solvated and heated to 550 °C (Brown and Brindley, 1980). The mineralogy of sandstones was determined in thin-sections, following Gazzi–Dickinson's method (Ingersoll *et al.*, 1984), in which 400 points were assessed using a point counter (Varela, 2011). They have been the key to

quantifying the paleolatitudinal climate gradient in North America during the late Middle Pennsylvanian.

Mineralogical analysis by XRD is used in conjunction with remotely sensed data in several research investigations. Volcanic rock avalanches and debris flows are potentially deadly natural phenomena capable of destroying entire communities with little precursory warning. For example, debris flows triggered in November 1985, by a minor eruption of Nevado del Ruiz volcano, killed approximately 23,000 people in the town of Armero, Columbia (Pierson *et al*, 1990; Voight, 1990). Elsewhere, the deposits of massive-prehistoric debris flows cover areas that today are densely populated. A dramatic illustration of this is provided by the Osceola Mudflow (ca. 5600 B.P.), which blankets some 108 km<sup>2</sup> of the Puget Sound Lowland near Mount Rainier, Washington (Crandell, 1971; Scott *et al*, 1995; Vallance & Scott, 1997). Research on debris-flow initiation and hydrodynamic processes, coupled with mapping of debris-flow deposits, has enabled detailed debris-flow hazard assessments for some volcanoes (e.g., Scott *et al.*, 1995). XRD is used to identify the minerals composing clay-rich, hydrothermally altered rocks that occur on several Cascade volcanoes (Crowley *et al*, 2003). Such rocks are believed to play an important role in the generation of large landslides and mudflows. XRD is used to analyze saline minerals, including borates (Dai *et al*, n.d.). Many saline hydrate minerals produce diagnostic spectral bands, and spectral data provide a basis for mineral exploration using remote-sensing data. Analysis of airborne imaging spectrometer data can directly map mineral occurrences by detecting diagnostic spectral absorption bands, the shape and position of which are determined by individual mineral structures. A detailed knowledge of sample

mineralogy, provided at least in part by XRD, is required to understand the observed spectral absorption features.

The major use of XRD in tephra analysis is as a conformationary tool for the mineralogy of the sample after interrogation by EPMA (Kylander *et al*, 2011; Larsen *et al*, 1999). XRD's use in this manner is highlighted by J. Kirkman *et al* where the morphology of volcanic glass particles in rhyolitic and andesitic tephra of central North Island and Taranaki areas of New Zealand were studied by scanning electron microscopy. Clay fractions (< 1.0/ $\mu$ m), after separation, were dried on a water bath, lightly crushed, and 15 mg of each pressed into a disk of 5 mm diameter, which after mounting on an aluminium stub and coating with carbon, was analysed for SiO<sub>2</sub>, Al<sub>2</sub>O<sub>3</sub>, Fe<sub>2</sub>O<sub>3</sub> and CaO using an X-ray wavelength spectrometer attachment on a scanning electron microscope (SEM). The surface of a platy primary mineral, believed to be feldspar, apart from two relatively clean areas, was covered with numerous particles of two different, but hypothesised closely related types of halloysite. The presence of feldspar and halloysite as well as the absence of other crystalline minerals was confirmed by X-ray powder diffraction (Kirkman, 1975, 1980).

Further use of XRD being used after SEM analysis of tephra can be observed in the works of Janice L. Bishop *et al* (characterization of alteration products in tephra from Haleakala, Maui: a visible-infrared spectroscopy, Mössbauer spectroscopy, xrd, EMPA and TEM study), G. Kelling *et al* (Basaltic tephra: potential new resource for ceramic industry), Giorgio Gasparotto *et al* (Contribution of grain size and compositional data from the Bengal Fan sediment to the understanding of Toba volcanic event) and M. Morley *et al* (The Campanian Ignimbrite (Y5) tephra at Crvena Stijena Rockshelter, Montenegro).

XRD does have its place in the analysis of tephra samples due to its position as the “gold standard” tool in mineralogical species identification. John Andrews *et al* have used PXRD to analyse tephra glass shards from non visible tephra layers in sea-bed silt (Andrews *et al*, 2010). In their work Quantitative X-ray diffraction (PXRD) analysis of the <2 mm sediment fraction from surface (sea floor) samples, and marine sediment cores that span the last 10e12 cal ka BP, are used to describe spatial and temporal variations in non-clay mineral compositions for an area between Kangerlussuaq Trough and Scoresby Sund, East Greenland. They discovered that Bedrock consists primarily of an early Tertiary alkaline complex with high weight% of pyroxene and plagioclase. Farther inland and to the north, the bedrock is dominantly felsic with a high fraction of quartz and potassium feldspars. Residual split samples from their sediment analyses were used (Andrews *et al*, 2002). One gram of the <2mm sediment fraction was mixed with 0.111 g of ZnO, milled, and run in a D5000 S XRD instrument between 5 and 65 2-theta at a 0.02 step with a 2 s count using Cu K-alpha radiation. The down core samples were prepared and run in a quasi-random order to avoid instrumental bias. The digital data are then pasted into “RockJock v.6” (Eberl, 2003), to derive a best fit between the observed and predicted XRD patterns. A Degree-Of-Fit (DOF) statistic is calculated based on comparison of all the HKL indices from qXRD runs of standard minerals, not just the 00L as is the case for oriented clay mineral analyses. They ran all the intensity data with the same non- clay and clay mineral compositions consisting of 23 non-clay and 10 clay minerals. Replication errors were in the range of 1% (Andrews, 2009). Their final data set consisted of 753 individual qXRD runs. The average DOF was 0.111. In order to alleviate issues associated with the closed-array problem (i.e. the total wt% sums to 100, hence if one species

increases in wt%, by definition one or more species have to decrease their wt%) the data were converted to their log ratios for statistical analyses (Aitchison, 1986). Tephra, mainly from Iceland, are becoming increasingly important in interpreting leads and lags in the Holocene climate system across NW Europe. In this paper it is demonstrated that Quantitative Phase Analysis of X-ray diffractograms of the <2 mm of marine sediment fraction (ie, sand, silt and clay) from Iceland and East Greenland can detect peaks in volcanic glass concentrations (weight%) even though discrete tephra layers are not visible; thus it provides a rapid overview of the probable location of volcanic glass within sediment sequences.

P Shiffman *et al* have used PXRD to analyse glassy, basaltic tephra from the summit regions of Kilauea and Mauna Kea volcanoes on the island of Hawaii. Their studies have shown the differences between palagonitization and pedogenic weathering of glassy basaltic tephra. In the young Hawaiian tephra studied, palagonitization has occurred in response to hydrothermal activity shortly after deposition. Although some, non-hydrothermally affected tephra may eventually become palagonitized, those that have been strongly desalinated by intense pedogenic weathering will probably never become palagonitized.

Raman spectroscopy is an inelastic light scattering technique usually used to study the vibrational properties of solids, liquids, and gases. There is currently an increasing interest in Raman scattering as a probe of structure and dynamics applied to many problems in geochemistry and mineralogy, but the technique is not new to these fields: Some of the first Raman spectra obtained were for

minerals and silicate glasses (Landsberg & Mandelstam 1928, Hollaender & Williams 1931).

In Geo-chemistry Raman spectroscopy is regularly used to study Gemstone and mineral identification, fluid inclusions, mineral and phase distribution in rock sections, phase transitions and mineral behaviour under extreme conditions (Davies *et al.*,2015). Generally speaking, it has largely been used as a means to identify specific materials in a sample rather than using it to interrogate the sample as a whole e.g. Acta *et al* utilising Raman Spectroscopy to identify a green rust mineral in a sample of reductomorphic soil (Acta *et al.*, 1997).

Raman spectroscopy has been regularly used in the identification of minerals of the type found in terrestrial soil samples. Richard Herman *et al* used Raman microprobe analysis to identify individual carbonate minerals (regularly found in the majority of soil samples) such as calcite, dolomite, and aragonite. Kamnev *et al* have used Fourier transform Raman spectroscopy (FT-Raman) in the study of the bacterium *Azospirillum brasilense*. *Azospirillum* is a bacterium known to be found in soils that can form an association with various plant species to stimulate the plant growth. In this study the bacterium were extracted from the soil before the structural features of their cells were studied with FT-Raman.

The methodologies used in the identification of minerals with Raman spectroscopy vary widely due to a number of analytical problems that can be caused by these materials. For example, when analysing the mineral content in soil samples fluorescence regularly masks any sample peak signals. This fluorescence is caused by the humic content of the soil samples and to date all Raman data on whole soil samples has been heavily corrected (Source, 2005). Raman spectroscopy can itself be a problem in the analysis of minerals and as

such a systematic development is required for the analysis of any new materials. Although laser Raman spectroscopy is a non-destructive technique, samples can undergo localized heating and oxidation if the laser power is too high (what is considered “high” laser power depends on the sample). An example of these spectral changes brought about by sample heating has been described by D.L.A. de Faria *et al.* In their work Hematite ( $\alpha\text{-Fe}_2\text{O}_3$ ), magnetite ( $\text{Fe}_3\text{O}_4$ ), wüstite ( $\text{FeO}$ ), maghemite ( $\gamma\text{-Fe}_2\text{O}_3$ ), goethite ( $\alpha\text{-FeOOH}$ ), lepidocrocite ( $\gamma\text{-FeOOH}$ ) and  $\delta\text{-FeOOH}$  were studied by Raman microscopy (Faria & Vena, 1997).

Volcanic ash has been the subject of much study using Raman spectroscopy (Gage & Farwell 1981, Ishizaki & Tu 1982, Tu 1982, Zotov *et al.* 1992, Chabiron *et al.* 2004, Zajacz *et al.* 2005, Thomas & Davidson 2006, Di Muro *et al.* 2006a, 2006b), although the majority of these studies have dealt with the characterization of water content of glasses rather than their mineral content which is vital in the separation and characterization of tephra samples. The most recent research into the use of Raman spectroscopy on tephra samples has been carried out by Emily J. Bathgate *et al* and published in the Journal of Raman Spectroscopy (Bathgate *et al*, 2015). The work focuses on the identification of mineral grains from basaltic tephra erupted by the Katla volcano. The authors had success in identifying several mineral grains within the samples including pyroxene, plagioclase, olivine, hematite, magnetite, and anatase. The aim of this body of work however was not to assess the use of Raman spectroscopy for tephrochronology but to assess its use in the future missions to Mars, including the European Space Agency 2018 ExoMars Rover mission and the National Aeronautics and Space Administration 2020 Rover. Beyond the use of tephra as an analogue material for the surface of Mars there is very little further work on the use of Raman spectroscopy for tephra analysis.

Robert Barletta published a paper entitled “Raman analysis of blue ice tephra: an approach to tephrochronological dating of ice cores” in 2012. The premise of the work was that Tephra in glacial ice provides a method to obtain a depth vs chronology correlation within an ice core. Currently, core sections containing particulate must be sacrificially analysed to determine the nature of the particulate (e.g. aerosol, micrometeor, volcanic ash), and, in the case of volcanic ash, the event tied to the particle. Characterization through melting and chemical analysis precludes, de facto, its use for other purposes. Barletta investigated the use of micro-Raman spectroscopy for this purpose. Spectra were obtained on samples of Antarctic blue ice tephra from different sources along with a reference ash sample of New Mexico Bandelier Tuff. Vitreous and crystalline particles in the samples were characterized. For vitreous material, a detailed analysis of the Raman-active vibrational bands of the glass structure was found to have the potential of being a unique identifier of the source of the glass. Barletta found that the analysis of ash samples with Raman spectroscopy provides a considerable analytical challenge. This is mainly due to the fact that, unlike aerosol particulates, for example, volcanic ashes are polyphase, containing both glass and minerals. The minerals exist as free crystals (phenocrysts) and also as small crystals within the volcanic glass (microlites). In the study Raman spectra were obtained that could be attributed to glasses and feldspars within the sample. However, Barletta did experience difficulties with glass optical elements and sample fluorescence that could only be overcome with post-acquisition data processing (Barletta, 2012).

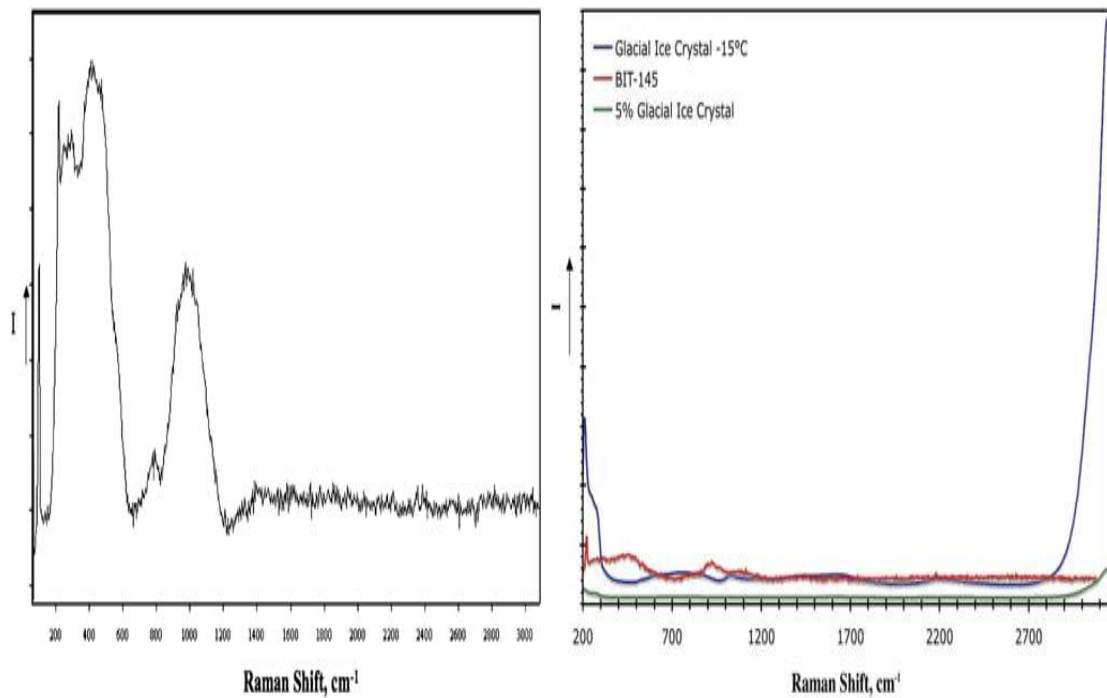


**Figure 2.1.2:** Images taken from Barletta's Paper " Raman analysis of blue ice tephra: an approach to tephrochronological dating of ice cores". On the left is the raw spectrum with the processed spectra on the right.

## 2.2- Methodology

### 2.2.1- X-ray Diffraction

Powder X-ray diffraction is the primary tool used in the characterisation of geological mineralogy, identifying and quantifying the mineralogy of crystalline compounds in rocks, soils and particulates. XRD has been an essential technique for identifying and characterising the nature of clay minerals, providing information which thus far had not been determined by any other method(<mailto:www-bgs@bgs.ac.uk>).

X-Ray diffractometers consist of three basic elements: an X-ray tube, a sample holder, and an X-ray detector.

X-Rays are generated in a cathode ray tube by heating a filament to produce electrons, accelerating the electrons toward a target by applying a voltage, and bombarding the target material with electrons. When electrons have sufficient energy to dislodge inner shell electrons of the target material, characteristic X-ray spectra are produced. These spectra consist of several components, the most common being  $K_\alpha$  and  $K_\beta$ .  $K_\alpha$  emission lines arise when an electron transitions into the “K” shell from the 2P orbital on the “L” shell.  $K_\alpha$  is typically by far the strongest X-ray spectral line for an element bombarded with energy sufficient to cause maximally intense X-ray emission.  $K_\alpha$  consists, in part, of  $K_{\alpha 1}$  and  $K_{\alpha 2}$ .  $K_{\alpha 1}$  has a slightly shorter wavelength and twice the intensity as  $K_{\alpha 2}$  (Works, Can, It, & Tell, n.d.). When the two orbitals involved in the transition are adjacent (e.g.  $2 \rightarrow 1$ ), the line is called  $\alpha$ . When the two orbitals are separated by another shell (e.g.  $3 \rightarrow 1$ ), the line is called  $\beta$ . Since the transition for  $\beta$  is bigger than for  $\alpha$ , i.e.  $\Delta E_\beta > \Delta E_\alpha$ , then  $\lambda_\beta < \lambda_\alpha$ . The specific wavelengths are characteristic of the target material (Cu, Fe, Mo, Cr). Filtering, by foils or crystal monochrometers, is required to produce monochromatic X-rays needed for diffraction.  $K_{\alpha 1}$  and  $K_{\alpha 2}$  are sufficiently close in wavelength such that a weighted average of the two is used.  $K_\beta$  emission lines arise when an electron transitions into the “K” shell from the “M” shell.  $K_\beta$  Copper is the most common target material for powder-crystal diffraction, with  $\text{Cu}K_\alpha$  radiation =  $1.5418\text{\AA}$  (Shi *et al.*, 2011). These X-rays are collimated and directed onto the sample. As the sample and detector are rotated, the intensity of the reflected X-rays are recorded. When the geometry of the incident X-rays impinging the sample satisfies the Bragg Equation, constructive interference occurs and a peak in intensity occurs (Bond, 1960). Bragg's law gives the angles for coherent and incoherent scattering for a crystal lattice. Bragg diffraction occurs when

radiation, with wavelength comparable to atomic spacings, is scattered in a specular fashion by the atoms of a crystalline system, and undergoes constructive interference. For a crystalline solid, the waves are scattered from lattice planes separated by the interplanar distance  $d$ . When the scattered waves interfere constructively, they remain in phase since the path length of each wave is equal to an integer multiple of the wavelength. The path difference between two waves undergoing interference is given by  $2d\sin\theta$ , where  $\theta$  is the scattering angle. The effect of the constructive or destructive interference intensifies because of the cumulative effect of reflection in successive crystallographic planes of the crystalline lattice. This leads to Bragg's law, which describes the condition on  $\theta$  for the constructive interference to be at its strongest:

$$2d \sin \theta = n\lambda,$$

where  $n$  is a positive integer and  $\lambda$  is the wavelength of incident wave.

A detector records and processes this X-ray signal and converts the signal to a count rate which is then output to a device such as a printer or computer monitor. A goniometer is used to maintain the angle between the x-ray source, sample and the detectors. The angle between the source and the detector is defined as  $2\theta$  and is systematically varied through the collection process, most commonly through  $5 - 70^\circ$ .

The powder X-Ray diffractograms were obtained using a Bruker AXS D8 Advance X-Ray diffractometer in Bragg-Brentano geometry. Bragg-Brentano reflection geometry is where the divergent and diffracted beams are focussed at a fixed radius from the sample position. Bragg-Brentano differs

from Debye-Scherrer geometry which is one of the oldest known powder diffraction geometries, though originally it was used only with photographic film on a "powder diffraction camera". It uses a near-parallel incident beam of X-rays with sufficient cross-section to bathe the whole powder-sample. The X-Ray source was copper with a wavelength of 0.15406 nm, a voltage of 40 kV and a filament emission of 30 mA. Data was collected at 5-60 °, 1 second per step and a step size of 0.02°/min.

## **2.2.2- Raman Spectroscopy**

### **2.2.2.1 – Molecular Vibrations**

A molecular vibration occurs when atoms in a molecule are in periodic motion while the molecule as a whole has constant translational and rotational motion. The frequency of the periodic motion is known as a vibration frequency and typical frequencies of molecular vibrations range from less than  $10^{12}$  to approximately  $10^{14}$  Hz("NIR-Chem.pdf," n.d.).

In general, a molecule with  $N$  atoms has  $3N - 6$  normal modes of vibration, but a *linear* molecule has  $3N - 5$  such modes, as rotation about its molecular axis cannot be observed("NIR-Chem.pdf," n.d.). The normal modes of vibration of polyatomic molecules are independent of each other but each normal mode will involve simultaneous vibrations of different parts of the molecule such as different chemical bonds.

If a molecule absorbs a single quantum of energy,  $E$ , corresponding to a vibrational frequency,  $\nu$ , according to the relationship;  $E = h\nu$  (where  $h$  is

Planck's constant) then that particular vibration is excited (Raman, Vogels, & Ketterle, 2001). A fundamental vibration can be excited when a molecule in its ground state absorbs one such quantum of energy. Motion in a normal vibration can be approximated by a simple harmonic vibration. In this approximation the vibrational energy is a quadratic function with respect to the atomic displacements (Arkani-hamed *et al*, 2000). This simple harmonic motion is neither driven nor damped and is described simply as an oscillation about an equilibrium position in a sinusoidal pattern. A body in a simple harmonic motion experiences a single force, given by Hooke's Law, ( $F=kx$ ) which states that force is directly proportional to the displacement,  $x$ , and points in the opposite direction (Ho *et al*, 1999).

In reality, vibrations are anharmonic and excitation of the higher overtones requires progressively less energy and eventually leads to the dissociation of the molecule as the potential energy of the molecule is more like a Morse potential (Ho *et al.*, 1999).

### **2.2.2.3 – Co-ordinates**

The coordinate of a normal vibration is a combination of *changes* in the positions of atoms in the molecule. When the vibration is excited, the coordinate changes sinusoidally with a frequency,  $\nu$ . (Guirgis *et al*, 2000).

*Internal coordinates*- a description of each atom in a molecule in terms of its atomic number, bond length, bond angle, and dihedral angle- are of the following types, illustrated with reference to the planar molecule ethene (fig 2.2.2.3.1).

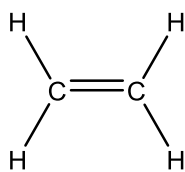


Figure 3.2.2.3.1: Structure of ethene

- Stretching: a change in the length of a bond, such as C-H or C-C
- Bending: a change in the angle between two bonds, such as the HCH angle in a methylene group
- Rocking: a change in angle between a group of atoms, such as a methylene group and the rest of the molecule.
- Wagging: a change in angle between the plane of a group of atoms, such as a methylene group and a plane through the rest of the molecule,
- Twisting: a change in the angle between the planes of two groups of atoms, such as a change in the angle between the two methylene groups.
- Out-of-plane: a change in the angle between any one of the C-H bonds and the plane defined by the remaining atoms of the ethylene molecule. Another example is in  $\text{BF}_3$  when the boron atom moves in and out of the plane of the three fluorine atoms.

In a rocking, wagging or twisting coordinate the bond lengths within the groups involved do not change, but the angles do (Kayalvizhi *et al*, 2012). Rocking is distinguished from wagging by the fact that the atoms in the group stay in the same plane (Kayalvizhi *et al.*, 2012).

In ethene there are 12 internal coordinates: 4 C-H stretching, 1 C-C stretching, 2 H-C-H bending, 2  $\text{CH}_2$  rocking, 2  $\text{CH}_2$  wagging, 1 twisting. Note that the H-C-

C angles cannot be used as internal coordinates as the angles at each carbon atom cannot all increase at the same time.

#### **2.2.2.4- Raman Spectroscopy Theory**

Raman spectroscopy is a spectroscopic technique used to study vibrational, rotational, and other low-frequency modes in a system (Ho *et al.*, 1999). It relies on inelastic scattering, or Raman scattering, of monochromatic light, usually from a laser in the visible, near infrared, or near ultraviolet range. The laser light interacts with molecular vibrations, phonons or other excitations in the system, resulting in the energy of the laser photons being shifted up or down. The shift in energy gives information about the vibrational modes in the system (Chourpa *et al.*, 2005).

As the vibrational information is specific to the individual chemical bonds in the molecule Raman spectroscopy allows the identification of different molecules in a molecular system. Solid state molecules usually have characteristic phonon modes- vibrations occurring in a rigid crystal lattice- that can help in identification. Raman spectroscopy also allows for the observation of low frequency excitations.

The Raman effect occurs when light impinges upon a molecule and interacts with the electron cloud and the bonds of that molecule ( Delhi *et al*, 2008). For the spontaneous Raman effect a photon excites the molecule from the ground state to a virtual energy state. When the molecule relaxes it emits a photon and it returns to a different rotational or vibrational state. The difference in energy between the original state and this new state leads to a shift in the frequency of

the emitted photon's away from the excitation wavelength (fig 2.2.2.4.1). The Raman effect should not be confused with absorption (as with fluorescence) where the molecule is excited to a discrete (not virtual) energy level (Journal *et al.*, 2008). If the final vibrational state of the molecule is more energetic than the initial state, then the emitted photon will be shifted to a lower frequency in order for the total energy of the system to remain balanced. This shift in frequency is designated as a Stokes shift. If the final vibrational state is less energetic than the initial state, then the emitted photon will be shifted to a higher frequency, and this is designated as an Anti-Stokes shift. Raman scattering is an example of inelastic scattering because of the energy transfer between the photons and the molecules during their interaction.

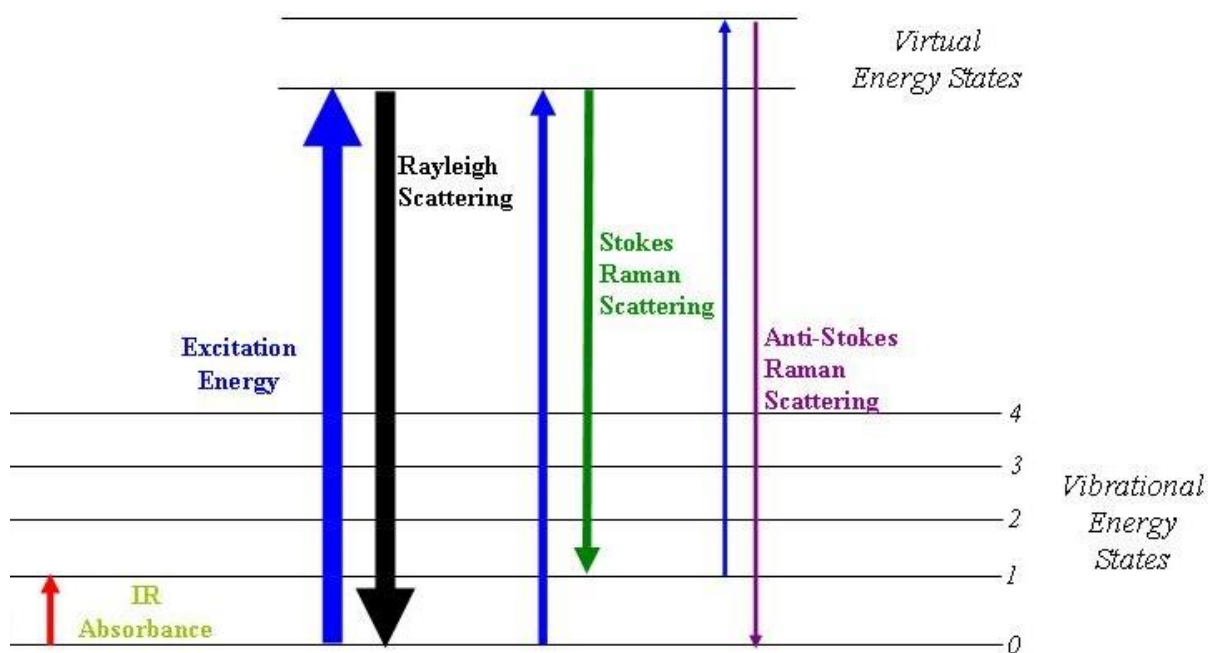


Figure 2.2.2.4.1: Energy level diagram showing the states involved in Raman signals. The line thickness is representative of the signal strength from the different transitions (Gardiner, D.J., 1989).

The energy difference between the vibrational energy states, the virtual energy levels,  $\bar{\nu}$  and the Raman shift,  $\text{cm}^{-1}$  (wave numbers) can be calculated by;

$$\bar{\nu} = \frac{1}{\lambda_{\text{incident}}} - \frac{1}{\lambda_{\text{scattered}}}$$

In this equation  $\lambda_{\text{incident}}$  is the wavelength of the incident and  $\lambda_{\text{scattered}}$  is the wavelength of the Raman scattered photons.

To be Raman active a molecule must have a change in polarizability during a molecular vibration such that;

$$\left(\frac{\partial \alpha}{\partial Q}\right) \neq 0$$

Here the normal co-ordinator of vibration is defined as Q. Polarizability of molecules related to the induced dipole moment,  $\mu$ , by the equation;

$$\mu = \alpha E.$$

the electric field strength at time t can be given by;

$$E = E_0 \cos 2\pi \nu t,$$

Where  $E_0$  is the electric field amplitude and  $\nu$  is the laser frequency. The frequency  $\nu$  can be expressed in terms of the speed of light; wavelength  $\lambda$  and c ( $3 \times 10^8 \text{ms}^{-1}$ ). Wavenumbers,  $\bar{\nu}$ , may be introduced to give;

$$\nu = \frac{c}{\lambda},$$

$$\bar{\nu} = \frac{\nu}{c} = \frac{1}{\lambda} (\text{cm}^{-1}).$$

By considering the transfer of energy from an electric field to a molecule (occurring when the two interact) an expression of the energy difference,  $\Delta E$ , can be expressed as;

$$\Delta E = h\nu = h \frac{c}{\lambda} = hc\bar{\nu}$$

In the above equation  $h$  is Planck's constant ( $6.626 \times 10^{-34}$  Js) The magnitude of  $\Delta E$  depends on the vibrational transition between  $3 \times 10^3$  and  $10^2 \text{ cm}^{-1}$ .

One of the critical components of Raman scattering is the formation of vibrational states. Interactions between the incident photon and the molecule occur practically instantaneously to the emission of the scattered photon. As a result, no real states are involved in the process. It is because of these virtual states that we can explain why the non-resonance Raman effect is not dependent on the wavelength of the excitation lasers. The spectra do not depend on the laser excitation. However, when the excitation photon's energy gets close to the energy required for transition between the two states one will observe either resonance Raman or fluorescence. Time scales for the two effects vary with a Raman transition being completed in a maximum of one picoseconds with fluorescence requiring a minimum of  $10^{-9}$  seconds.

The presence of both Raman and fluorescence resonance effects is dependent of the wavelength of the excitation laser. The difference between these two processes is related to the time scales involved, as well as with the nature of the intermediate states. In contrast with resonant fluorescence, relaxed fluorescence results from the emission of a photon from the lowest vibrational level of an excited electronic state, following a direct absorption of the photon and relaxation of the molecule from its vibrationally excited level of the

electronic state back to the lowest vibrational level of the electronic state. A fluorescence process typically requires more than  $10^{-9}$  s. In contrary, a Raman transition is completed within a picosecond or less. Fluorescence usually hides Raman features, particularly those with a low intensity, as fluorescence is far more intense than Raman scattering. Fluorescence will only occur if the excitation photon provides sufficient energy to the molecule. Therefore, one of the best methods of avoiding fluorescence is in the careful selection of the laser excitation wavelength. Near Infra-Red (NIR) lasers usually avoid the fluorescent emissions as the laser photons do not have enough energy to initiate fluorescence. Fluorescence can also be derived from impurities in a sample or its surrounding matrix. These issues can be lessened or avoided with the use of a Raman microscope by targeting the sample from which the Raman spectrum is to be recorded.

The Raman spectra were obtained using a Renishaw InVia Reflex dispersive spectrometer using the *Reflex* Raman microscope with a diode laser operating at either 785 or 633nm with a thermoelectrically cooled charged coupled device (CCD) detector. The instrument is coupled with a *Leica* microscope with 5x, 20x and 50x objective lenses. The diffraction grating of the instrument provides a spectral range of  $3200-100\text{ cm}^{-1}$  with a spectral resolution of  $2\text{ cm}^{-1}$ . The instrument was calibrated daily by recording the Raman spectrum of pure silicon (1 accumulation, 10 seconds exposure time, 100% laser power in static scan mode). When necessary drift corrections were performed to ensure the position of the silicon band was at  $520.5 \pm 0.1\text{ cm}^{-1}$ . The tephra and soil samples ( $\sim 0.1\text{ g}$ ) were spread on a glass slide and placed on the stage in the spectrometer. In total 50 spectra of each sample were collected over random sampling sites.

Spectra were obtained with an accumulation of ten scans, ten seconds exposure time, 1% laser power (approximately 50 mW at source) and 633 nm excitation as these settings had been shown to be the optimum collection parameters. All the spectra collected were taken using the 20x objective lens giving us a spectral footprint of  $5\mu\text{m}$  in diameter. The spectrometer was controlled using a PC and Renishaw WiRE 2 as the control software. The Inspector Raman <sup>TM</sup> is equipped with a diode laser operating at 785 nm, a thermoelectrically cooled CCD detector and a 25 mm focal length nose piece. The spectral range is 200 to 2000  $\text{cm}^{-1}$  with a spectral resolution of 8  $\text{cm}^{-1}$ . The output power of the laser is 120 mw at source and 35 mw at the sample. Daily calibration of the instrument is necessary and this was achieved by obtaining the Raman spectrum of polystyrene using the inbuilt calibration routine. Spectra were recorded with 5 scans and an exposure time of ten seconds per scan. The spectrometer was controlled via a portable note book PC using the instrument control software, Nu Spec <sup>TM</sup>.

#### **2.2.2.5- Fluorescence**

Raman scattering and Fluorescence emission are two competing phenomena, which have similar origins. Many materials are coloured and often, these materials absorb light in a specific part of the visible spectrum. But most of the light is transmitted or reflected; this light fraction can be observed as the complementary colour of the absorbed light (Hartschuh *et al*, 2003).

The absorbed light excites electrons of the material to higher energy levels for a very short time. Usually, the electrons return quickly to the ground state by emitting light of the same energy or wavelength, respectively. However, in some materials this return needs by far more time and is accompanied by losing part

of its energy due to internal molecular processes. As a result, light is emitted at longer wavelengths compared to the absorbed light. This process is called fluorescence (Ramos & Ruis, 2005).

If Raman scattering is excited close to an electronic transition, it sometimes coincides with fluorescence. Since fluorescence is typically much more intense, with a broad emission, already very low amounts of fluorescent species can cover the Raman scatter of a material. Without Raman scattering enhancement techniques, detection limits are in the range of about 0.1% to 1%. Since fluorescence is typically several orders of magnitude stronger than Raman scattering, already fluorescent traces of impurities below the detection limit may avoid the detection of the Raman spectrum of the major material (Ramos & Ruis, 2005).

Fluorescence can be caused by several differing factors and it is often impossible to know the cause of the fluorescence in the sample. In most cases the only option is to eliminate potential causes one by one. Common causes of fluorescence are:

- Contamination or impurities in the sample. These issues can be overcome by Photo-bleaching where irradiating the sample with intense light for a few minutes, preferably by the Raman laser, decomposes fluorescent species. This method is applicable for solid samples where fluorescence originates from impurities. One can also “purify” the samples by removing contaminants by techniques such as washing, digestion or physical removal.
- Electronic transition of the sample being close to the wavelength of the laser. Selecting an excitation wavelength far away from any electronic

transition of the sample generally avoids fluorescence. Fluorescence can be avoided most effectively by NIR FT Raman spectroscopy.

- Detection of fluorescence from outside of the laser focus. Spatial filtering by the pinhole of a confocal microscope reduces the detected fluorescence from outside of the laser focus and detects the Raman scatter within the laser focus. Applicable to relatively small intense fluorescent samples.

Fluorescence from any of the above mentioned techniques can also be removed through use of one or all of the following techniques (Ramos & Ruis, 2005).

- Spatial filtering by the pinhole of a confocal microscope reduces the detected fluorescence from outside of the laser focus and detects the Raman scatter within the laser focus. Applicable to relatively small intense fluorescent samples.
- Two Raman spectra are collected subsequently at slightly different laser wavelengths. Subtracting the spectra from one another removes the unchanged fluorescence background. The Raman spectrum is reconstructed from the difference spectrum by a mathematical procedure.
- Baseline correction where small, intense fluorescent background is removed via a mathematical procedure. Typically applied for removing a remaining low-intense fluorescent background after photo-bleaching.

By further investigating the quantum interpretation of the Raman effect, it can be shown that the power of the scattered light,  $P_s$ , is equal to the product of the

intensity of the incident photons,  $I_o$ , and a value known as the Raman cross-section,  $\sigma_R$ . It can be shown that,

$$\sigma_R \propto \frac{1}{\lambda^4},$$

where  $\lambda$  equals the wavelength of the incident photon. Therefore,

$$P_s \propto \frac{I_o}{\lambda^4}.$$

It is clear that there is a linear relationship between the power of the scattered light and the intensity of the incident light as well as a relationship between the power of the scattered light and the inverse of the wavelength to the fourth power. Therefore, by using a shorter wavelength we can increase the Raman signal (Bahram, Bro, Stedmon, Afkhami, & Roskilde, 2007).

## 2.3- References

- Acta, C., Gi, M. R., Bourrii, G., Ceclex, R., Physique, C., Poincar, C. H. (1997). SCIENTIFIC COMMENT Identification of a green rust mineral in a reductomorphic soil by Mossbauer and Raman spectroscopies, *61*(5), 1107–1111.
- Andrews, J. T., Jennings, A. E., Coleman, G. C., & Eberl, D. D. (2010). Holocene variations in mineral and grain-size composition along the East Greenland glaciated margin ( ca 67 e70 N ): Local versus long-distance sediment transport. *Quaternary Science Reviews*, *29*(19-20), 2619–2632. doi:10.1016/j.quascirev.2010.06.001
- Arkani-hamed, N., Dimopoulos, S., Sundrum, R., & Kaloper, N. (2000). A small cosmological constant from a large extra dimension, (May), 193–199.
- Bahram, M., Bro, R., Stedmon, C., Afkhami, A., & Roskilde, D.-. (2007). Handling of Rayleigh and Raman scatter for PARAFAC modeling of fluorescence data using interpolation, (January), 99–105. doi:10.1002/cem
- Barletta, R. E. (2012). Raman analysis of blue ice tephra: an approach to tephrochronological dating of ice cores. *Antarctic Science*, *24*(02), 202–208. doi:10.1017/S0954102011000885
- Bathgate, E., Maynard-Casely, E., Caprarelli, G., Xiao, L., Stuart, B., Smith, K., & Pogson, R. (2015). Raman, FTIR and XRD study of Icelandic tephra minerals: implications for Mars. *Journal of Raman Spectroscopy*, *46*, 855.
- Bond, B. Y. W. L. (1960). Precision Lattice Constant Determination, *Acta Crystallographica.*, 10–11.
- Cardell, C., Guerra, I., Romero-pastor, J., Cultrone, G., & Rodriguez-navarro, A. (2009). Micro-X-Ray Diffraction , Scanning Electron Microscopy-Based Mineral Maps , and Diffuse Reflectance Infrared Fourier Transform Spectroscopy to Characterize Archeological Artifacts, *81*(2), 604–611.
- Chourpa, I., Douziech-Eyrolles, L., Ngaboni-Okassa, L., Fouquenot, J.-F., Cohen-Jonathan, S., Soucé, M., Marchais, H., *et al.* (2005). Molecular composition of iron oxide nanoparticles, precursors for magnetic drug targeting, as characterized by confocal Raman microspectroscopy. *The Analyst*, *130*(10), 1395–403. doi:10.1039/b419004a
- Crowley, J. K., Hubbard, B. E., & Mars, J. C. (2003). Analysis of potential debris flow source areas on Mount Shasta , California , by using airborne and satellite remote sensing data, *87*, 345–358. doi:10.1016/j.rse.2003.08.003
- Dai, H., Gong, J., Kim, H., & Lee, D. (2002). A novel method for preparing ultra-fine alumina-borate oxide fibres via an electrospinning technique, *Nanotechnology*, *674-677*.

- Dinelli, E., & Tateo, F. (2002). Different types of fine-grained sediments associated with acid mine drainage in the Libiola Fe – Cu mine area ( Ligurian Apennines , Italy ), *Applied Geochemistry*, 17, 1081–1092.
- Faria, D. L. a., & Lopes, F. N. (2007). Heated goethite and natural hematite: Can Raman spectroscopy be used to differentiate them? *Vibrational Spectroscopy*, 45(2), 117–121. doi:10.1016/j.vibspec.2007.07.003
- Faria, D. L. A. D., & Vena, S. (1997). Raman Microspectroscopy of Some Iron Oxides and Oxyhydroxides, *Journal of Raman Spectroscopy*, 28(February), 873–878.
- Gardiner, D.J. (1989). Practical Raman spectroscopy. Springer-Verlag. ISBN 978-0-387-50254-0.
- Guirgis, G. A., Zhu, X., Yu, Z., & Durig, J. R. (2000). Raman and Infrared Spectra , Conformational Stability , Normal Coordinate Analysis , Vibrational Assignment , and ab Initio Calculations of 3 , 3-Difluorobutene, *Journal of Physical Chemistry*, 4383–4393.
- Hartschuh, A., Pedrosa, H. N., & Novotny, L. (2003). Simultaneous Fluorescence and Raman Scattering from Single Carbon Nanotubes, *Science*, 301(September), 1354–1357.
- Henry, J., County, K., Brownfield, M. E., Affolter, R. H., Cathcart, J. D., Johnson, S. Y., Brownfield, I. K., *et al.* (2005). Geologic setting and characterization of coals and the modes of occurrence of selected elements from the Franklin coal zone , Puget, 63, 247–275. doi:10.1016/j.coal.2005.03.021
- Ho, R. Y. N., Roelfes, G., Feringa, B. L., Que, L., & Tpa, L. (1999). Raman Evidence for a Weakened O-O Bond in Mononuclear Low-Spin Iron ( III ) 264–265.
- Delhi, T. (2008). Characterization Techniques for nanotechnology Applications in Textiles, *Journal Fibretextile & Studies*, (August 2015).
- Kayalvizhi, R., Vidhya, M. S., Ferdinand, A. C., & Meenakshi, G. (2012). Spectroscopic Analysis of Expired and Pure Melmet, 11(4), 427–435.
- Kylander, M. E., Lind, E. M., Wastegård, S., & Löwemark, L. (2011). Recommendations for using XRF core scanning as a tool in tephrochronology, (June). doi:10.1177/0959683611423688
- Larsen, G., Dugmore, a., & Newton, a. (1999). Geochemistry of historical-age silicic tephros in Iceland. *The Holocene*, 9(4), 463–471. doi:10.1191/095968399669624108
- Mukhopadhyay, P. K., Goodarzi, F., & Crandlemire, A. L. (1998). Comparison of coal composition and elemental distribution in selected seams of the Sydney and Stellarton Basins , Nova Scotia , Eastern Canada..

- Raman, C., Vogels, J. M., & Ketterle, W. (2001). Observation of Vortex Lattices in Bose-Einstein Condensates, *292*(April), 476–480.
- Ramos, P. M., & Ruis, I. (2005). Noise and background removal in Raman spectra, (June), 848–856. doi:10.1002/jrs.1370
- Shi, J. H., Li, Z. Q., Zhang, D. W., Liu, Q. Q., Sun, Z., & Huang, S. M. (2011). Fabrication of Cu ( In , Ga ) Se 2 thin films by sputtering from a single quaternary chalcogenide target, (May 2010), 160–164. doi:10.1002/pip.1001
- Source, S. L. (2005). Spatial Distribution and Speciation of Lead around Corroding Bullets in a Shooting Range Soil Studied by Micro-X-ray Fluorescence and Absorption Spectroscopy, *39*(13), 4808–4815.
- Tuffen, H., & Castro, J. M. (2009). The emplacement of an obsidian dyke through thin ice: *Journal of Volcanology and Geothermal Research*, *185*(4), 352–366. doi:10.1016/j.jvolgeores.2008.10.021
- Varela, A. N., Veiga, G. D., & Poiré, D. G. (2012). Sequence stratigraphic analysis of Cenomanian greenhouse palaeosols: A case study from southern Patagonia , Argentina. *Sedimentary Geology*, *271-272*, 67–82. doi:10.1016/j.sedgeo.2012.06.006

## Chapter 3

### 3.1- Introduction

Soil samples have been traditionally analysed via examinations of colour, texture and mineral content by physical or chemical methods. These methods leave any organic or water-soluble fractions unexamined (Ruffell & McKinley, 2005). A range of analytical techniques has been applied in this area in order to study both the organic and inorganic soil fractions. This study uses Raman spectroscopy in order to assess both the mineralogical and the water-soluble organic fractions in soil samples. Soil samples were collected from both urban and rural environments comprising the city of Bradford in England and an arable farming district in Lincolnshire. A further test of the methods was carried out on soil samples collected along the route of the A65 road between Bradford and Kirkby Lonsdale, a route that crosses over several bedrock types and contains both urban and rural locations. This study demonstrates how, with the use of oxidative preparation methods, Raman spectroscopy can be used to successfully discriminate between soil types using mineralogy as well as the organic and water-soluble fractions of soils.

Forensic soil comparisons use a physical and microscopic comparison of texture, colour, mineralogical content density gradient, microbiology and Palynology (Cengiz *et al*, 2004). Often, polarized light microscopy will then be used in aiding additional mineral identification whilst a laser granulometer will be used to measure particle size and distribution. X-Ray fluorescence and diffraction approaches are routinely used to confirm the mineralogical composition of the sample (Ruffell & McKinley, 2005). These methods are

useful tools for the discrimination of soil samples, but have one major disadvantage in that they are unable to interrogate amorphous fractions, particularly the complex organic fractions of soil. In principle, Raman spectroscopy may be able to provide further discrimination of the sample by providing information about the organic content (humic material, and other organic components), which are largely neglected by the current methods.

### 3.1.1 – Sample Collection

Preliminary soil samples were collected locally from around the university campus (Figure 3.1.1.1). These sample points were chosen to offer a wide range of soil uses from a confined area of known bedrock. At each location three samples of the surface soil were collected (approximately 50g each) and agglomerated to form one sample of approximately 150g per collection point.



Figure 3.4.1.1: Sample collection points form locations around the University of Bradford campus.

Secondary soil samples were collected from two distinctly different locations both in a geological and an environmental context. At each location ten soil samples were collected and combined to achieve two aggregated samples, one from each location.

The first set of samples was collected from around the city of Bradford, United Kingdom (Figure 3.1.1.2), a densely populated area with a rich industrial history. The geology of this sampling area comprises Carboniferous sand, gritstone and some coal measures overlain by glacial till of Devensian age.

The second set of samples was collected from an arable farming district of Lincolnshire, United Kingdom (Figure 3.1.1.3), from a twenty mile radius surrounding the village of Bitchfield. The geology of this sampling area is dominated by the Jurassic Oxford Clay formation overlain by Mid-Pleistocene diamicton and till.

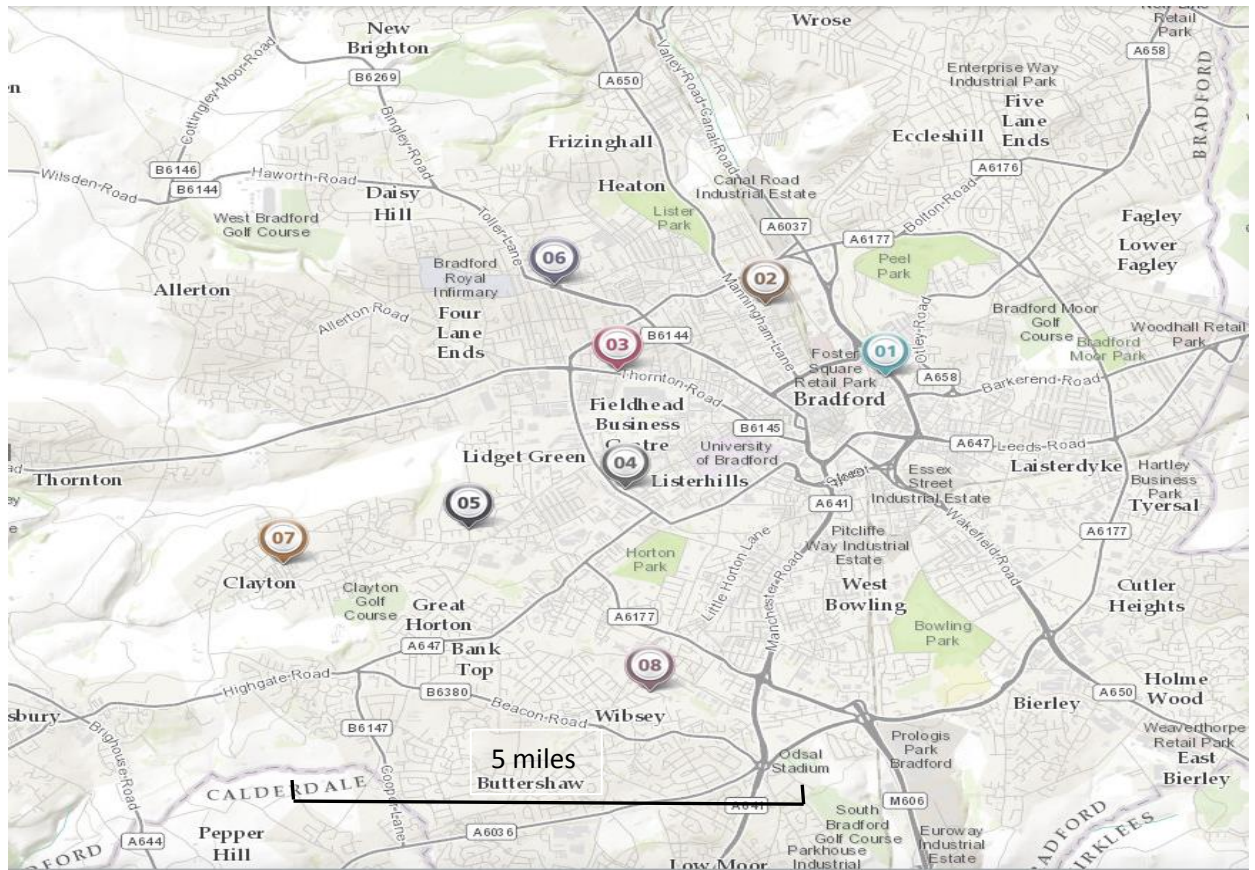


Figure 3.1.1.5: Sample collection points from locations around the city of Bradford, West Yorkshire.

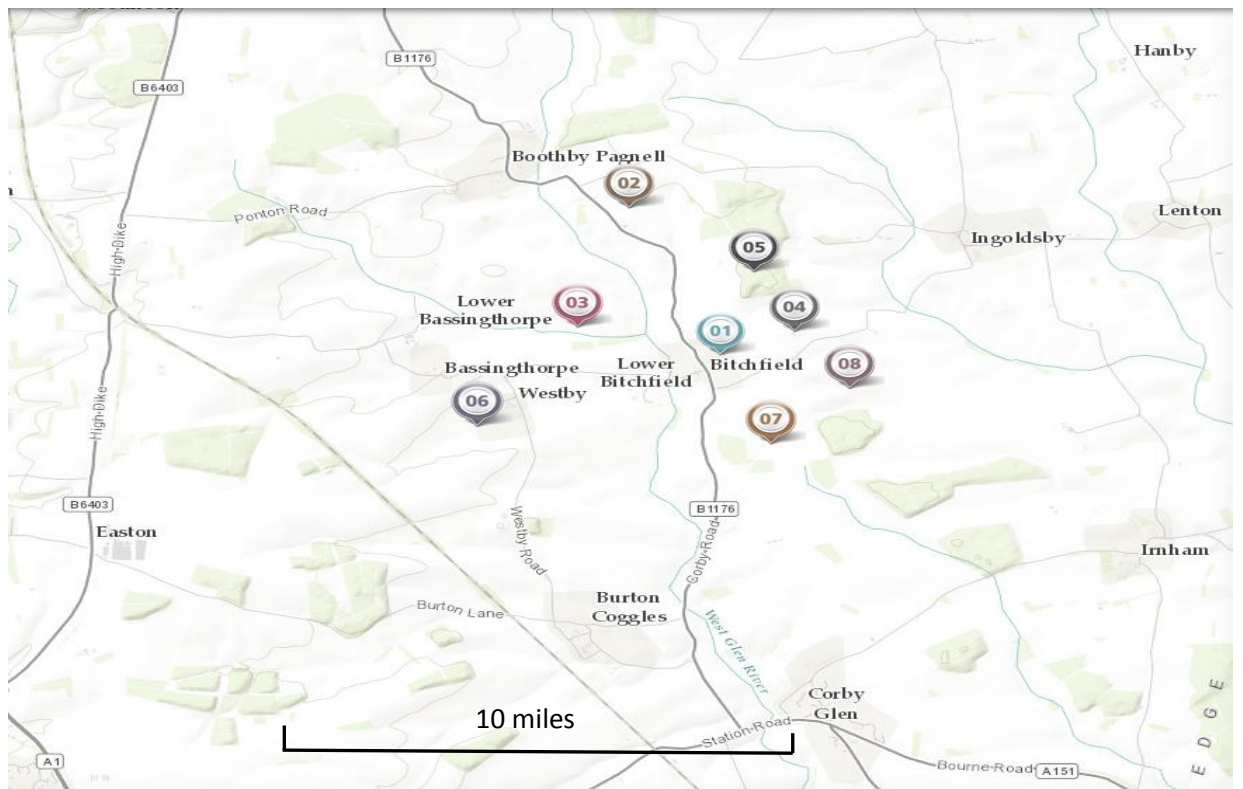
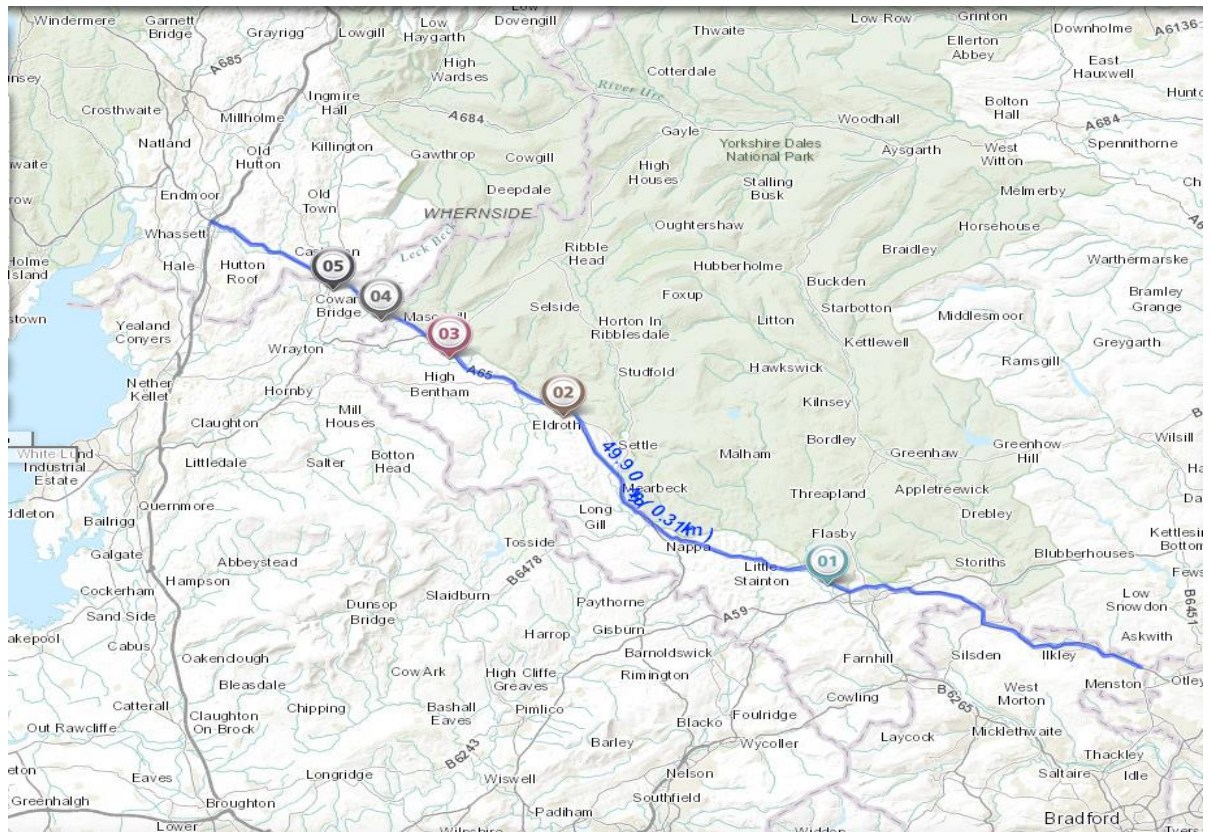


Figure 6.1.1.3: Sample collection points from the farming areas around Bitchfield, Lincolnshire.

A final, third set of soil samples was collected along the route of the A65 road between Bradford and Cumbria with the sample collection points starting outside of Skipton and concluding at Kirkby Lonsdale (Figure 3.1.1.4). This route travels over the Laurentian Basement covering the Midland Valley Proterozoic Crystalline basement and the Sothern Uplands Proterozoic Crystalline basement. Along this route and overlying the bedrock types are a variety of soil types. Mafic Lava, Felsic Lava, Millstone grit and siltstone are all types that were expected to be collected over this area. At each sampling point five samples were collected. Commercial farming fields line the whole of the sampling route along the A65. At each collection point samples were collected from each of the four corners of the field and a final, fifth, sample collected from the center of the field. The reason for these sampling points was to introduce an element of randomness to the samples, to ensure that the samples were representative of the soils found at those locations. These samples were later combined to form one aggregated sample.



**Figure 3.1.1.4: Sample collection points along the route of the A65, between Bradford and Kirkby Lonsdale. The highlighted route is 49.9 miles from start to finish.**

### **3.2.2 – Method of Sample Collection**

All of the samples were collected in a pitman tin before being placed inside a polythene bag and refrigerated. A pitman tin is a metal ring, six inches in diameter and two inches in height. It is pushed into the soil and then removed bringing with it a disk of soil thus ensuring a regular sample size from each of the locations. At each of the locations the grid position was taken using a handheld GPS and photographs taken to enable easy identification of the sight if further samples were to become necessary.

### **3.2 – Instrumentation**

### **3.2.1 - Renishaw InVia Reflex dispersive spectrometer**

Raman spectra were obtained using a Renishaw InVia Reflex Raman microscope with a diode laser operating at 785 nm and a thermoelectrically cooled charge coupled device (CCD) detector. The instrument was coupled with a Leica microscope with a 50x, 20x and 5x microscope objective providing a spectral footprint of approximately 2 – 5 microns. The diffraction grating (1200 lines / mm) provides a spectral range of 100 – 3200  $\text{cm}^{-1}$  with a spectral resolution of 2  $\text{cm}^{-1}$ .

Daily calibration of the instrument was achieved by recording Raman spectrum of silicon with 1 accumulation and 10 seconds exposure in static mode. When necessary an offset correction was performed to ensure that the position of the silicon band was at  $520 \pm 0.1 \text{ cm}^{-1}$ . The spectra were obtained with a 20x lens. Spectra were obtained with an accumulation of one scan, ten seconds exposure time and 50% laser power (approximately 50 mW at source). The spectrometer was controlled by a PC using the instrument control software, Renishaw WiRE 2<sup>TM</sup>.

### **3.2.2 – Delta Nu Inspector Raman FSX**

The Inspector Raman<sup>TM</sup> is equipped with a diode laser operating at 785 nm, a thermoelectrically cooled CCD detector and a 25 mm focal length nose piece. The spectral range is 200 to 2000  $\text{cm}^{-1}$  with a spectral resolution of 8  $\text{cm}^{-1}$ . The output power of the laser is 120 mw at source and 35 mw at the sample. Daily calibration of the instrument is necessary and this was achieved by obtaining the Raman spectrum of polystyrene using the inbuilt calibration routine. Spectra were recorded with 5 scans and an exposure time of ten seconds per scan. The

spectrometer was controlled via a portable note book PC using the instrument control software, Nu Spec™.

### **3.2.3 - Bruker AXS D8 Advance X-Ray Diffractometer**

Powder X-ray diffractograms were obtained using a Bruker AXS D8 Advance X-ray diffractometer in Bragg-Brentano geometry. The X-ray source was copper with a wavelength of 0.15406 nm, a voltage of 40 kV and a filament emission of 30 mA. Data was collected at 5-60 °, 1 second per step and a step size of 0.02.

### **3.3 – Data Analysis**

Raman spectra from all instruments were exported in the Galactic \*.SPC format. Spectra were then compared using Grams AI (version 8.0, Thermo Electron Corp, Waltham, MA, USA); some of the Raman spectra were subjected to spectral smoothing and baseline corrections.

All X-ray diffractograms were viewed and compared using the Diffrac+ EVA software. The diffractograms were not subjected to any data manipulation or processing techniques and are reported as collected.

### **3.4 – Soil sample analysis**

#### **3.4.1- Preliminary study on the soils collected from the University of Bradford Campus**

A preliminary study into the effectiveness of Raman spectroscopy on soil samples was carried out with the dried samples after the first stage of sample collection (see 3.1.1, paragraphs 1 and 2). Initially a small fraction of the dried

sample was placed on a microscope slide and interrogated via Raman spectroscopy. A total of five different samples were run in this fashion with a total of 100 spectra collected (20 for each sample). The results showed that the organic fraction of the soil was too high and caused a large amount of fluorescence, which overpowered any signal from the other minerals in the soil sample (Figure 3.4.1.1 ).

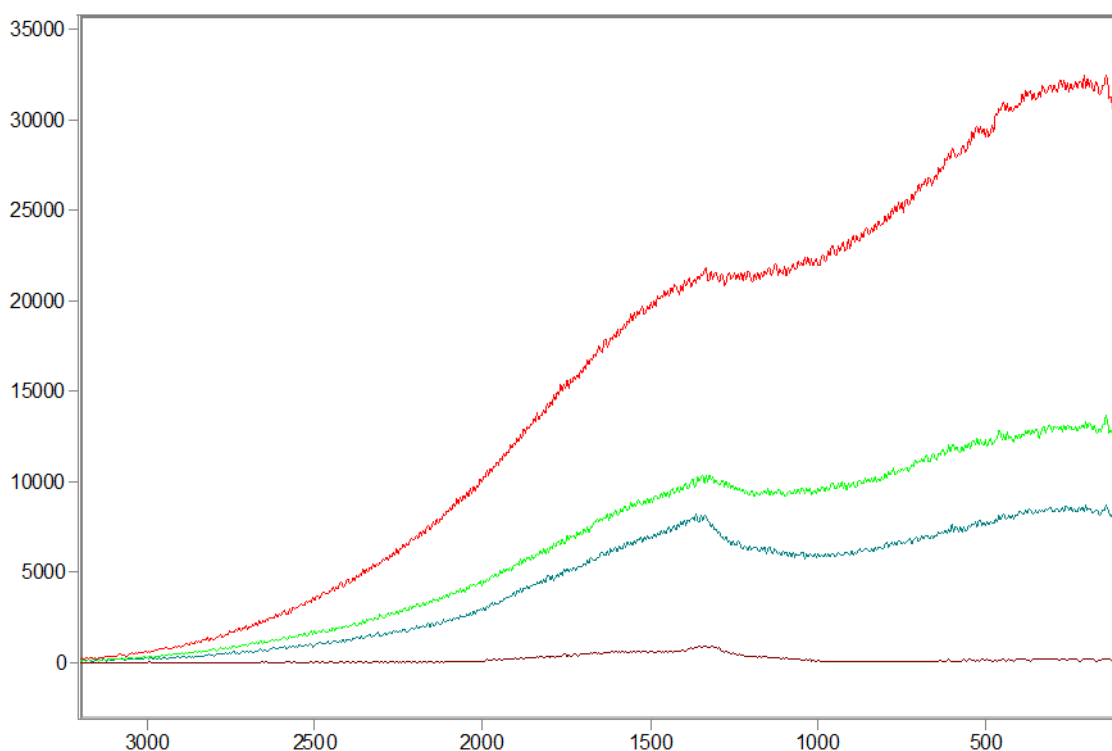


**Figure 3.4.1.1: Examples of the fluorescence observed in the preliminary study of the soil samples collected from locations around Bradford University.**

### **3.4.2 – Method development of the oxidative sample preparation to reduce sample fluorescence.**

The reason that very little work has been carried out on soil utilising Raman spectroscopy is due to the fluorescence of soil samples (Ewald *et al*, 1983).

Currently the signature peaks from the soil components are masked by large fluorescent backgrounds caused by the humic content in the soil. In principle, Raman shifts can provide information on both mineralogical and organic (humic) materials. Systematic development of sample preparation is thus necessary in order to limit sample fluorescence.

Hydrogen peroxide is commonly used in the treatment of soils in order to remove contaminants such as unsaturated aliphatic and aromatic compounds (Remediation, 2011). The interactions between hydrogen peroxide and organic soil material have been well studied (Goi *et al*, 2009). Organic soil material can be split into two fractions- particulate organic matter (POM) and non-particulate organic matter (NPOM). Studies have shown that the total destruction of organic material is directly proportional to the dosage of hydrogen peroxide used. It has also been shown that the majority of the destruction occurs in the NPOM fraction (Bissey, 2006).

In order to reduce the amount of fluorescence within the soil samples some of the organic material (humic and fulvic acids as well as any organic contaminants) had to be removed. This is routinely carried out using hydrogen peroxide. The following experiments were carried out to ensure that not all of the organic material was removed- just enough to ensure that the fluorescence caused by organic material did not mask the Raman signals (fig 3.4.2.5).

In order to assess the correct amount of hydrogen peroxide required for each reaction a sample of soil was collected from Dirkhill Road, Bradford (BD7 1QA) and treated as described below. This soil was of a peaty type, suggestive that there is a large organic fraction (TGA confirmed an organic fraction of approximately 24%) and was used solely for the determination of hydrogen

peroxide concentration and amount. Initially, a Raman spectrum was recorded for this sample. A large amount of fluorescence was observed and the spectrum yielded no useful information. This spectrum became the control for which improvements in spectral quality were compared.

The hydrogen peroxide used was purchased from Sigma Aldrich, product code 516813. It was bought in 500 ml bottles at 50% H<sub>2</sub>O<sub>2</sub> in H<sub>2</sub>O.

Initially, 2 g of soil was placed in each of 5 round bottomed flasks with 2 cm<sup>3</sup> of H<sub>2</sub>O<sub>2</sub> 50% in water. These flasks were then heated at 30, 40, 50, 60 and 70 °C for a total of one hour. Excess peroxide was removed by washing with an excess of distilled water and the soil samples dried in an oven at 60°C for one hour. The samples were re-weighed after drying and Raman spectra were collected for each sample (Table 3.4.2.1).

In the second stage of the development process it was decided that the concentrations of peroxide were too high and destroying too much of the organic residues. This was based on the final weights of the sample showing approximately 50% of the organic materials had been removed (based on TGA data). A range of solutions were made up ranging from 0% to 50% H<sub>2</sub>O<sub>2</sub> (Table 3.4.2.2).

Hydrogen peroxide solution (50 cm<sup>3</sup>) was added to the soil sample (2 g) and refluxed until the reaction reached 50 °C, the end point of the reaction was judged when the effervescence had ceased. The peroxide was washed with an excess of distilled water and the soil samples dried in an oven at 60 °C for one hour. The samples were re-weighed after drying and Raman spectra were collected for each sample (Table 3.4.2.3 and Figure 3.4.2.1).

**Table 3.4.2.1: This table demonstrates the mass loss of the samples, collected from the University of Bradford campus, as the temperature of reflux is increased.**

Sample Number	Starting Weight (g)	Temperature (°C)	Final Weight (g)
1	2.00	30	1.821
2	2.00	40	1.796
3	2.00	50	1.793
4	2.00	60	1.776
5	2.00	70	1.785

**Table 3.4.2.2: This table shows the range of H<sub>2</sub>O<sub>2</sub> solutions made up in order to try and reduce the total amount of organic material lost through reflux.**

Solution Number	Amount H <sub>2</sub> O (cm <sup>3</sup> )	Amount H <sub>2</sub> O <sub>2</sub> (cm <sup>3</sup> )	Overall Concentration H <sub>2</sub> O <sub>2</sub> (%)
1	50	0	0
2	40	10	10
3	30	20	20
4	20	30	30
5	10	40	40
6	0	50	50

**Table 3.4.2.3: Sample mass loss after being refluxed at 50°C with a 25% H<sub>2</sub>O<sub>2</sub> solution.**

Sample Number	Starting Weight (g)	Temperature (°C)	Final Weight (g)
1	2.000	50	1.921
2	2.000	50	1.819
3	2.000	50	1.814
4	2.000	50	1.796
5	2.000	50	1.781

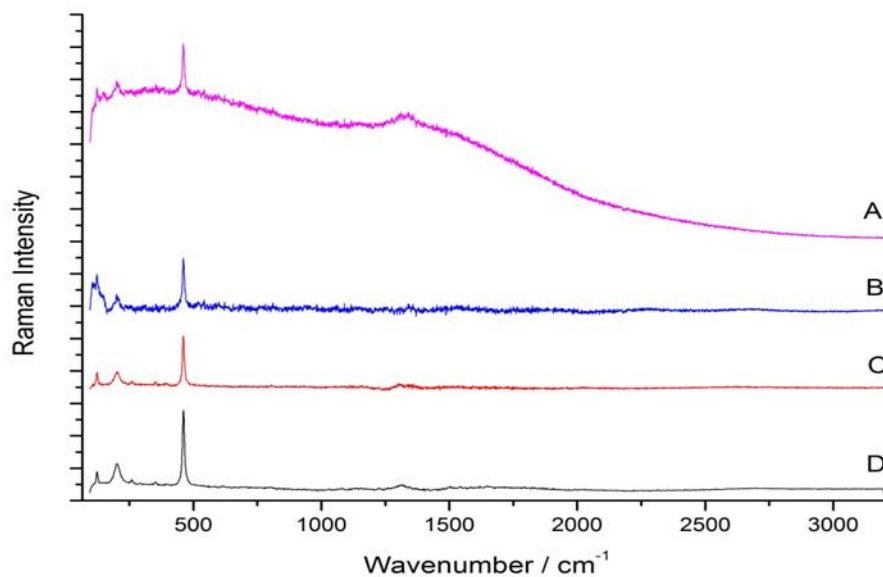


**Figure 3.4.2.1: This stacked plot demonstrates the improvements gained in the noise to signal ratio and the fluorescence level in the spectra of quartz with increasing strength of hydrogen peroxide. A shows the spectra untreated, B has been treated with a 10% H<sub>2</sub>O<sub>2</sub> solution, C with a 25% H<sub>2</sub>O<sub>2</sub> solution and D with a 50% H<sub>2</sub>O<sub>2</sub> solution.**

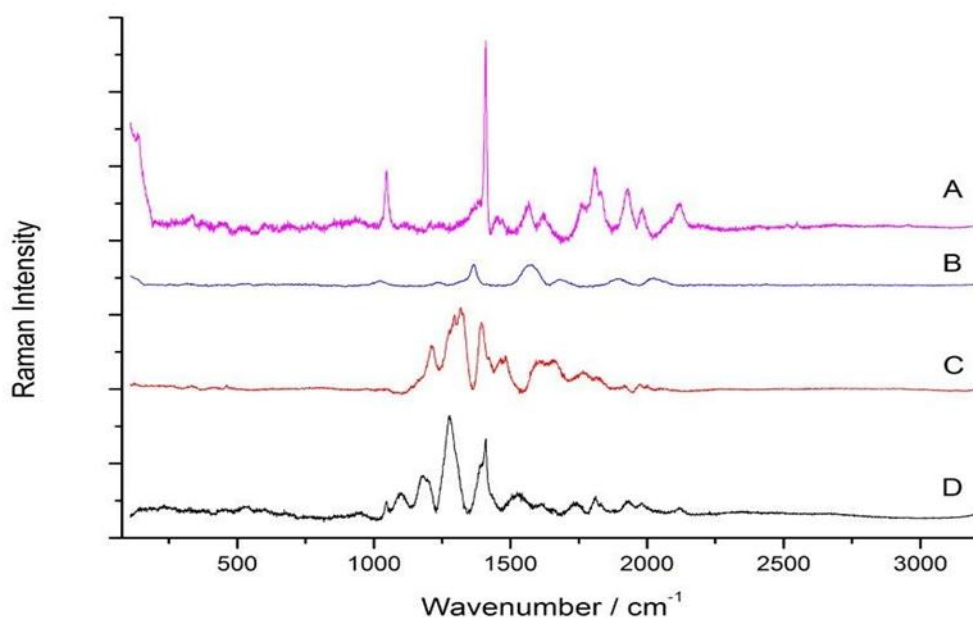


**Figure 3.4.2.2: Stacked plot demonstrating the spectra that can be observed of the humic/ fulvic fraction of the soil after the oxidative process. A shows the spectra untreated, B has been treated with a 10% H<sub>2</sub>O<sub>2</sub> solution, C with a 25% H<sub>2</sub>O<sub>2</sub> solution and D with a 50% H<sub>2</sub>O<sub>2</sub> solution.**

### **3.4.3 – Sample Preparation**

The soil samples collected from each individual location were combined to form one aggregated sample representative of the soil conditions from the different areas. All the samples were oven dried at a temperature of 60 °C for a total of three hours to remove all the moisture. These conditions were confirmed to be adequate for the removal of sample moisture by thermogravimetric analysis.

Once dried the samples were dry sieved through a mesh of 60 µm and stored in sealed glass jars in an air tight container.

A portion (2 g) of all the soil samples were placed in a round bottomed flask with hydrogen peroxide (50 cm<sup>3</sup>, 25%) and brought to reflux at 50 °C. After the effervescence from the solid surface had ceased the reflux was terminated (~30-50 mins). The resulting slurry was oven dried at 60 °C for between two and three days until dry. The dry sample was then ground ready for analysis

by Raman and PXRD.

#### **3.4.4 – Sample Analysis**

The Raman spectra were obtained using the Renishaw InVia Reflex dispersive spectrometer. The soil sample (0.1 g) was placed on a glass microscope slide and placed on the stage in the spectrometer. The spectra were obtained with a 20x lens. Spectra were obtained with an accumulation of one scan, ten seconds exposure time and 50% laser power (approximately 50 mW at source) as this had been shown to be adequate collection parameters. The instrument was calibrated by recording the Raman spectrum of silicon (1 accumulation, 10 seconds exposure time, 100% laser power in static scan mode).

#### **3.5- Results and discussion**

Due to sample fluorescence Raman spectra of soil samples have never been recorded (see chapter 1). Instead, a multi proxy method is used for the analysis of soil samples. However, Raman spectroscopy has much scope in this area and was investigated as a technique for use in soil sample analysis. In order to advance this theory multiple steps were taken. Firstly, the effect of sample fluorescence had to be measured and observed. This was carried out by the analysis of soil samples from the campus of the University of Bradford with Raman spectroscopy. After observation of these results a systematic development of an oxidative sample preparation method was developed with the aim of removing enough organic material to obtain reasonable spectra whilst retaining a representative proportion of the organic material for observation. As a result of this process, the sample loses between 10 and

14% of mass depending on its initial organic content. Results have shown that this reduces Raman fluorescence and the signal to noise ratio sufficiently enough to observe the constituent peaks whilst still allowing organic peaks to be observed.

Once the oxidative sample preparation method had been developed it was tested on soil samples from distinctly different geographical and geological locations. The aims of this study were twofold. The primary aim was to test the effectiveness of the oxidative treatment on two distinctly different soil types. The soils had different concentrations of organic material so this was a good test to ensure that the process worked across a whole range of different organic concentrations. The secondary aim was to discover whether or not Raman spectroscopy was capable of discriminating between soils from different locations.

In the final study five soil samples were collected from similar geographical locations along the route of the A65 from Skipton to Kirkby Lonsdale. Although geographically similar the locations are geologically distinct due to their bedrock. The aim of this study was to provide a more rigorous evaluation of the discriminatory value of Raman spectroscopy on soil samples.

In all three studies the samples were also analysed with powder X-ray diffraction. The purpose of this analysis was to confirm the mineral species identified by Raman spectroscopy. The samples were also subjected to PXRD after treatment with hydrogen peroxide. This was to ensure that the oxidative treatment did not affect the mineralogical composition of the soil

samples.

### **3.6.1 – Preliminary Study**

The samples collected for the preliminary study were collected from the campus of the University of Bradford. The samples were collected from distinct sites of the campus that may have provided different soil conditions. Samples were collected from land that has been left as a nature reserve, planted areas regularly maintained with the additions of peat and scarred areas of land showing traces of Bradford clay in the soil streaks.

In the preliminary study the soil samples were untreated. Therefore the analysis was carried out on the whole soil fraction as it would normally be found. Two-hundred different spectra were recorded from random locations across the mounted sample with poor results. No useful information about the minerals or the organic material was identified in the samples due to high fluorescence.

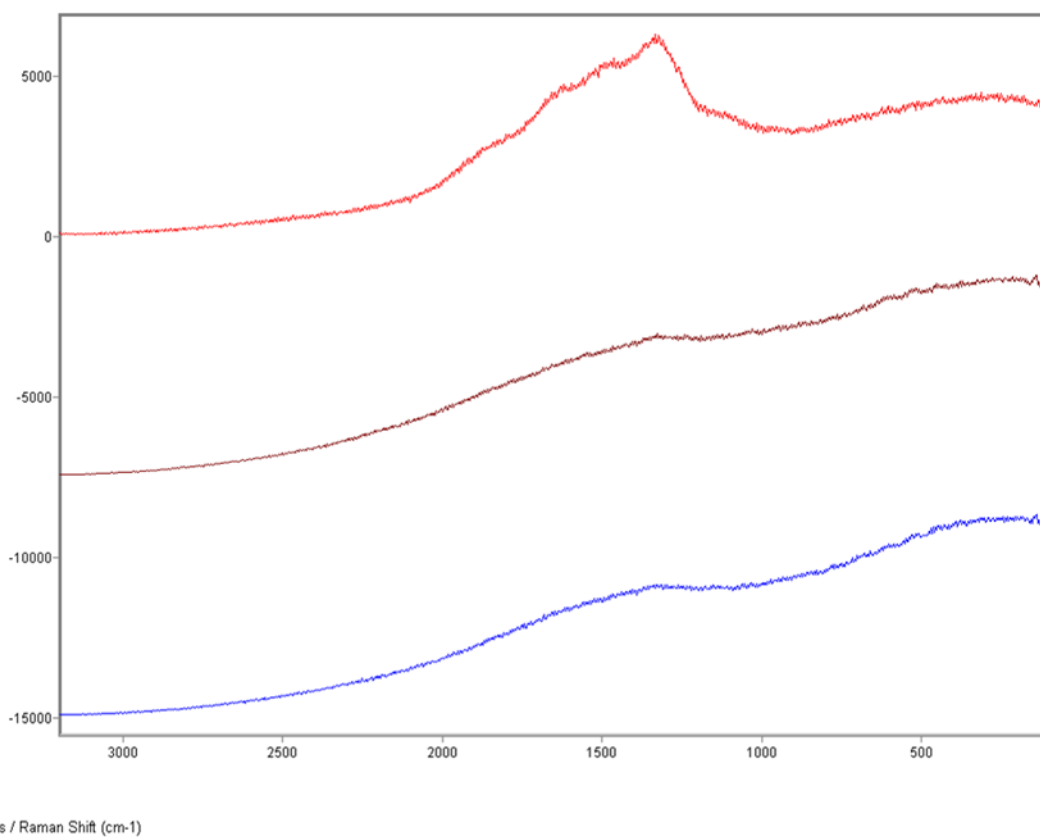
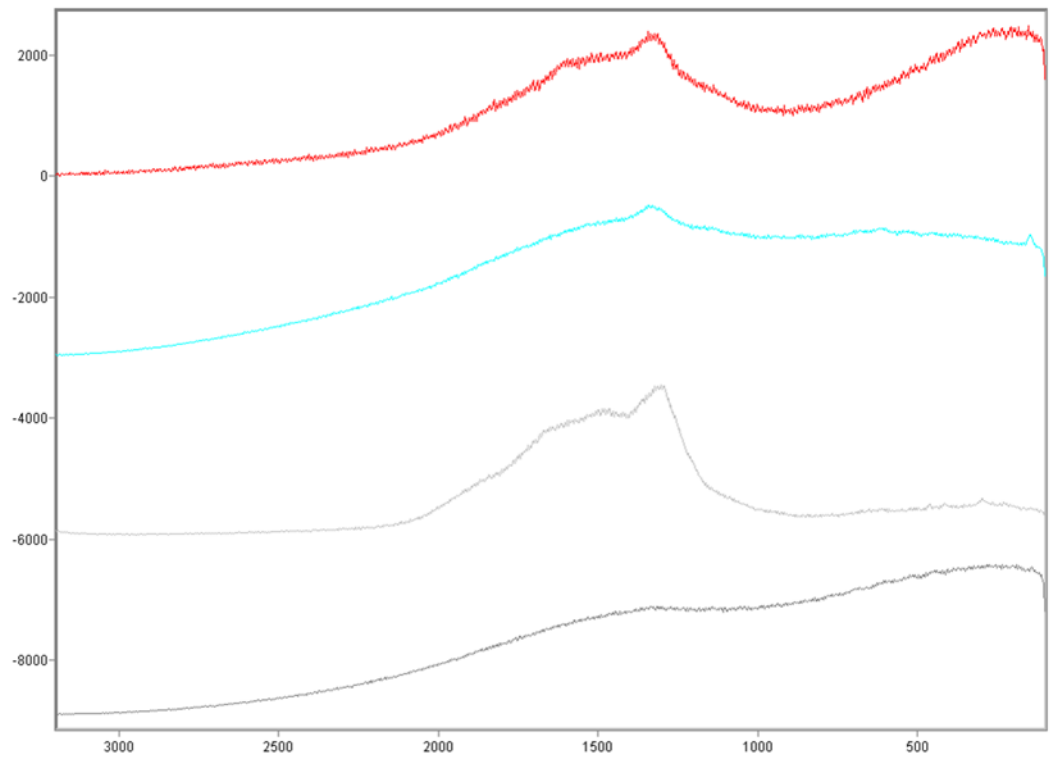


**Figure 3.6.1.1: Stacked plot of preliminary interrogation of soil samples (taken from the University of Bradford campus) with Raman spectroscopy.**

Figures 3.6.1.1 and 3.6.1.2 show a selection of representative spectra from the preliminary study. They demonstrate the problems associated with the study of soil samples utilising Raman spectroscopy, with high fluorescence obscuring any peaks in the Raman spectra. One may also observe the large humps between 1000 and 2000 cm<sup>-1</sup>. These are caused by glass flair, a phenomenon associated with Raman instrumentation with an unknown cause.



Counts / Raman Shift (cm-1)

Stacked X-Zoom CURSOR

**Figure 3.6.1.2: Stacked plot of preliminary interrogation of soil samples (taken from the University of Bradford campus) with Raman spectroscopy**

Figure 3.6.1.3 shows the powder X-ray diffractogram of the soil sample used in this preliminary study. Several mineral species can be seen in this diffractogram and these species and their corresponding positions are displayed in table 3.6.1.1.

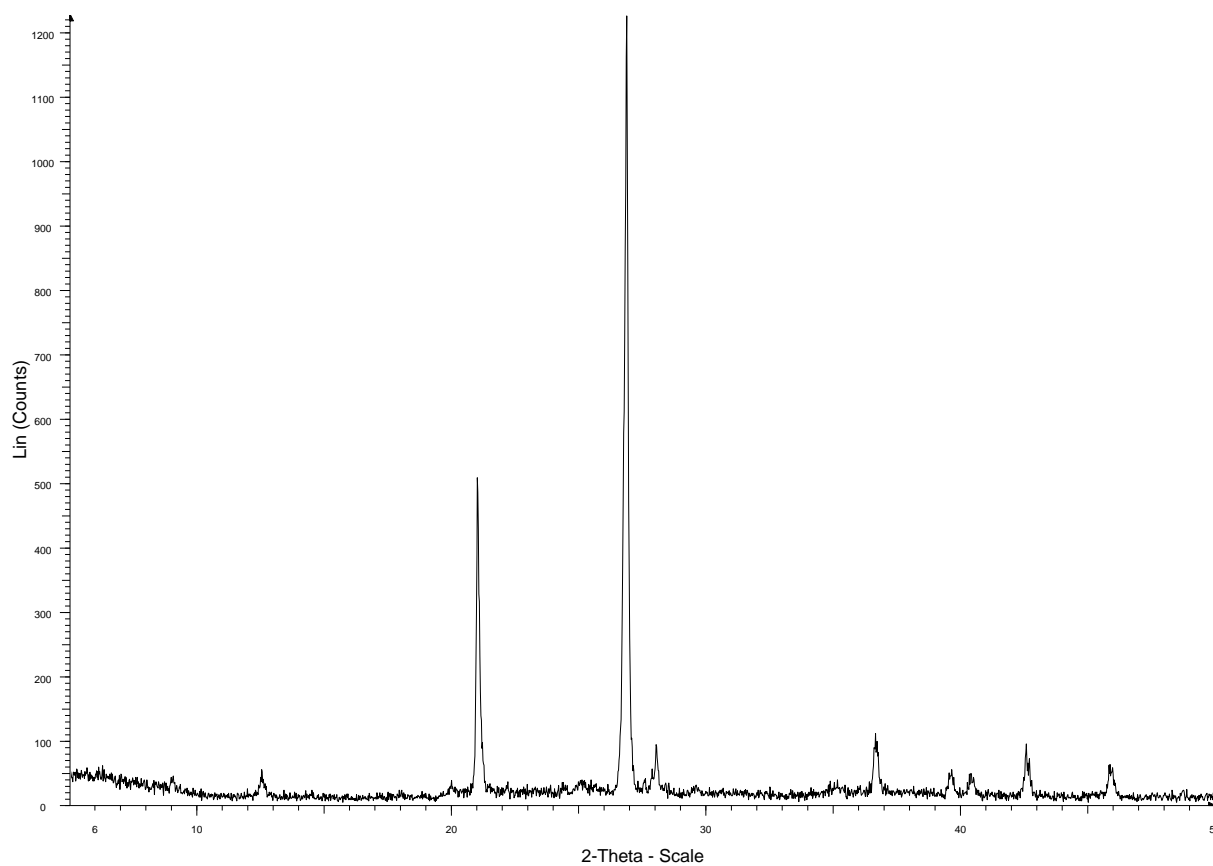


Figure 3.6.1.3: PXRD of preliminary soil samples (taken from the University of Bradford campus).

Table 2.6.1.1: Mineral species found in soil samples taken from the city of Bradford.

Mineral Species	Position (2-theta)	Reference
Kaolinite	12.3	Jackson
Quartz	20.4	Chisholm
	26.8	Chisholm
K-Feldspar	27.7	Grew
Dolomite	31.1	Lumsden
Calcite	36.3	Smyth

### **3.6.2 – Secondary Study**

The secondary study focussed on using the oxidative sample preparation (see 3.4.2) in order to differentiate between soils of two distinctly different locations, one urban and one rural. Ten soil samples were collected from around the city of Bradford, England, a densely populated area with a rich industrial history therefore increasing the likelihood of contaminants. The geology of this sampling area comprises Carboniferous sand and gritstone and some coal measures overlain by glacial till of Devensian age (Cr, n.d.). The second set of ten samples was collected from an arable farming district of Lincolnshire from a twenty mile radius surrounding the village of Bitchfield. The geology of this sampling area is dominated by the Jurassic Oxford Clay formation overlain by Mid-Pleistocene diamicton and till (Atlas, 2013). The Bradford samples comprise of peaty soils that are rich in humic compounds (Scheurmann, 2000). These humic compounds make up approximately twenty percent of the total soil composition (University C, 2009). The soils from Lincolnshire are comprised of organic clays that have been affected by ploughing. The soil samples were combined to achieve two aggregated samples (one from Bradford, one from Lincolnshire) for this experimental study.

#### **3.6.2.1 – Urban Samples (Bradford)**

The major mineral species found in the urban soil samples was quartz, see figure 3.6.2.1.1. It was expected that quartz would be one of the major components in all samples due to its large abundance in the earth's crust where it is the second most abundant mineral. Quartz is identified through the

fundamental vibration wavenumber found at wavenumber  $490\text{cm}^{-1}$  and the peak at  $200\text{cm}^{-1}$ . These peaks are indicative of the stretching and bending of the  $\text{S}(\text{SO}_4)$  molecule (Perrillat et al., 2003).

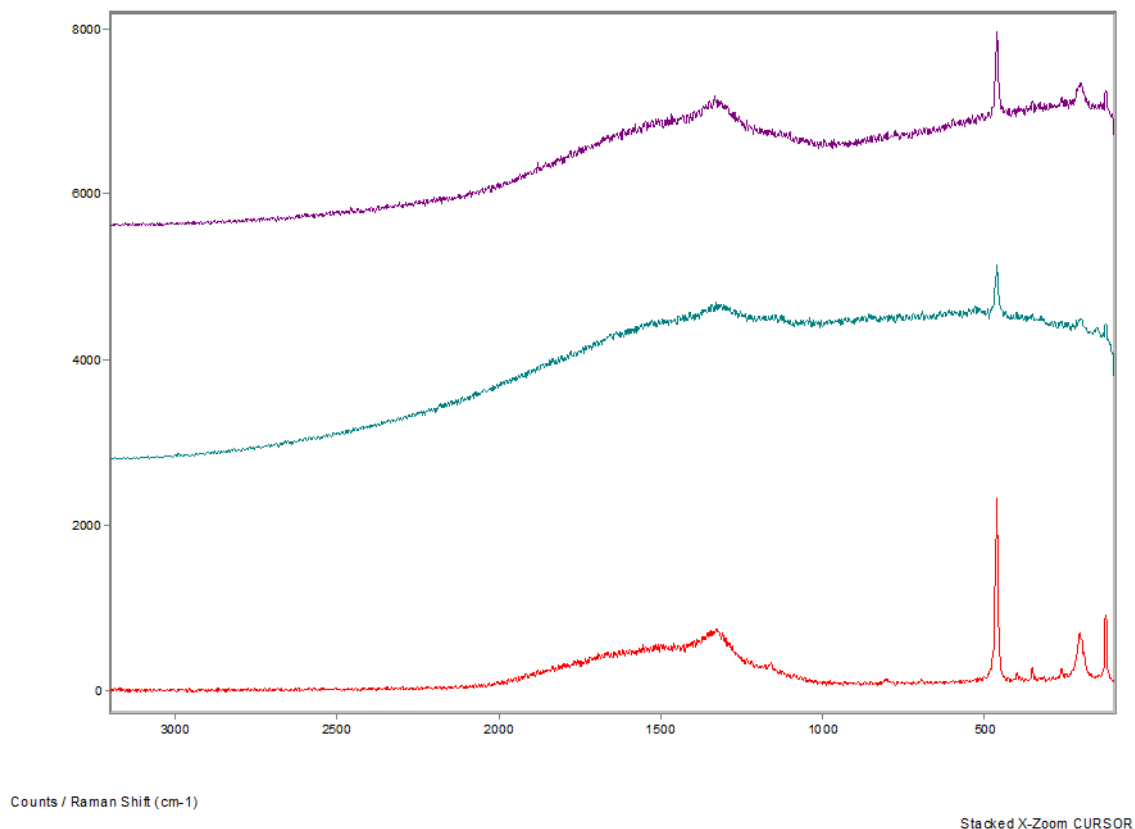


**Figure 3.6.2.1.1: Representative Raman spectra found in the urban soil samples.**

Also found within the urban soil samples were traces of Haematite. Hematite is identified by the expected seven phonon lines at 225, 247, 293, 299, 412, 498 and  $613\text{cm}^{-1}$  (Legodi *et al*, 2007) (see table 3.4) . Figure 3.6.2.1.2 shows the traces of Haematite the mineral form of iron (III) oxide, found within the sample.

**Table 3.6.2.1.1: Expected Raman peaks for Haematite (González *et al*, 2000).**

Raman Peak (cm-1)	Symmetrical species	Ions Involved
225	A1g	Fe,O
247	Eg	Fe,O
293	Eg	Fe,O
299	Eg	Fe,O
412	Eg	Fe,O
498	A1g	Fe,O
613	Eg	Fe,O

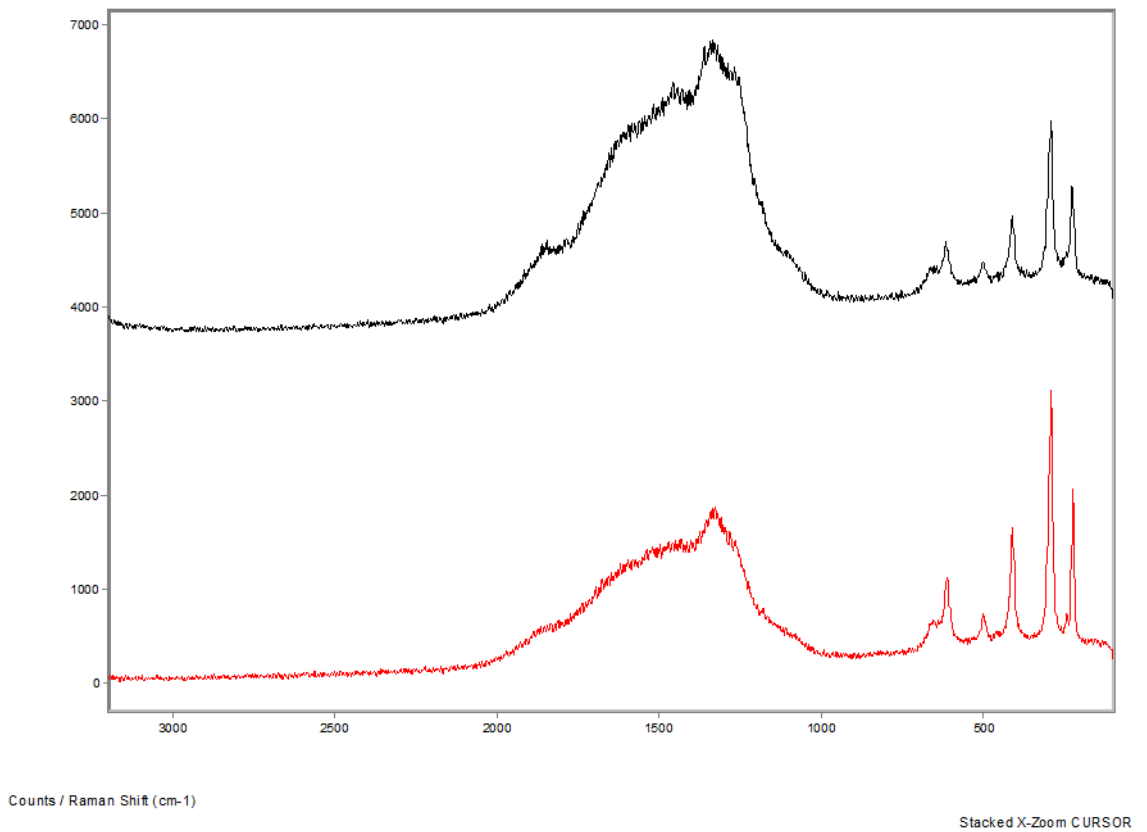


**Figure 3.6.2.1.2: Representative stacked plot showing the Haematite peaks found within the urban soil samples.**

### 3.6.2.2 – Rural Samples (Lincolnshire)

Again, in the rural samples, one observed a large proportion of quartz in the samples. However, the count rate for these peaks was, on average, lower than those observed in the urban samples. It was also observed that there were, on the whole more traces of quartz found in these samples compared to the urban samples.

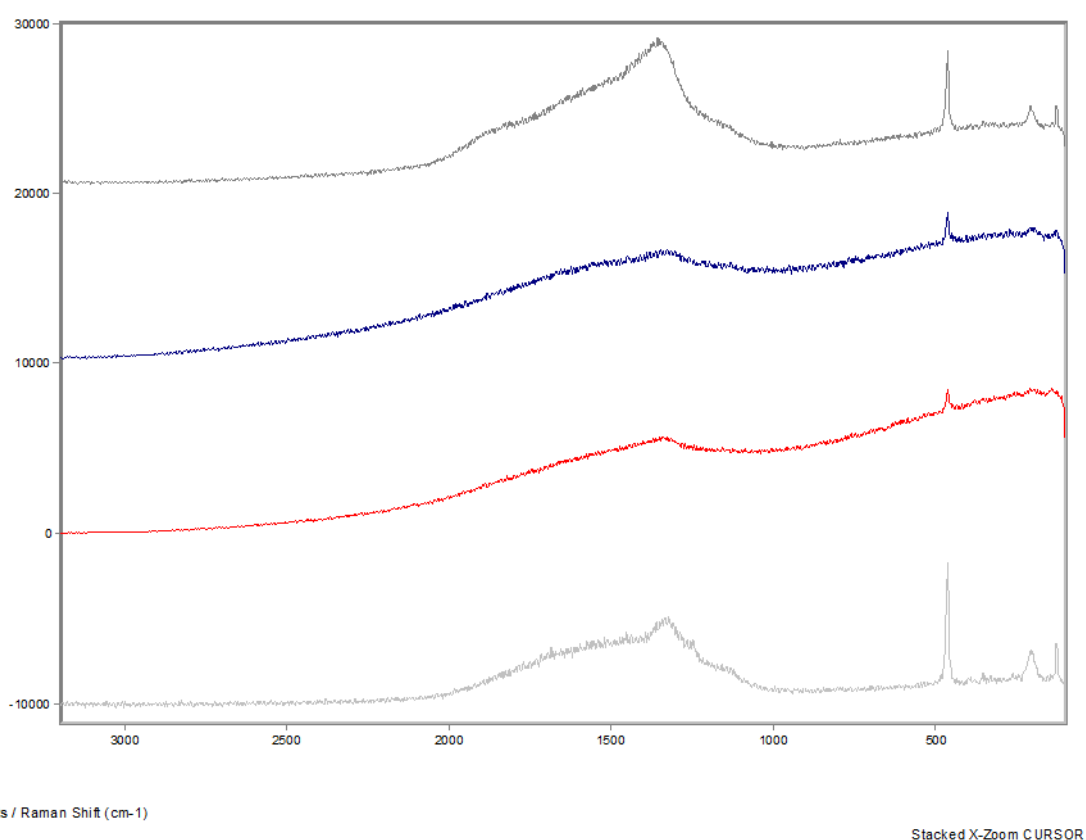


**Figure 3.6.2.2.1: A larger number of sampling sites in the rural samples were shown to contain quartz, more than we observed in the urban samples.**

In the rural soil samples we also observed several peaks associated with calcite. Calcite was expected in both samples according to PXRD data but it was only

observed in the rural samples. Calcite can be identified through the transitional and rotational lattice modes of the crystal structure found at  $278\text{ cm}^{-1}$  and  $151\text{ cm}^{-1}$  respectively (Taylor *et al.*, 2008). The peak at  $1092\text{ cm}^{-1}$  is the symmetric  $\text{CO}_3$  stretch with the deformation at  $716\text{ cm}^{-1}$  (Taylor *et al.*, 2008).

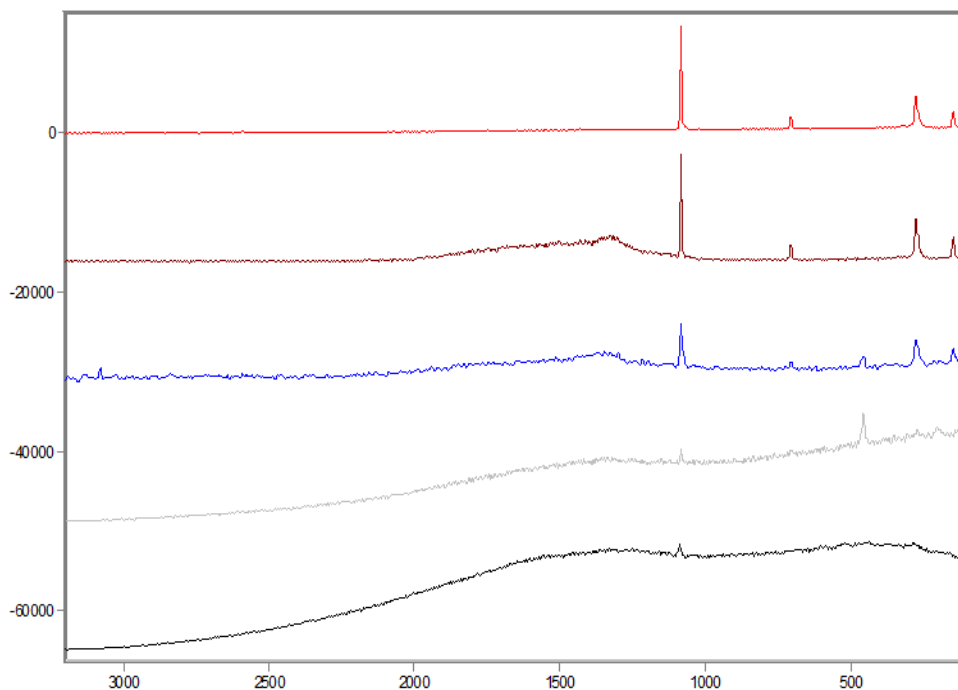
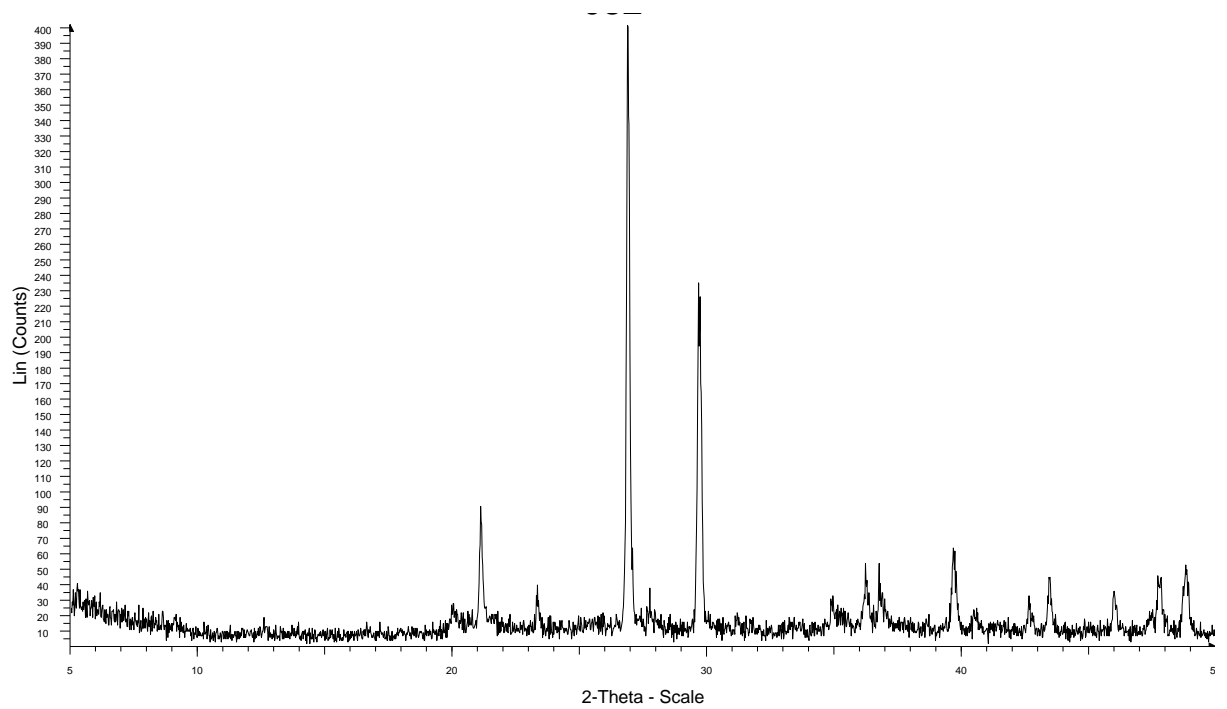


Figure 3.6.2.2.2: Representative stack plot of the calcite spectra observed in the rural soil samples.

### 3.6.2.3 – Urban Samples (Bradford)

The urban soil diffractogram again shows peaks of calcite and quartz. Peaks at  $\sim 21^\circ$  and  $26^\circ$  are attributed to goethite, an iron oxide, which is not found in the rural sample (Legodi *et al.*, 2007). This may be attributed to the haematite traces found by Raman spectroscopy as the two are known to interconvert given the correct conditions (Faria & Lopes, 2007).



**Figure 3.6.2.3.1: Powder X-ray diffractogram of the urban soil sample.**

### **3.6.2.4 – Rural Samples (Lincolnshire)**

As expected the rural soil samples differ from the urban soil sample with the inclusion of two peaks, those of Illite and Kaolinite at  $8^\circ$  and  $12^\circ$  respectively (Hu & Liu, 2003).

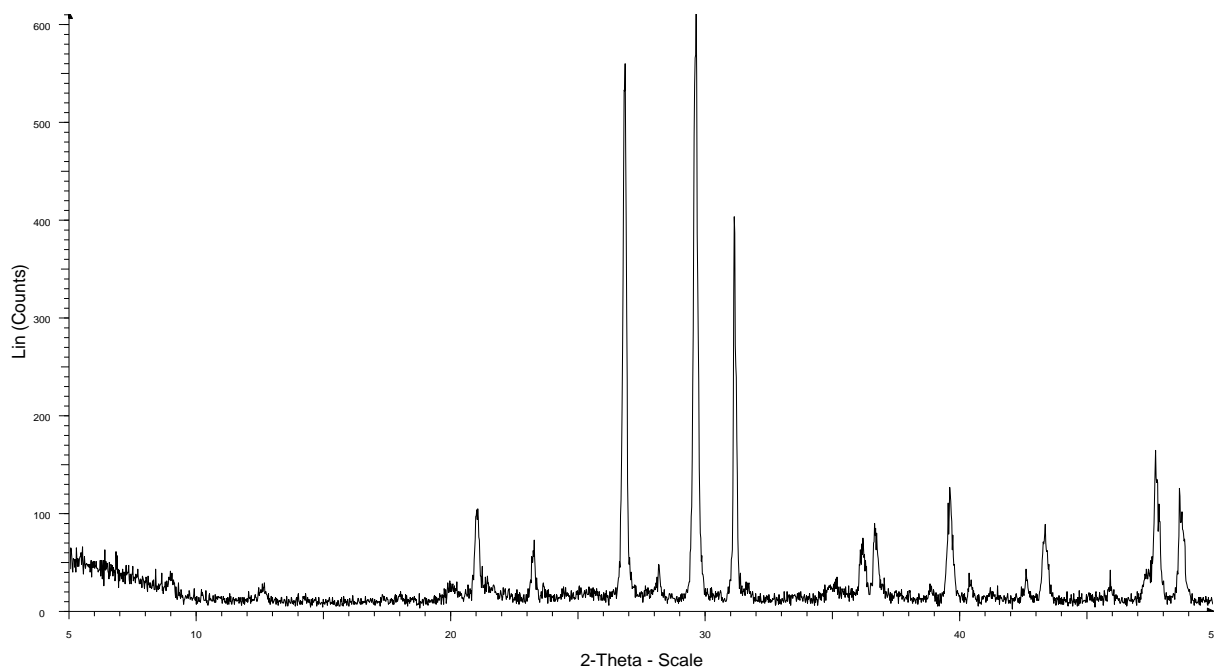


**Figure 3.6.2.4.1: Powder X-ray diffractogram of the rural soil sample.**

These fall within the smectite range of the diffraction, an indication of the clay nature of the soil type. The other large peak that does not appear in the urban sample is at  $31^\circ$ , attributed to calcite through peak matches with an internal standard. Further observed peaks include quartz and k-feldspar.

### 3.6.3 – Final Study (Soil samples from the route A65)

All the sampling points taken from the area around Ireby showed the spectra characteristic of quartz (Perrillat *et al.*, 2003). No other mineralogy or organic features were observed. Figure 3.6.3.1 shows a representation stack of all the spectra recorded from the soil samples around Ireby.

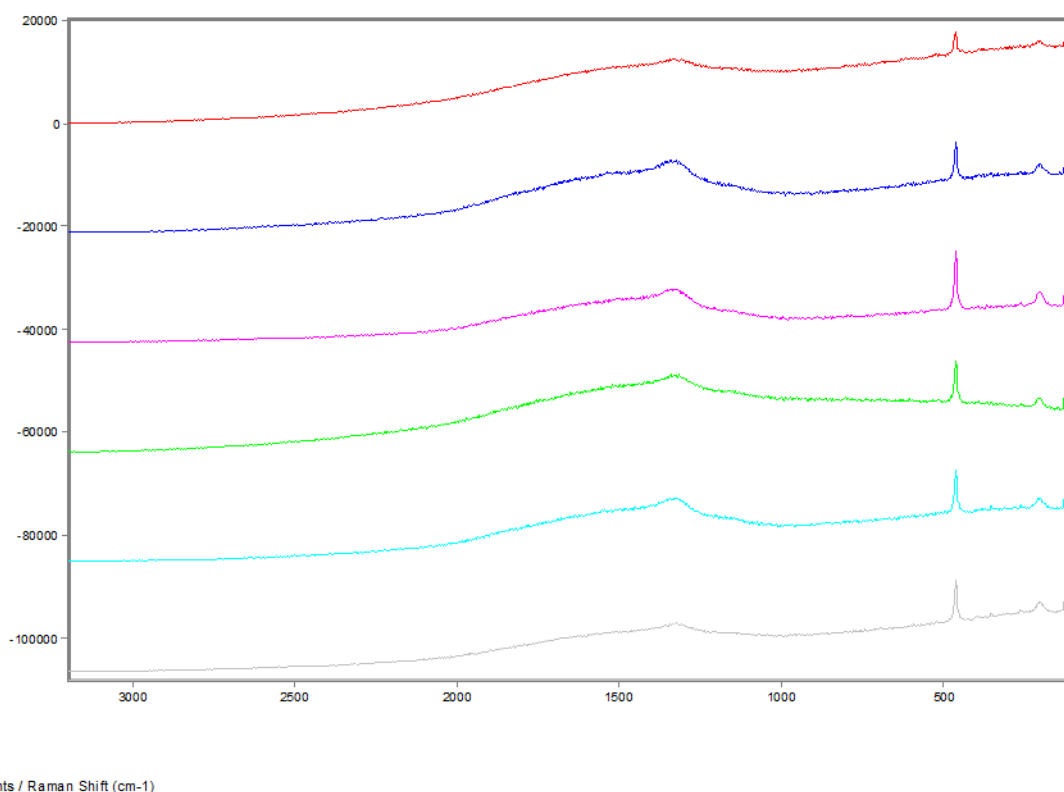


**Figure 3.6.3.1: Representative stacked spectra displaying characteristic quartz modes from soil samples taken from Ireby.**

As with Ireby, the soil samples from around the village of Ingleton showed a large proportion of the in-organic fraction consisted of quartz. These inorganic traces can be observed in figure 3.6.3.2.

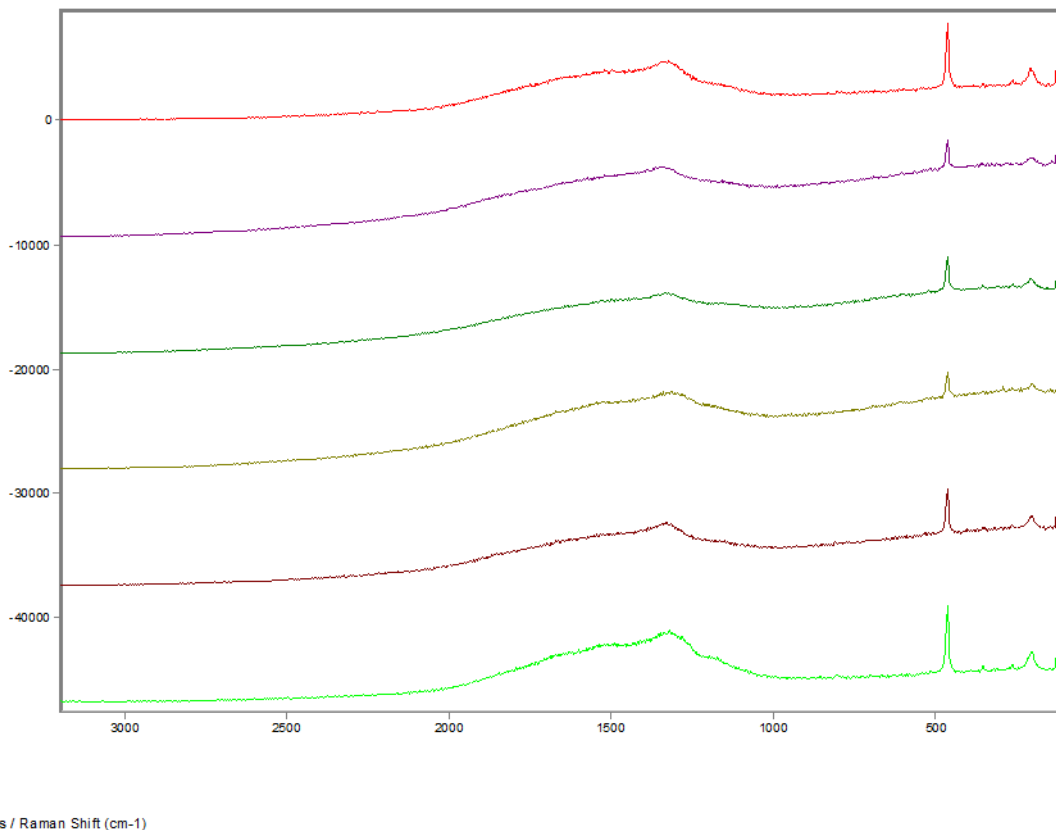


**Figure 3.6.3.2: Stacked plot showing the characteristic quartz modes found in the soil samples taken from Ingleton.**

The samples also showed several peaks in the organic region. In the upper trace these peaks are observed at 1368, 1580, 1675, 1887 and 2017  $\text{cm}^{-1}$  (fig 3.6.3.3). These peaks have been attributed to the symmetric CO stretch (Otto 2005), aromatic ring chain vibrations (Otto 2005), silicon (Viera, 2001), the CO stretch (Marrett, 1969) and the CO vibrations respectively. One can also observe the characteristic vibrations for quartz within this spectra.

On the lower trace the organic peaks are a lot broader and not as intense (fig 3.6.3.3). The peaks are observed at 1047, 1200, 1269 and 1406  $\text{cm}^{-1}$ . These

peaks have been identified as the nitrate peak ( $\text{NO}_3$ ) (Holthoff, Stratis-cullum, & Hankus, 2011), the amorphous carbon vibration of graphite (Mao, Mao, & Eng, 2003), the  $\text{CH}_2$  deformation and the  $\text{CH}_3$  deformation.

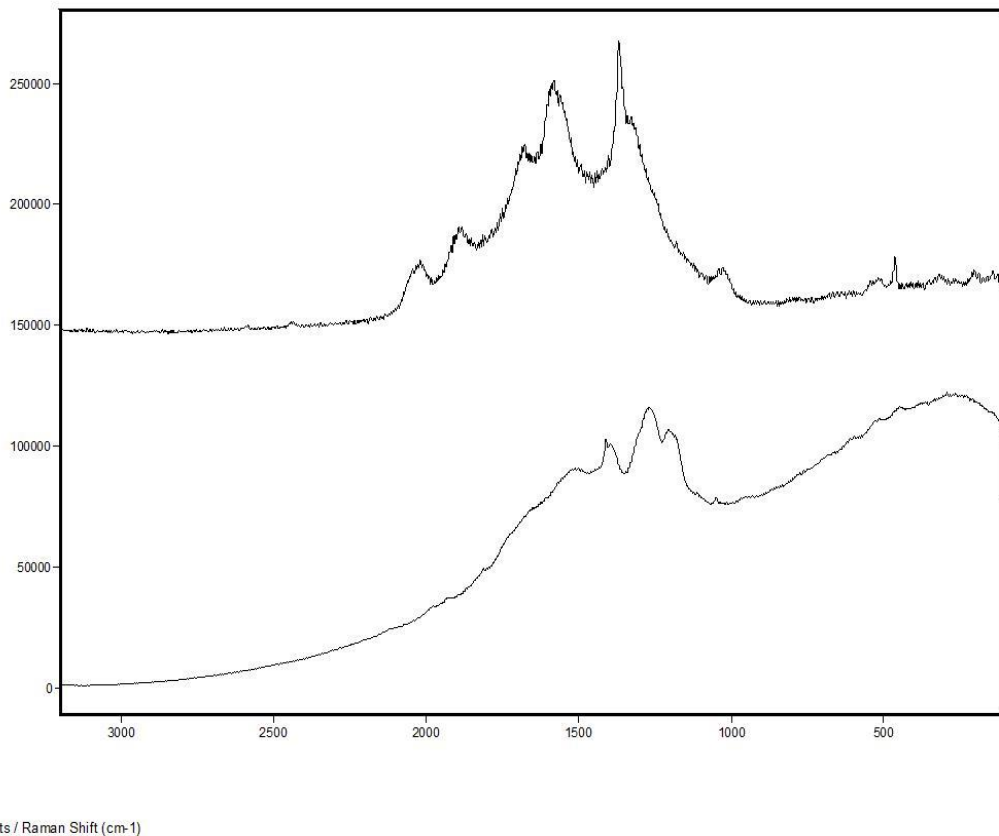


**Figure 3.6.3.3: Spectra displaying peaks associated with humic and fulvic acids found in the soil samples taken from Ingleton.**

Large amounts of quartz were identified in the samples from the area of West Barbon (fig 3.6.3.4).

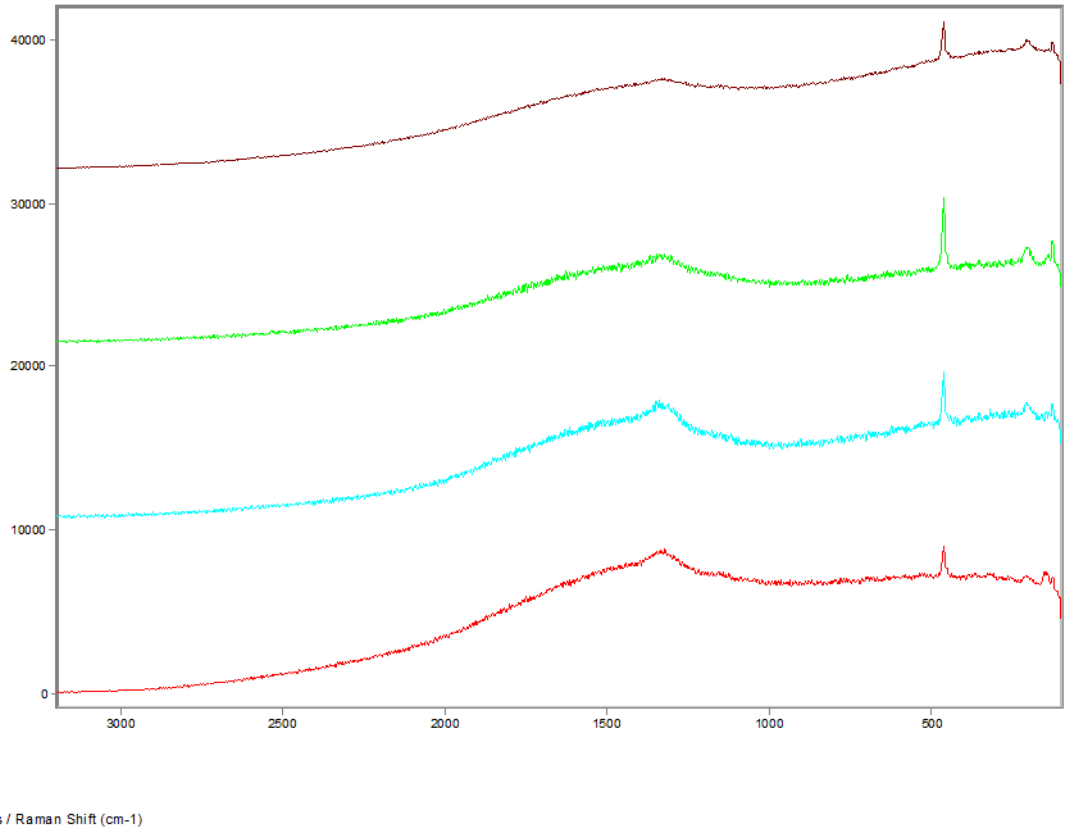


**Figure 3.6.3.4: Spectra displaying peaks characteristic with quartz. The spectra were produced from soil samples from West Barbon.**

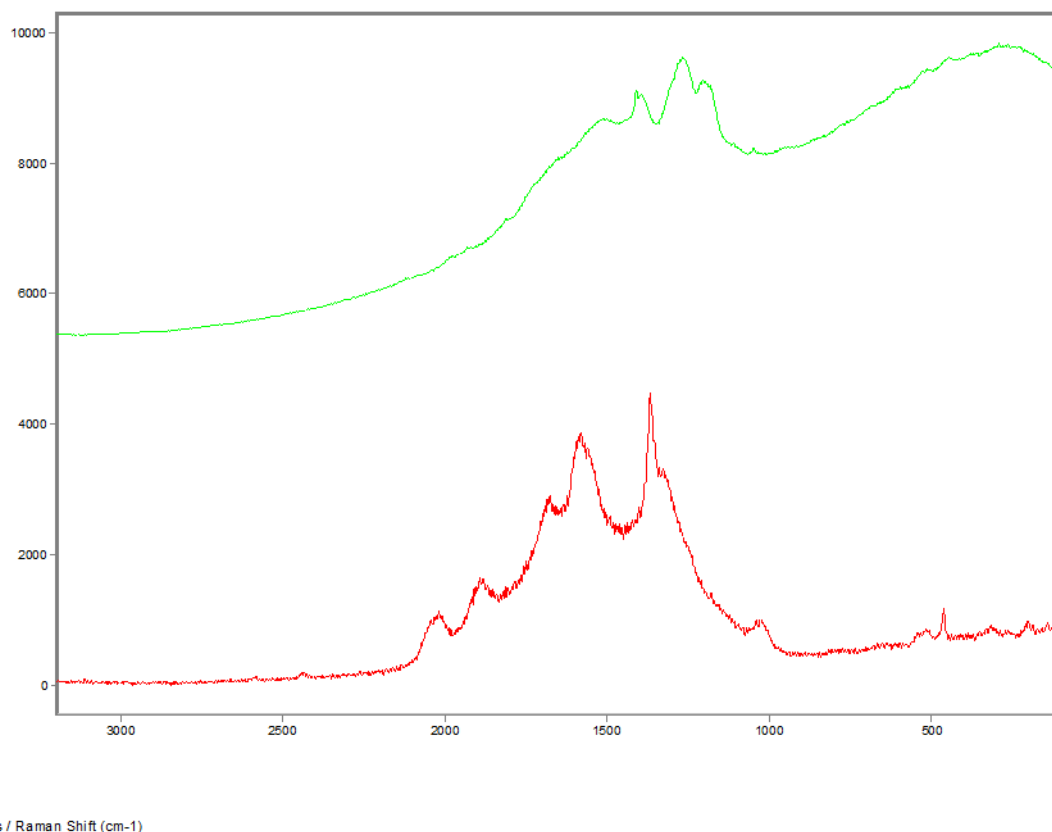


**Figure 3.6.3.5: These traces display some of the peaks attributed to the organic fractions of the soil taken from West Barbon**

Two of the spectra (figure 3.6.3.5) yielded some organic information about the soil samples and the composition of the fulvic acid fraction of the soils. The upper trace in figure 3.6.3.5 shows four main peaks in the organic region at 1204, 1269, 1409 and 1518  $\text{cm}^{-1}$ . These peaks are attributed to the  $\text{CH}_2$  deformations,  $\text{CH}_3$  deformation and the amorphous carbon vibration of graphite (Mao *et al.*, 2003). The lower trace shows five peaks located at 1368, 1580, 1682, 1887 and 2017  $\text{cm}^{-1}$ .

These peaks are assigned to the symmetric CO stretch (Otto, 2005) aromatic ring chain vibrations (Jyh-Hsin, 1994),  $\text{H}_2\text{O}$  bending mode the CO stretch and the CO vibrations respectively.

The samples taken from Kirkby Lonsdale yielded very little useful spectral information, of the 100 spectra taken only 23 contained any information. All 23 recorded spectra showed traces of quartz although the peak height was much lower than the quartz spectra recorded at all the other sites. The fundamental vibration for quartz also had a much lower intensity than that in the other samples.

As with all the locations sampled the samples from Skipton showed a large amount of quartz.

Several of the spectra also revealed a large, broad peak at  $1324\text{ cm}^{-1}$ . In some cases this peak was observed along with other soil mineralogy (second and third traces of figure 3.6.3.6 show the peak alongside quartz signals). This peak has been attributed to the diamond  $\text{C}\pm\text{C}$  stretching peak (Edwards *et al.*, 2011).

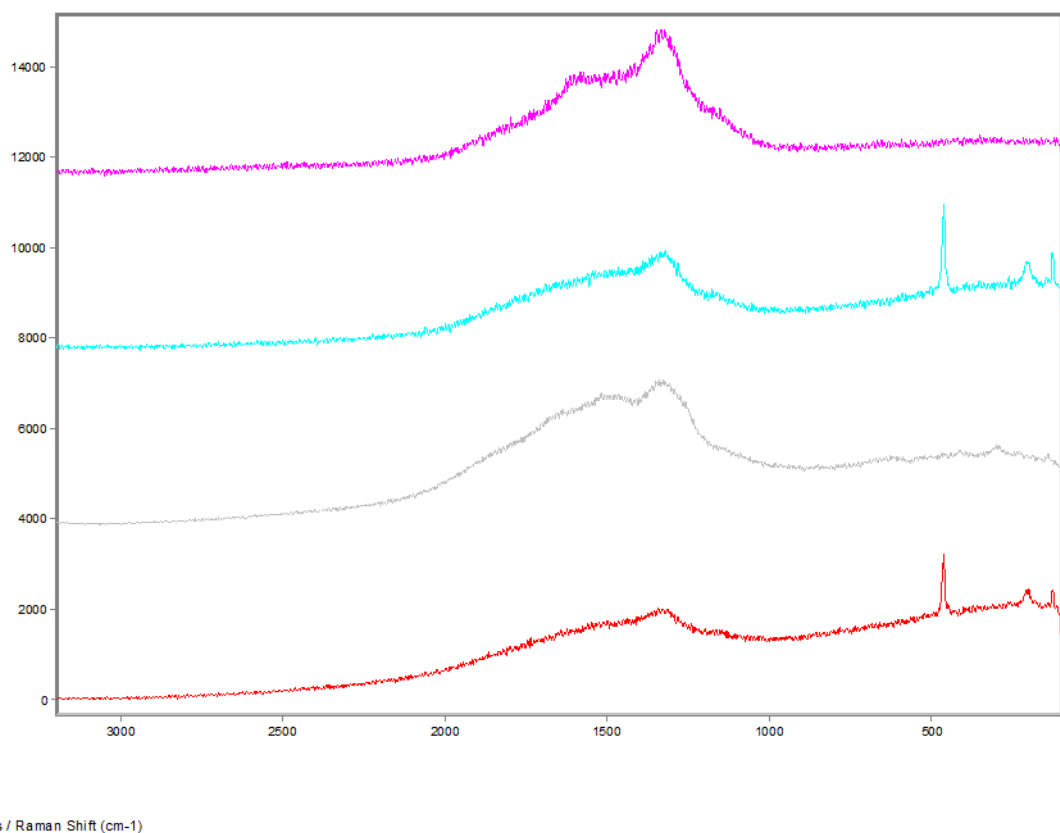


**Figure 3.6.3.6:** Traces showing the broad peak at  $1324\text{ cm}^{-1}$  attributed to the  $\text{C}\pm\text{C}$  stretch of diamond.

Three further organic spectra were recorded from the Skipton sampling sights. In the upper trace of figure 3.6.3.7 one can observe the graphite peak at  $1600\text{ cm}^{-1}$  (Mao *et al.*, 2003). The middle trace yields peaks at 2020, 1890, 1682, 1600 and  $1368\text{ cm}^{-1}$ . These peaks have been assigned as the CO vibration, the CO stretch, the H<sub>2</sub>O bend mode, graphite and the symmetric CO stretch. The final trace shows three small, broad peaks at 1440, 1351 and  $1276\text{ cm}^{-1}$ . These peaks have been assigned as being those of tin (Tamm *et al.*, 2012).

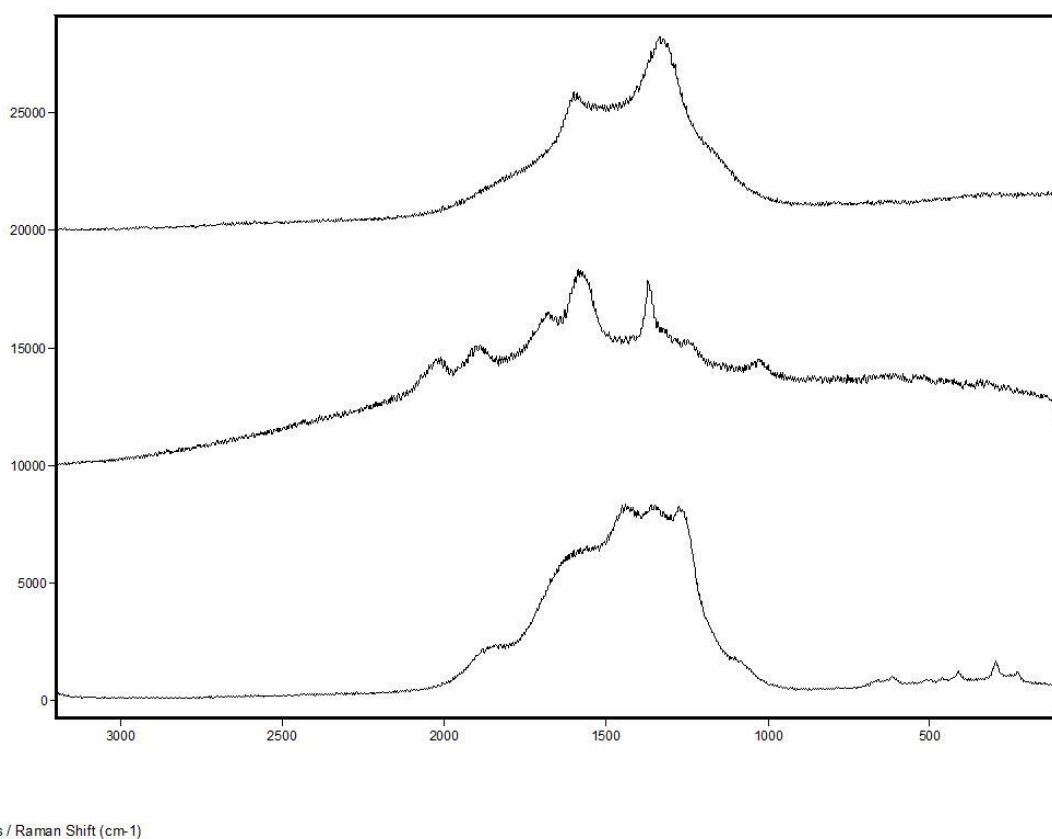


**Figure 3.6.3.7: Spectra attributed to the organic materials found in soil samples from Skipton.**

### **3.6.3.1 – Powder X-Ray Diffraction**

In all of the five samples collected along the A65 the powder X-ray diffractograms showed identical mineralogy. The only slight differences between the samples are greater or lower peak intensities. Figure 3.6.3.1.1 demonstrates this identical mineralogy by way of overlaid diffractograms for all five sampling sights.

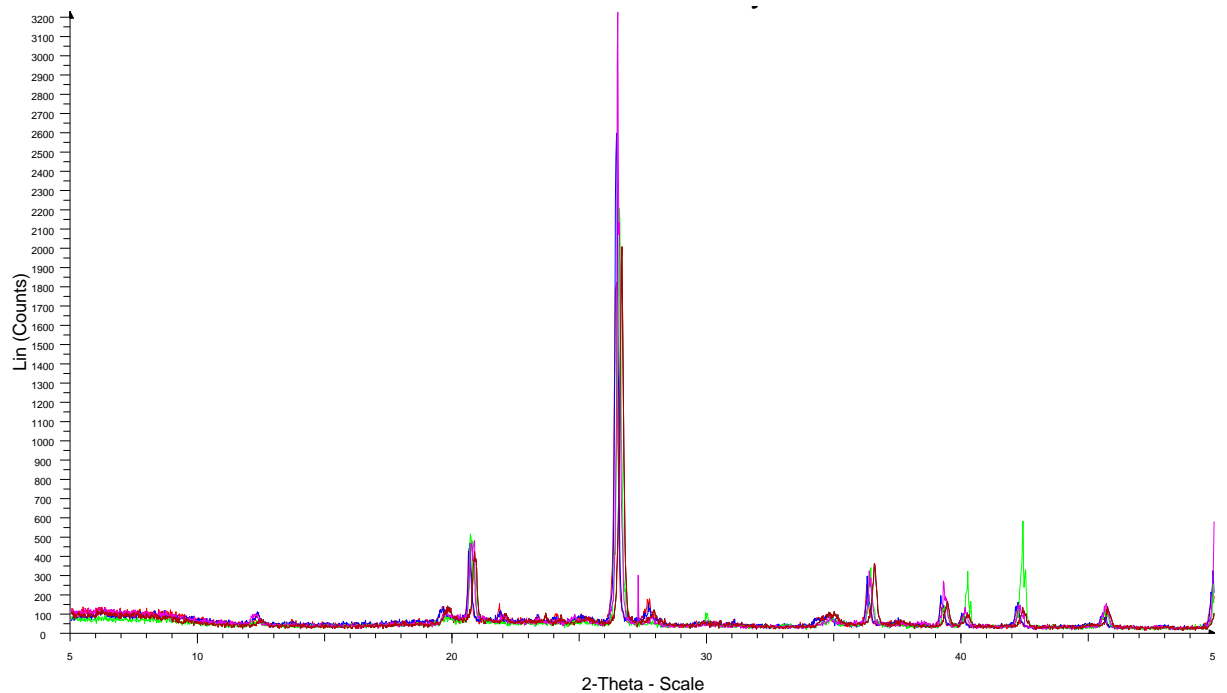


**Figure 3.6.3.1.1: Overlay of the diffractograms taken from all the sampling sites in the final soil study.**

The diffractogram shows four main mineral species are found in these soil samples. The peak at  $12.3^{\circ}$  is that of Kaolinite (Hu & Liu, 2003) whilst quartz can be observed at  $20$  and  $26^{\circ}$  (Perrillat *et al.*, 2003). One can also observe the peaks for Goethite at  $45.5$ ,  $40.2$ ,  $36.7$  and  $27.9^{\circ}$ . The peaks for Montmorillite are observed at  $42.1$ ,  $39.6$ ,  $34.1$ ,  $20.5$  and  $19.8^{\circ}$  (Wood & Details, 1932).

### 3.7- Conclusions

The preliminary study using whole, untreated soil fractions demonstrated the difficulties associated with the analysis of soil samples utilising Raman spectroscopy. The only signal of note that was observed in just two of the one-hundred sampling points was the broad band suggestive of the amorphous carbon vibration of graphite at  $1518\text{ cm}^{-1}$ . No other Raman signals were observed in any other spectra. This issue is caused by both sample fluorescence due to the organic content and the lack of scattering of the laser beam due to its absorption by the dark colouring of the sample.

This small study demonstrated the need for a technique to remove part of the organic content of the soils in order to lessen the effect of fluorescence as well as to lighten the colour of the samples to enable more scattering of the laser light.

The initial tests carried out into the effectiveness of using  $\text{H}_2\text{O}_2$  as a treatment to address the issues raised in section 6.1 showed a marked improvement in spectral quality. The resulting spectra were a vast improvement on the untreated spectra with small peaks showing traces of quartz and calcite. However, there were no traces of any organic residues having presumably been removed by the initial oxidative process. The treatment with the peroxide removed all of the organic content and enabled the observation of some mineralogical peaks (quartz and calcite) with Raman spectroscopy. However, the aims of this study were to utilise Raman spectroscopy in the interrogation of whole soil fractions, not just the mineralogical content. Therefore development of this oxidative method was necessary in order to retain some of the samples organic content whilst retaining the ability to record useful Raman data.

The tests were repeated however this time a range of peroxide concentrations were used. It was found that concentrations of 20% or lower were insufficient and had retained too much of the organic content to be able to record and useable spectra. Concentrations at 30% had removed sufficient amounts of organic residue to record clear spectra of both organic and inorganic fractions of the soil sample but the peak intensity was at its best and was most clear in the samples that had been treated with a 40% solution of hydrogen peroxide. After comparison of the collected spectra it was decided that the reflux carried out with the 40% H<sub>2</sub>O<sub>2</sub> solution showed the best overall improvement in spectral quality and enabled the study of both organic and inorganic fractions of the soil. For this reason all further samples in the following studies were treated under reflux with a 40% solution in water of hydrogen peroxide.

The purpose of the study of samples taken from the urban environment of Bradford and the rural environment of Lincolnshire was two-fold. Firstly it was used as a test as to the effectiveness of the oxidative treatment and secondly to see if it is possible to differentiate between two different soil samples utilising Raman spectroscopy.

Clear Raman spectra were recorded for both samples. Of most interest are the mineral spectra of Haematite in the rural samples. This is because of the inclusion of some organic signals on the Haematite samples. Organic materials of fulvic acid are known to attach to iron oxides (Ktigel-knabner, 1997) and it is this spectra that is a clear indicator that the oxidative treatment enables the study of both the organic and the inorganic fractions of a soil sample. The oxidative preparation method has been shown to provide clear spectral quality

with the ability to interrogate both the organic and the inorganic fractions of the soil.

What we can observe from the two different soil samples is the difficulty of utilising this technique to discriminate between two different soil samples utilising Raman spectroscopy. In the rural and the urban samples a small difference was observed, namely with the finding of Haematite in the rural samples and not in the urban samples. However, Haematite was only observed in a very small percentage of the rural samples and one can not be sure that it was not present in the urban samples.

Discrimination was expected based on the compositional differences of the soil types, one high in smectites and one in organic materials. Initially it was suspected that the oxidative treatment may have removed not only the organic content but some of the smectite range as well as causing a change in the sample mineralogy. However, PXRD data taken both before and after the oxidative treatment shows clear evidence that that is not the case. The lack of discrimination between samples may be due to the random nature of the sampling points. Utilising Raman spectroscopy only small areas of the sample are analysed by focusing the laser beam rather than larger areas. It is possible that the laser beams simply did not focus on all the components of the sample and that is the reason for a lack of whole soil fraction identification.

The study using soil samples from five different bedrock conditions aimed to be the final test into the discriminatory abilities of Raman spectroscopy on soil samples. The PXRD diffractograms surprisingly showed identical mineralogy from all five locations. PXRD is the gold standard for soil identifications in forensic case work and so these samples were there to provide a stern test for

Raman spectroscopy, could it provide sample discrimination where commonly used forensic methods could not.

Using the oxidative preparation method and Raman spectroscopy we were able to provide some further discrimination between some of the five soil samples. The majority of the spectra revealed large amounts of quartz which is of no value in soil discrimination because of the large amounts of quartz found in the earth's surface. Where we were able to provide some discrimination between the soils was within the organic content as well as providing some insight as to the land usage. In the samples taken from around the village of Ingleton showed traces of nitrates in the soil. Ingleton is a small farming village in the north of Yorkshire and the traces of nitrates suggest contamination in the soils. Through knowing about the number of farms surrounding the village we may conclude that the nitrate traces within the soil has come from agricultural fertilisers. It was the presence of these nitrates that enabled the samples from Ingleton to be separated from all the other samples taken. From the samples taken from Skipton we were able to distinguish them from the other soil samples by the presence of tin. Clearly a soil contaminant tin was found in none of the other samples. Looking back through the industrial records, there is no industrial heritage to explain the presence of tin in the soil samples. However, tin is a metal found regularly in everyday life and the proposal is that the tin contamination has come through a lack of waste management.

### **3.8- Further Work**

It is clear from the improvement in spectral quality that the oxidative process has enabled the interrogation of soil samples with Raman spectroscopy. However, it has become clear through the secondary and tertiary studies that

the methods of sample analysis are not currently sufficient for full discrimination between soil samples. Therefore, further development of the sampling methods is required to utilise the potential of Raman spectroscopy to its fullest. One believes that this may become possible with the design of a sampling map utilising the mapping facility of the control software. This would enable multiple sampling points across the whole of the sample in a regular and uniform pattern, allowing for reproducible results under a standard method. In order to fully assess the discrimination value of Raman spectroscopy in soil science a full forensic interrogation of at least one sample must be carried out and the results of this compared to the results obtained *by Raman spectroscopy* for the same sample. Techniques should include, but not be limited to, PXRD, SEM-EDX, soil pH indexing and colour identifications.

One believes that this technique may find its greatest use in the field. There is a large body of work looking at soil contamination, soil typing, and forensic soil placement. The geological potential of an *in situ* field test that can identify full soil fractions is huge whether the purpose is forensically looking to place people at a scene, discover contaminants or as a geological surveyor looking to document or discover. Portable Raman spectroscopy is not possible directly for the issues of fluorescence. However, it may be possible to develop the oxidative method further in order to allow the use of portable Raman spectroscopy for the *in-situ* analysis of soil samples. If it becomes possible for the *in-situ* analysis of soil samples with portable Raman spectroscopy then a large body of experimentation will be necessary in order to develop a representative and reproducible protocol for the testing of the samples. It has been shown that this is difficult under laboratory conditions and this will make it more so in the field.

This work has focussed on the analysis of organic and inorganic species in geological samples. This method of analysis has demonstrated a greater discriminating power than many of the current techniques available, particularly in mineralogical species identification. Considering this the technique may have wider applications in the areas of geochemistry, particularly in mineralogical interrogation. The possibilities of this technique being used as a standard geological method will be explored against current established geological methods. Initially this study will begin by looking at tephra samples. Tephra chronology is used extensively in geology particularly in dating techniques where the identification of tephra layers can accurately be dated through historical records (Larsen, 1983). However, thus far the discrimination of some tephra layers has become impossible due to the principle components of the tephra being identical (Rea *et al*, 2012). Raman spectroscopy has been proven in this study to be able to distinguish between samples of similar principle component and the potential to transfer this discriminatory power to tephra chronology should be explored.

### 3.9- References

- Atlas, B. S. (2013). STRATEGIC STONE STUDY A Building Stone Atlas of, (July).L.L. Bissey, J.L. Smith, R. J. Watts, *Water Research*. **2006**; *40*, 2477.
- Cengiz, S., Karaca, A., Cakir, I., Uner, H., Sevindik, A., *Forensic Science International*. **2004**; *141*, 33.
- Corrado, G., Sanchez-Cortes, S., Francioso, O., Garcia-Ramos, J., *Analytica Chimica Acta*. **2008**; *616*, 69.
- Cr, C. R. (n.d.). Commissioned Report CR/04/172N.
- Edwards, H., Munshi, T., Scowen, I., Surtees, A., & Swindles, G. T. (2011). Development of oxidative sample preparation for the analysis of forensic soil samples with near-IR Raman spectroscopy. *Journal of Raman Spectroscopy*, (July 2010), n/a–n/a. doi:10.1002/jrs.3031
- Ewald, Belin, Berger, J. H. Weber, *Environmental Science and Technology*. **1983**; *17*, 501.
- Faria, D. L. a., & Lopes, F. N. (2007). Heated goethite and natural hematite: Can Raman spectroscopy be used to differentiate them? *Vibrational Spectroscopy*, *45*(2), 117–121. doi:10.1016/j.vibspec.2007.07.003
- Faria , Venâncio Silva , M. T. D. Oliveira, *Journal of Raman Spectroscopy*. **1997**; *28*, 873.
- Goi A., Trapido, M., Kulik, M., *Engineering and Technology*. **2009**; *59*, 185.
- González, G., Sagarzazu, A., & Villalba, R. (2000). Study of the mechano-chemical transformation of goethite to hematite by TEM and XRD. *Materials Research Bulletin*, *35*(14-15), 2295–2308. doi:10.1016/S0025-5408(00)00434-7
- Holthoff, E. L., Stratis-cullum, D. N., & Hankus, M. E. (2011). A Nanosensor for TNT Detection Based on Molecularly Imprinted Polymers and Surface Enhanced Raman Scattering, 2700–2714. doi:10.3390/s110302700
- Hu, Y., & Liu, X. (2003). Chemical composition and surface property of kaolins, *16*, 1279–1284. doi:10.1016/j.mineng.2003.07.006
- Jyh-Hsin M. Tsai, J.G.H., James C. Martin, Tracy P. Hamilton, Mark van der Woerd, Michael J. Jablonsky, Joseph S. Beckman, *Role of Conformation of Peroxynitrite Anion (ONOO-) with Its Stability and Toxicity*. *Journal of the American Chemical Society*, 1994. **116**(9): p. 1.
- Ktigel-knabner, I. (1997). <sup>15</sup>N NMR spectroscopy as a tool in soil organic matter studies, *80*, 243–270.

- Larsen, G. (1983). The Hekla Eruption 1980-1981, *46*(August 1980).
- Legodi, M. A., Waal, D. D., & Africa, S. (2007). The preparation of magnetite , goethite , hematite and maghemite of pigment quality from mill scale iron waste, (February).
- Mao, W. L., Mao, H., & Eng, P. J. (2003). Bonding Changes in Compressed Superhard Graphite, *302*(October), 425–428.
- Merritt, R.W.M.a.J.A., Infrared and Raman spectra of 1-methylcyclopropene. *Spectrochimica Acta Part A: Molecular Spectroscopy*, 1969. **25**(12): p. 8.
- Otto, A., *The 'chemical' (electronic) contribution to surface-enhanced Raman scattering*. *Journal of Raman Spectroscopy*, 2005. **36**: p. 12.
- Perrillat, J. P., Daniel, I., Lardeaux, J. M., Cardon, H., Sciences, L. D. E., Terre, D. E. L. A., Cnrs, U. M. R., *et al.* (2003). Kinetics of the Coesite ± Quartz Transition: Application to the Exhumation of Ultrahigh-Pressure Rocks, *44*(4), 773–788.
- Rea, H. a., Swindles, G. T., & Roe, H. M. (2012). The Hekla 1947 tephra in the north of Ireland: regional distribution, concentration and geochemistry. *Journal of Quaternary Science*, *27*, . doi:10.1002/jqs.1566
- Ruffell, A., McKinley, J., *Earth-Science Reviews*. **2005**; 69, 235.
- S. S. Remediation, *Vol. 2010*, **2011**.
- Scheurmann, I., *The Natural Aquarium Handbook*, 2 ed., Barron's Educational Series, **2000**.
- Tamm, A., Dimri, M. C., Kozlova, J., Aidla, A., Tätte, T., Arroval, T., Mäeorg, U., *et al.* (2012). Atomic layer deposition of ferromagnetic iron oxide films on three-dimensional substrates with tin oxide nanoparticles. *Journal of Crystal Growth*, *343*(1), 21–27. doi:10.1016/j.jcrysgro.2011.09.062
- Taylor, P. D., Kudryavtsev, A. B., & Schopf, J. W. (2008). Calcite and aragonite distributions in the skeletons of bimineralic bryozoans as revealed by Raman spectroscopy, *127*(1), 87–97. doi:10.1111/j.1744-7410.2007.00106.x
- University, C., *Vol. 2009*, **2009**.
- Viera, G., and Boufendi, L., Crystal size and temperature measurements in nanostructured silicon using Raman spectroscopy *Journal of Applied Physics*, 2001. **90**(8): p. 9.

Wood, L. A., & Details, E. (1932). Adsorption of Water Vapor by Montmorillonite.  
11. Effect of Exchangeable Ions and Lattice Swelling as Measured by X-Ray Diffraction, 5–8.

## Chapter 4

### 4.1- Introduction

Tephrochronology (the dating of sedimentary sequences using volcanic ash layers) is an important tool for dating and inter-environmental correlation of sedimentary archives of palaeoenvironmental change. In addition, tephra layers provide valuable information on the frequency and nature of ash fallout from volcanic activity. Successful tephrochronology is based on the geochemical identification of the tephra which has, until now, been based primarily on the analysis of major element oxide composition of glass shards using electron probe microanalysis (EPMA) (Hunt & Hill, 1993). However, it is often impossible to discriminate between key tephra layers using EPMA alone. For example, the Hekla AD 1947 and AD 1510 tephras which are found in Iceland and also as 'crypto-tephra' microscopic layers in NW Europe are currently indistinguishable using EPMA as it only shows the major element composition of the sample (Rea *et al.*, 2012). Therefore, other stratigraphic or chronological information is needed for their reliable identification. Raman spectroscopy is commonly used in chemistry, since vibrational information is specific to the chemical bonds and symmetry of molecules and can provide a fingerprint by which these can be identified. Here, we demonstrate how near-IR Raman spectroscopy can be used for the successful discrimination of mineral species in tephra. Raman spectroscopy is a valuable tool for both proximal and distal tephrochronology, due to its non-destructive nature, and can be used to discriminate Hekla 1510 from Hekla 1947. Distal tephrochronology in NW Europe is a well established tool for the correlation and dating of sedimentary sequences and palaeoclimate records (Larsen *et al.*, 1999; Haflidason *et al.*, 2000; Swindles *et al.*, 2011).

There have been many studies where geochemical correlation of distal tephra deposits with volcanic sources in Iceland was achieved successfully. This has primarily been achieved using electron probe microanalysis (EPMA) on the volcanic glasses, usually through the analysis of individual shards. However, discrimination based on EPMA alone has limitations as the glass composition of tephra erupted from same vent or from multiple volcanic sources in any given volcanic cluster (Iceland, Hawaii, Japan, etc.) may have indistinguishable major element composition. In fact, the widely used volcanic rock classification schemes (so called "TAS diagrams, for total alkalis vs.  $\text{SiO}_2$ , or the "K vs.  $\text{SiO}_2$ " diagram; see Maitre, 2002) are designed on the fact that bulk rock major element compositions of global volcanic rock datasets form clusters (for basalt, andesite, dacite, rhyolite, etc.). Moreover, the process of basaltic magma evolution and the predictable crystal fractionation of common rock forming minerals (olivine, pyroxenes, feldspars, oxides of Fe and Ti, etc.) can lead to very similar residual glass major element compositions. This is especially true for felsic (dacitic or rhyolitic) eruptions, which always erupt pumice with very low MgO and FeO and very high alkali and  $\text{SiO}_2$  contents (Di Carlo *et al.*, 2010).

Hekla is one of the most active volcanoes in Iceland, it is a morphological stratovolcano located near the rift-transform fault junction in the area where Iceland's South and Eastern Seismic Zones meet. Hekla's repeated fissure eruptions result in the formation of a vaulted ridge of about 5 km (*Heklugjá* fissure) that opens along its entire length during major eruptions.

Due to the small glass shard sizes there has been no mineral species discrimination based on the standard optical microscopy (e.g. Rea *et al.*, 2012) of tephtras from the Hekla eruption of 1510 and 1947 AD. This is particularly true

for the more distal deposits in peats, where often only a few glass shards can be successfully retrieved. We demonstrate how near-IR Raman spectroscopy can be used to distinguish between tephra grains with otherwise indistinguishable major oxide compositions. Through this discrimination we also demonstrate how Raman spectroscopy is able to definitively distinguish between the two tephtras for the first time without the aid of optical or other destructive analytical techniques. We also demonstrate how Raman spectroscopy has the potential to offer greater discriminatory power compared to the widely used EPMA analysis approach alone.

## **4.2- Tephra**

Tephra is fragmental material produced by a volcanic eruption regardless of composition, fragment size or emplacement mechanism. Volcanologists also refer to airborne fragments as pyroclasts. Once clasts have fallen to the ground they remain as tephra unless hot enough to fuse together into pyroclastic rock or tuff (Thornalley *et al.*, 2011).

The distribution of tephra following an eruption usually involves the largest boulders falling to the ground quickest and therefore closest to the vent, while smaller fragments travel further — ash can often travel for thousands of miles, even circumglobal, as it can stay in the stratosphere for days to weeks following an eruption. When large amounts of tephra accumulate in the atmosphere from massive volcanic eruptions (or from a multitude of smaller eruptions occurring simultaneously), they can reflect light and heat from the sun back through the atmosphere, in some cases causing the temperature to drop, resulting in a climate change: "volcanic winter". Tephra mixed in with precipitation can also be acidic and cause acid rain and snowfall.

Tephra-chronology is one of the key uses of tephra and is defined as; “use of tephra layers as isochrons (time-parallel marker beds) to connect and synchronize sequences and to transfer relative or numerical ages to them using stratigraphy and other tools”(Swindles *et al*, 2010). While residence time in the atmosphere of the very finest of these particles can be substantial, the deposition of the bulk of volcanic ejecta can be considered instantaneous from a geological, archaeological, and evolutionary perspective. Therefore, the occurrence of tephra from a given eruption in stratigraphic sequences provides a powerful means of dating such deposits, or of refining available dating schemes. Furthermore, the occurrence of tephra from the same eruption across sites, regions and in various types of depositional contexts (ice-cores, terrestrial, marine, cultural) holds the potential of linking and thus elucidating the tempi and causes of both environmental and cultural change.

It is this need for refinement of chronological dating that drives the study of tephra, particularly with the accuracy of radio-carbon dating being called into question for the dating of samples post-1900's due to nuclear testing and the increased consumption of fossil fuels (Higham *et al.*, 2009).

Tephra are usually identified through a number of chemical and non-chemical tests. Techniques used to detect and map cryptotephra or thin, visible tephra include field or ship-board instruments such as core scanners and magnetic susceptibility meters (e.g., Vogel *et al.* 2009). Some techniques are destructive, others are not (Gehrels *et al.*, 2008). They include ground-penetrating radar (Lowe, 1985), magnetic susceptibility and remanent magnetisation (Takemura *et al.*, 2000), X-radiography (Lowe, 1988; Dugmore and Newton, 1992; Turner *et al.*, 2008; Marshall *et al.*, 2010), X-ray fluorescence (XRF) (Hogg and McCraw,

1983; Gehrels *et al.*, 2008) including XRF-based core scanning (Vogel *et al.*, 2009; Révillon *et al.*, 2010), and scanning X-ray analytical microscopy (Katsuta *et al.*, 2007). Further techniques include spectrophotometry (reflectance, luminescence) (Gehrels *et al.*, 2008), high-resolution micropetrography (Vleeschouwer *et al.*, 2008), high-resolution trace element analysis by instrumental neutron activation analysis (INAA) (Lim *et al.*, 2008), and measurements of particle size distribution, total organic carbon, and loss-on-ignition (Gehrels *et al.*, 2008).

However, the gold standard tool for the analysis of tephra is electron probe microanalysis (EPMA). Geochemical fingerprinting of tephra to match them with source eruptions can be achieved very reliably and rapidly by EPMA. Discrimination between the majorities of tephra layers is usually achieved easily by analysis of the 10 major and minor elements present in the magma (Na, Mg, Al, Si, P, K, Ca, Ti, Fe, and Mn). Thus geochemical fingerprinting of tephra horizons by EPMA represents a very precise and cost effective dating tool.

### **4.3- Initial Study**

#### **4.3.1- Tephra**

In this work tephra from the Hekla volcanic eruptions of 1947 and 1510 AD were studied as the known EPMA data on the glass chemistry of these tephra has been published (Figure 4.3.1.1).

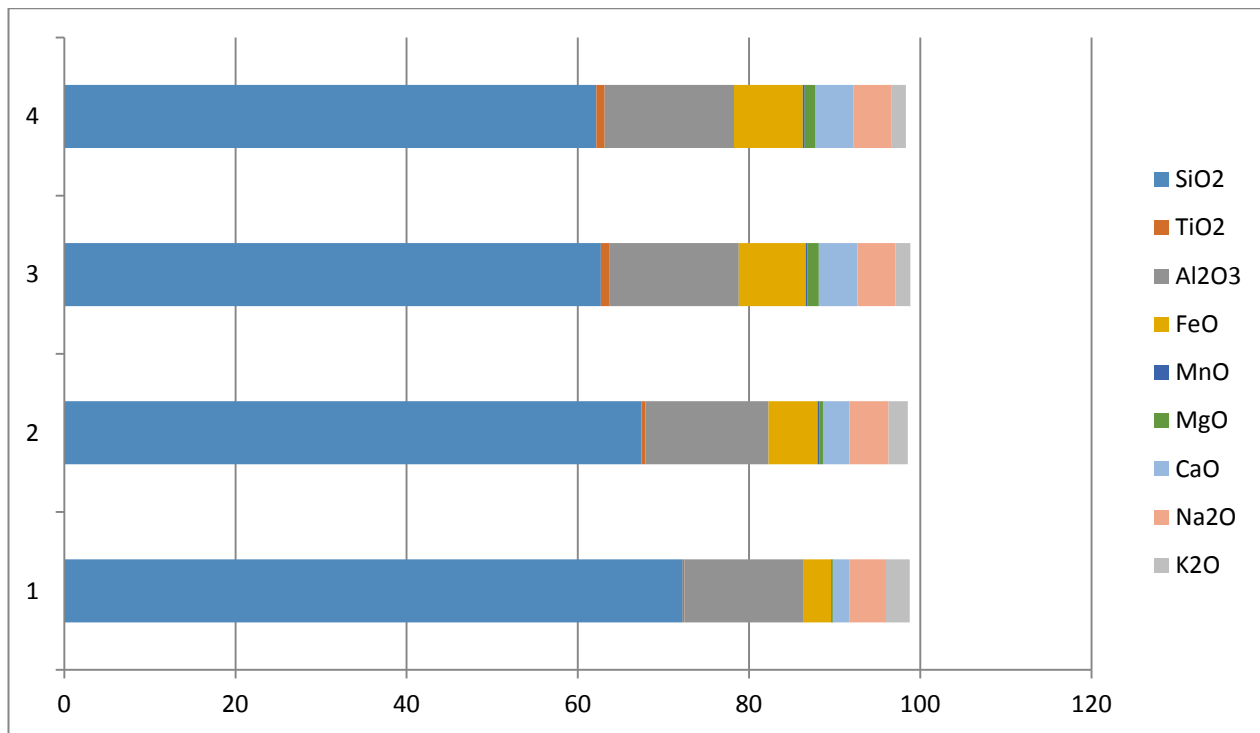


**Figure 4.3.1.1: Collated EMPA data of glass chemistry, where 1 is Hekla 1104 AD, 2 is Hekla 1158 AD, 3 is Hekla 1510 AD and 4 is 1947 AD (Rea *et al.*, 2012).**

The premise of tephrochronology is that each tephra deposit from a singular volcanic eruption has a unique chemical fingerprint. These tephra deposits form discrete layers and using the chemical fingerprints these layers can be distinguished from one another. These events form a chronological framework in which paleoenvironmental or archaeological records can be placed.



**Figure 4.3.1.2: Examples of visible tephra layers forming a chronological framework (Alber, 2012).**

The main advantages of the technique are that the volcanic ash layers can be relatively easily identified in many sediments (see fig. 4.3.1.2) and that the tephra layers are deposited relatively instantaneously over a wide spatial area. This means they provide accurate temporal marker layers which can be used to verify or corroborate other dating techniques, linking sequences widely separated by location into a unified chronology that correlates climatic sequences and events.

Recently tephra chronology is key in the dating of peat sequencing and examining inter-site records across specific isochrones allowing the spatial synchronicity of environmental changes to be scrutinised. Tephra horizons are sometimes visible to the naked eye (see figure 4.3.1.2) yet criptotephra samples invisible to the naked eye have been found in many more areas around the world further away from their volcanic source. In some cases these tephra horizons can be assigned a known calendar date based on historical, documented evidence (Hekla 1947, 1510 and 1104) (Sverrisdottir, 2007). Other tephra horizons have been aged utilising radiocarbon techniques such as wiggle match dating of the surrounding deposits in which they are found and

Bayesian age modelling. These ageing techniques can only be achieved if accurate, quantitative distributional and geochemical data are obtained from the tephra layer in question.

#### **4.3.1.2- Hekla**

Hekla ([hɛ<sup>h</sup>kla]) is a stratovolcano located in the south of Iceland with a height of 1,491 metres (4,892 ft). Hekla is one of Iceland's most active volcanoes; over 20 eruptions have occurred in and around the volcano since 874.

Hekla is part of a volcanic ridge, 40 kilometres (25 mi) long. However, the most active part of this ridge, a fissure about 5.5 km (3.4 mi) long named *Heklugjá*, is considered to be the volcano Hekla proper. Hekla looks rather like an overturned boat, with its keel being in fact a series of craters, two of which are generally the most active. The volcano's frequent large eruptions have covered much of Iceland with tephra and these layers can be used to date eruptions of Iceland's other volcanos. 10% of the tephra created in Iceland in the last thousand years has come from Hekla, amounting to 5 km<sup>3</sup>. The volcano has produced one of the largest volumes of lava of any in the world in the last millennium, around 8 km<sup>3</sup>.

Hekla has a morphological type between that of a crater row and stratovolcano sited at a rift-transform junction in the area where the south Iceland seismic zone and eastern volcanic zone meet. The unusual form of Hekla is found on very few volcanoes around the world, notably Callaqui in Chile. Hekla is situated on a long volcanic ridge of which the 5.5 km *Heklugjá* fissure is considered Hekla proper. This fissure opens along its entire length during major eruptions and is fed by a magma reservoir estimated to have a top 4 km below the surface with centroid 2.5 km lower. Hekla's basaltic andesite lava generally

has a SiO<sub>2</sub> content of over 54%, compared to the 45-50% of other nearby transitional alkaline basalt eruptions. It is the only Icelandic volcano to produce calc-alkaline lavas. Phenocrysts in Hekla's lava can contain plagioclase, pyroxene, titanomagnetite, olivine & apatite (Larsen, 1983).

When not erupting Hekla is often covered with snow and small glaciers, it is also unusually aseismic with activity only starting 30–80 minutes before an eruption. Hekla is located on the mid-ocean ridge, a diverging plate boundary. Hekla is closely studied today for parameters such as strain, tilt, deformation and other movement and seismic activity.

Hekla (currently 1491m in height) is one of the most active volcanoes in Iceland. Hekla is a morphological stratovolcano located near the rift-transform fault junction in the area where Iceland's South and Eastern Seismic Zones meet. Hekla's repeated fissure eruptions result in the formation of a vaulted ridge of about 5 km (*Heklugjá* fissure) that opens along its entire length during major eruptions. The magma reservoir(s) under Hekla appears to be not well constrained but it is generally agreed that it is situated between 4 km (Linde *et al.*, 1993) and 8 km (Kjartansson and Gronvold, 1983).

All known Hekla eruptions have begun with an explosive phase followed by more effusive eruptions. After the eruptions in 1693, 1845 and 1947, tephra fallouts were recorded in contemporary written accounts (Thorarinsson, 1981), and among the most recent eruptions of Hekla only two are accompanied by physical evidence on the ground (Salmi, 1948). This is a common problem in tephrochronology and is due to the fact that tephra blankets can either disappear (often completely after major erosion due to an associated rainfall event) or have never been deposited at a particular site. During the last 1100

years Hekla has produced 17 wide spread silicic tephra layers (Hafliðason *et al.*, 2000). All of these tephra layers have been analysed with EMPA and the eruptions responsible for producing these tephras have been well-dated.



**Figure 4.3.1.2.1: Hekla and its location on the map of Iceland (Pfeiffer, 2003).**

Details of the 1510 eruption were not recorded until a century later. It started on July 25 and was particularly violent, (VEI 4) firing volcanic bombs as far as Vörðufell, 40 km west. Tephra was deposited over Rangárvellir, Holt and Landeyjar, 0.2 km<sup>3</sup> in total.

The 1947 eruption started on March 29, 1947 and ended on April 21, 1948. At VEI 4 it is likely that this was both the second greatest lava eruption of Hekla whilst Iceland was inhabited and the second greatest lava eruption in the world in the period 1900-1970. A total lava volume 0.8 km<sup>3</sup> was produced with 0.21 km<sup>3</sup> of tephra (Rea *et al.*, 2012). The height of Hekla was 1447 m before the eruption, increasing to a maximum of 1503 m, before dropping to 1491 m subsequently.

Further details of the 1510 and 1947 eruptions of Hekla are to be found in chapter one.

#### **4.4- Samples**

Two samples were supplied by Dr Graeme Swindles at the University of Leeds. The first was an ash sample of tephra from the 1510 AD eruption of Hekla. The second sample was lapilli (grain size of between 2 and 6 mm) from the 1947 AD eruption of Hekla.

##### **4.4.1- Initial study**

Initially, small amounts of the samples were placed on a glass slide and analysed with Raman spectroscopy. When carrying out a Raman examination for the first time one must consider several parameters. Firstly the excitation level of the laser must be considered. In selecting the laser one needs to choose one as far from the electronic transmission of the sample as possible in order to avoid or to minimise sample fluorescence. After the selection of the laser one must consider the lasers power, the exposure time and the number of spectral accumulations one wishes to take.

The power of the laser is a very important consideration in Raman spectroscopy. Since Raman scattering is relatively weak compared to Rayleigh scattering, one of the main historical problems with Raman spectroscopy had been separating out the weak Raman signal from the strong Rayleigh signal. One method with which one can increase the strength of Raman scattering is by increasing the laser power. Therefore, with increased laser power comes an increase in peak

height. However this laser power needs to be balanced against the risk of sample damage. By increasing the laser power one also increases the localised heating at the focal point of the laser. Depending on the sample type this heating can have the effect of destroying the sample or causing chemical changes with the sample.

Signal accumulation is a very efficient method of reducing random noise that is often found in Raman spectra. It works by selecting the user selecting number of spectra (NS) that they want to be accumulated. The software will then collect NS successive spectra adding each spectrum to an accumulating buffer. When NS spectra have been acquired and summed the data collection is complete. The noise is reduced by the square root of the NS spectra that have been summed.

The exposure time refers to the amount of time in which the spectrally dispersed light is allowed to strike the CCD array and produce charge. With increased exposure time comes increased pixel charge in the CCD and thus increased peak height on the spectra.

The initial analysis was carried out using a Renishaw InVia Reflex Raman microscope with a diode laser operating at 785 nm and a thermoelectrically cooled charge coupled device (CCD) detector. Spectra were obtained with an accumulation of one scan, ten seconds exposure time and 50% laser power (approximately 50 mW at source).

Initially, one-hundred spectra were collected from each sample. This number was taken to give a balanced view on the spectral quality achievable throughout the samples. These collections were randomly collected to ensure that the number of spectra collected were representative of the whole sample.

#### 4.4.2- Method development

With this technique never having been successfully applied to tephra glass shards there was no precedent to follow in terms of laser choice and parameter settings. Settings needed to be devised based on the interpretation of initial spectra gathered using known parameter settings. The settings used were decided upon based on their success in gathering useable spectra in the analysis of the mineralogical species in soil samples.

Of the two hundred spectra collected, only seven showed any spectral detail (although the peaks were broad and low in count). Although the peaks visibility was hindered by fluorescence they were in the areas associated with iron oxides. This was to be expected given the known FeO presence through several EPMA studies. All the spectra showed a large amount of fluorescence and most had a large degree of "glass flair".

It was important to overcome the issue of fluorescence due to the fact that whilst the fluorescence would always mask any spectral peaks and therefore needed to be removed before any serious study on the tephra's mineralogy study could be carried out.

In order to remove the fluorescence from further spectra the first consideration was to ensure the sample was free from any impurities by acid digestion. This is a commonly used procedure in tephra chronology and is designed to remove organic residues from the tephra whilst not changing the mineralogy of the sample. It was very important to remove any organic residues for two main reasons. Firstly, organic material is known to strongly fluoresces in Raman spectroscopy and thus drown out the any peaks relating to the tephra's mineralogy. Secondly, any organic material within the samples must be from

the post eruptive phase. This means that any organic materials are not related to the tephra itself but from the surrounding matrix. Therefore, one cannot accurately differentiate two tephtras based on organic materials.

Before acid digestion was carried out on the samples that were to be analysed a small experiment was carried out to ensure that the method was correct and that the mineralogy was indeed unaffected by the procedure and that the procedure was necessary to reduce fluorescence. For the purpose of these tests a tephra sample from the Hekla eruption of 1341 was used. This tephra was selected as it has similar elemental composition to the tephtras from the 1510 and 1947 Hekla eruptions, is well studied and avoided the risk of potentially destroying the 1947 and 1510 samples that were needed for analysis.

Raman spectroscopy was carried out on the sample using the same laser excitation and parameter settings that had initially been used on the 1510 and 1947 Hekla tephra samples. The diode laser operated at 785 nm and spectra were obtained with an accumulation of one scan, ten seconds exposure time and 50% laser power. It was observed that the spectra obtained from the 1341 Hekla sample displayed very similar traits to those gathered from the 1510 and 1947 spectra, namely a large amount of fluorescence, glass flair and very little mineralogical information.

XRD analysis was then carried out on the 1341 Hekla tephra sample carried in order to record its mineralogy. The same sample was then placed in a beaker and flooded with distilled water before being placed in a sonic bath for five hours. The water was then filtered off and the sample placed in a drying oven for two hours. XRD analysis was then carried out on the same sample. Washing the sample with water did not change any of the mineralogy.

Raman spectroscopy was then carried out on the washed sample under the same conditions as described above. The spectra from this washed sample were compared to the spectra from the unwashed spectra using an overlay. There was no significant change between the two spectra. The fluorescence was very slightly reduced but not by a significant amount, therefore necessitating the use of an acid digestion.

The acid digestion used is a common digestion method used in tephrochronology. The method used initially followed that of the method on tephabase. In this method 2 cm<sup>3</sup> of tephra was added to a conical flask along with 50 cm<sup>3</sup> of 98% Sulphuric acid. The mixture was then boiled for approximately two hours until the mixture has ceased reacting. At this stage five drops of 72% nitric acid was added and boiling was continued. Again, when the reaction has subsided further nitric acid was added, in this case approximately ten drops. The solution was boiled until it turned to a pale yellow or colourless clear liquid. It is then diluted with distilled water and centrifuged to allow the solid tephra to settle out of solution. The solid was then dried in an oven.

Utilising this method there was a reduction in the amount of fluorescence observed in the sample spectra. However, the digestion method itself caused a few difficulties: firstly, during the addition of the sulphuric acid a large amount of effervescence occurred causing the mixture to bubble out of the flask and as a result some of the sample was lost and secondly, the flask kept boiling dry. According to the method this is common and the solution is to simply add more sulphuric acid. The result of this is that far more sulphuric acid is used than the initial method suggested (in our case 145 cm<sup>3</sup>). The third problem we encountered was the mixing of the tephra and the acid. The tephabase method

did not call for any stirring and we could therefore not be certain that all of the tephra grains had been subjected to the digestion in order to rectify this the reaction was carried out with stirring.

The acid digestion was carried out again on a new batch of tephra from the Hekla eruption of 1341. This time some adjustments were made to the original method. Tephra (1 g) was added to sulphuric acid (50 cm<sup>3</sup>, 98%) and a stirring bead in a round bottomed flask. A reflux condenser attached to the flask and the contents were slowly brought to reflux. The contents of the flask were brought to reflux over one hour, this slow heating controlled the amount of effervescence thus ensuring that all the contents stayed in the flask. The contents were left to reflux, with stirring, for a total of one hour. The reflux ensured that the flask did not boil dry, nitric acid (72%) was then added drop wise until the addition of acid ceased to cause a reaction. At that point the mixture was refluxed for a further one hour. The mixture was left to cool before distilled water was added to neutralise the mixture. The mixture was then filtered using a vacuum. The tephra was then washed with further distilled water to ensure all of the acid had been removed and allowed to air dry under the pull of the vacuum. The tephra was dried in this manner to avoid any unnecessary heating.

The tephra was then analysed with PXRD and it was observed that the acid digestion had not caused any mineralogical changes to the sample.

Subsequently Raman spectra were collected on the sample, which displayed less fluorescence than the un-treated sample. However, there was still some fluorescence and the peaks were small and very broad.

One of the common methods to avoid the issue of fluorescence is to use a laser beam operating in the near infra-red wavelength as these generally are not energetic enough to cause the electronic excitation of the molecule that leads to fluorescence. The initial spectra taken of the Hekla samples were using a laser operating at 785nm in the Near-IR range. Therefore, simply changing the laser to one operating in the Near-IR would not be expected to significantly reduce the fluorescence.

Fluorescence is considered a problem in Raman spectroscopy because the Raman effect is comprised of a very small fraction (about 1 in  $10^7$ ) of the incident photons (Egerton *et al*, 1974). Therefore, even relatively small levels of fluorescence can easily swamp the Raman signals. As we are already operating in the Near-IR range the consideration to overcome the effect of fluorescence was in increasing the signal to noise ratio; by increasing the signal and maintaining the fluorescence level we should be able to observe the peaks more clearly.

It was decided that the laser operating at 633 nm should be used as it offered a shorter wavelength than the 785nm laser and therefore offered increased Raman signal whilst remaining in the Near-IR range and thus maintaining the fluorescence at similar levels.

The Raman spectra observed using the 633nm laser did show a reduction in fluorescence and much sharper, better defined peaks than were observed with the 785nm laser. It was also observed that the “glass flair” exhibited in the spectra taken with the 785nm laser were not present in the spectra taken with the 633nm laser.

Having reduced fluorescence through acid digestion and the selection of the 633 nm laser the selection of standardised parameter settings for the analysis of both tephras from the Hekla eruptions of 1947 and 1510 are necessary. The analytical parameters are required to produce the best possible spectra from both samples whilst leaving their mineralogy unchanged. The parameter settings need to be used on both samples to ensure standardised testing that will work to separate the samples.

The key consideration for this experiment was to work out the best laser power to use on the samples. First it is important to be aware that with some materials it is possible to damage or alter the sample with the excitation laser. This damage can be very obvious in extreme cases where the laser burns a hole in the sample; in other cases the damage can be more subtle and if care has not been taken to avoid damaging the sample, it may result in spectra that do not represent the true sample.

From EPMA data and our own initial studies we knew there were iron oxide species within the Hekla 1510 and 1947 samples. Iron oxide species such as magnetite, haematite, goethite and Wüstite have been well studied with Raman spectroscopy. Laser power has to be very carefully controlled, particularly when investigating iron oxides.

D. Faria has carried out several published studies on the effects of heat on the Raman spectra of iron oxides (Faria & Vena, 1997)(Faria & Lopes, 2007). She noted that changes in laser power cause shifts in Raman band positions or complete mineralogical conversions from one species to another. In her work it was discovered that changing laser power from 0.7 mW to 7 mW caused the

bands in haematite not only to broaden but to shift down in wavenumber. It was noted in this work that this reaction was reversible and when the laser power was reduced the Raman bands returned back to normal. However, when magnetite was treated to the same change in laser power new bands were observed in the spectra with the conclusion that haematite was being formed. This conversion was found to be irreversible (Faria & Lopes, 2007). This transformation is very common in nature and is referred to as martitization. It is also well documented that haematite can be formed through the heating of goethite. Indeed it was a practice used by early man when pigments, naturally rich in goethite, were heated to form darker colours, haematite, for use in cave paintings. Studies carried out utilising Raman spectroscopy show that this conversion begins at temperatures of around 300 °C. It is also worth noting that whilst this conversion is irreversible it is possible to distinguish between heated goethite and natural haematite using both Raman spectroscopy and XRD (González *et al.*, 2000). The bandwidths of Raman peaks of heated goethite are larger than those of natural haematite indicating a smaller degree of crystallinity this is confirmed by XRD.

Clearly the need for careful control of the laser power lies in gaining a truly representative spectrum of the tephra rather than a spectra arising through overheating of the sampling sight. In order to find a laser power that would not cause damage to the iron oxide mineralogy within the tephra sample a series of studies were carried out using pure samples of magnetite, haematite and goethite.

For this study the pure mineral samples were obtained from Sigma Aldrich. They were placed on individual glass slides and subjected to a series of Raman scans of increasing laser power from 0.1 % to 100% (633nm). The Raman spectra of each sample were then overlaid to observe the power at which each sample changed.

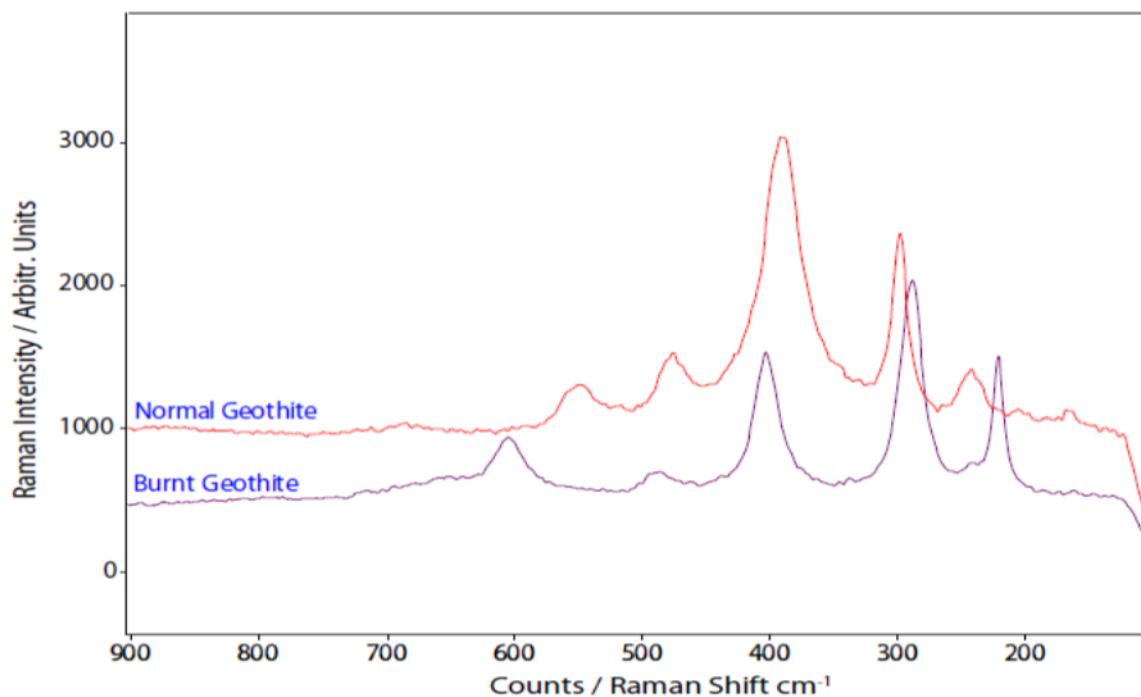
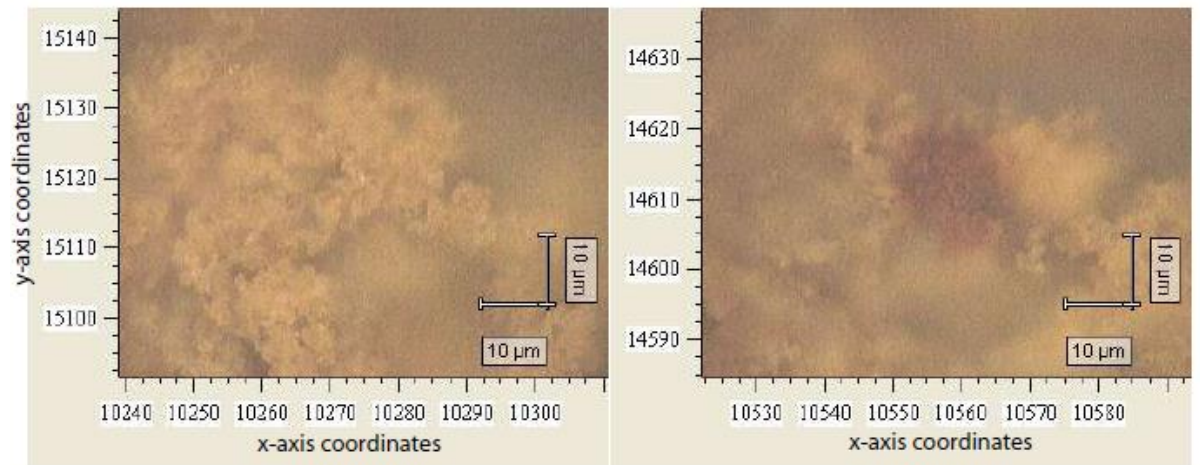


Figure 4.4.2.1: Overlaid spectra of Geothite. The lower trace shows the effect caused by high laser power, effectively "burning" the sample.

**Table 4.4.2.1: table showing the changes in laser power used in the development of the parameter settings for the interrogation of tephra samples with Raman spectroscopy.**

<b>Sample:</b>	<b>Exposure time (secs):</b>	<b>No. accumulations:</b>	<b>Laser power (%):</b>	<b>Spectral range (cm<sup>-1</sup>):</b>
<b>Goethite</b>	1	1	0.1	100- 2000
	1	1	0.5	100- 2000
	1	1	1.0	100- 2000
	1	1	5.0	100- 2000
	1	1	10.0	100- 2000
	1	1	50.0	100- 2000
	1	1	100.0	100- 2000
<b>Hematite</b>	1	1	0.1	100- 2000
	1	1	0.5	100- 2000
	1	1	1.0	100- 2000
	1	1	5.0	100- 2000
	1	1	10.0	100- 2000
	1	1	50.0	100- 2000
	1	1	100.0	100- 2000
<u>Magnetite</u>	1	1	0.5	100- 2000
	1	1	1.0	100- 2000
	1	1	5.0	100- 2000
	1	1	10.0	100- 2000
	1	1	50.0	100- 2000
	1	1	100.0	100- 2000

The sample of haematite appeared to be unaffected by increased laser power. The magnetite sample began to show spectral changes at 10 % laser power which were reversible; however at 50 % laser power the changes in peak width and position became irreversible. The goethite sample began to undergo spectral and physical changes above 10 % laser power. At 10 % laser power peaks typically associated with haematite were observed although, as shown in D. Faria's work, the peaks were not as sharp as those seen in natural haematite. We also observed a change in colour of the goethite sample subjected to the laser beam. The colour changed from a natural yellow-brown to a darker red colour as the laser power was increased (figure 4.4.2.2). This actively demonstrated the localised heating effect of the laser beam.



**Figure 4.4.2.2: Image showing the burn caused by high laser power on a sample of geothite**

As was expected the peak heights of each sample increased with the laser power as did their clarity. This study demonstrated that changes to the materials occurred when the power jumped from 5 % to 10 % indicating that the localised heating within this range was causing these changes, with the exception of the haematite sample. It was therefore decided that 1 % laser power offered the best peaks whilst leaving the mineralogy of the sample unchanged.

Whilst the exposure time and the number of accumulations were not likely to effect the mineralogy of the samples the settings needed to be worked out in order to ensure the best possible data collection.

These settings were worked out in a similar manner to the laser power; with a series of collections being carried out on the three iron oxides before the spectra were compared to decide upon the best settings.

**Table 4.4.2.2: table showing the changes in exposure time used in the development of the parameter settings for the interrogation of tephra samples with Raman spectroscopy.**

<b>Sample:</b>	<b>Exposure time (secs):</b>	<b>No. accumulations:</b>	<b>Laser power (%):</b>	<b>Spectral range (cm<sup>-1</sup>):</b>
<b>Goethite</b>	1	1	1	100- 2000
	2	1	1	100- 2000
	5	1	1	100- 2000
	10	1	1	100- 2000
	30	1	1	100- 2000
	60	1	1	100- 2000
	120	1	1	100- 2000
	<b>Hematite</b>	1	1	1
2		1	1	100- 2000
5		1	1	100- 2000
10		1	1	100- 2000
30		1	1	100- 2000
60		1	1	100- 2000
120		1	1	100- 2000
<b>Magnetite</b>		1	1	1
	2	1	1	100- 2000
	5	1	1	100- 2000
	10	1	1	100- 2000
	30	1	1	100- 2000
	60	1	1	100- 2000
	120	1	1	100- 2000

Looking at the exposure times it was decided that 10 seconds offered better spectra than those achieved at 1, 2 or 5 seconds exposure. Exposure times above 10 seconds offered very little improvement in spectral quality, the additional collection time proving to not offer better value in terms of time vs. spectral detail.

**Table 4.4.2.3: table showing the changes in accumulation number used in the development of the parameter settings for the interrogation of tephra samples with Raman spectroscopy.**

<b>Exposure time (secs):</b>	<b>Sample:</b>	<b>No. accumulations:</b>	<b>Laser power (%):</b>	<b>Spectral range (cm<sup>-1</sup>):</b>
10	<b>Goethite</b>	1	1	100- 2000
10		3	1	100- 2000
10		5	1	100- 2000
10		10	1	100- 2000
10		20	1	100- 2000
10		50	1	100- 2000
10		100	1	100- 2000
10	<b>Hematite</b>	1	1	100- 2000
10		3	1	100- 2000
10		5	1	100- 2000
10		10	1	100- 2000
10		20	1	100- 2000
10		50	1	100- 2000
10		100	1	100- 2000
10	<b>Magnetite</b>	1	1	100- 2000
10		3	1	100- 2000
10		5	1	100- 2000
10		10	1	100- 2000
10		20	1	100- 2000
10		50	1	100- 2000
10		100	1	100- 2000

Having decided on optimum laser power and exposure time a series of scans were carried out at these settings but with increasing numbers of accumulations. Again, these spectra were overlaid and compared to determine the optimum number of accumulations to carry out on each spectrum. 10 accumulations were far superior in terms of spectral quality in comparison to 1, 3 or 5 accumulations. Twenty accumulations offered a tiny improvement on ten accumulations but no further spectral improvements were noted above twenty. The difference between the spectral quality at 10 and 20 accumulations was marginal and again not worth the huge increase in time it took to collect each spectrum. It was therefore decided that ten accumulations was more than sufficient for the analysis of the tephra samples.

#### 4.4.3- Sample analysis

The acid digestion method described in this chapter was used on the tephra samples from the Hekla eruptions of 1510 and 1947. This digestion process ensured that both samples were free of any contamination and particularly from organic residues which may mask the mineral signal peaks in the Raman spectrum.

The samples were then spread on a glass slide and placed under the lens of the Raman instrument. As we did in the initial study, 100 spectra were collected from across the surface of each sample. The sample were collected with accumulations of ten scans, ten seconds exposure time, 1% laser power (approximately 50 mW at source) and 633nm excitation.

The results from these scans were a huge improvement on the results observed in the initial study. However, out of the total 200 spectra only 114 displayed any peaks. Although an improvement from our previous studies, 86 of the scanning sites failed to provide any spectral information. Where information was observed it appeared far less hindered with fluorescence than our initial study and showed peaks suggestive of all haematite, magnetite and goethite- showing that the experimental parameters were not causing the degradation or complete change of the iron oxides.

Whilst the results were encouraging it was decided to look at the specific sampling sites being used. During the above experiment sampling sites were selected using a grid pattern with auto-focus. It became obvious that this may not be the best sampling method because of the heterogeneous nature of our sample and the differences in size of each grain makes it difficult for the auto-focus tool.

The portions of the tephra that we were interested in are the shards of rhyolitic glass found within the samples, looking for the microlites and intratelluric mineral phases that can definitely be attributed to the tephra shards, which are unique to each eruption of the volcano. It is very important to avoid phenocrysts as these are mineral inclusions that are picked up by the magmatic flow after an eruption (fig 4.4.3.1). While they contain important mineralogical information, it relates to the environment around the location of the eruption rather than the specific eruption itself.

The cleaned samples were again spread onto glass slides with a 3 x 3 square grid drawn onto it and placed under the lens on the Raman microscope. The grid enabled us to examine small sections of the tephra at a time. The tephra was observed under 5x magnification until a shard of glass was observed. The glass was identified due to its catching of the illumination light from the microscope causing it to glint thus enabling us to identify it from the dull pumice surrounding material.

Once a glass shard was identified we increased the magnification to 20x enabling us to study it in closer detail. The microlites were identified and these were sharply focussed on as these are unique to specific eruptions rather than just to the volcano's environment. Microlites were visually identified as they appear as needle like crystals. Phenocrysts, that we were keen to avoid as they are not unique to specific eruptions, appear as a relatively large and usually conspicuous crystal distinctly larger than the grains of the tephra mass. Thus it is relatively easy to visually distinguish between the two.

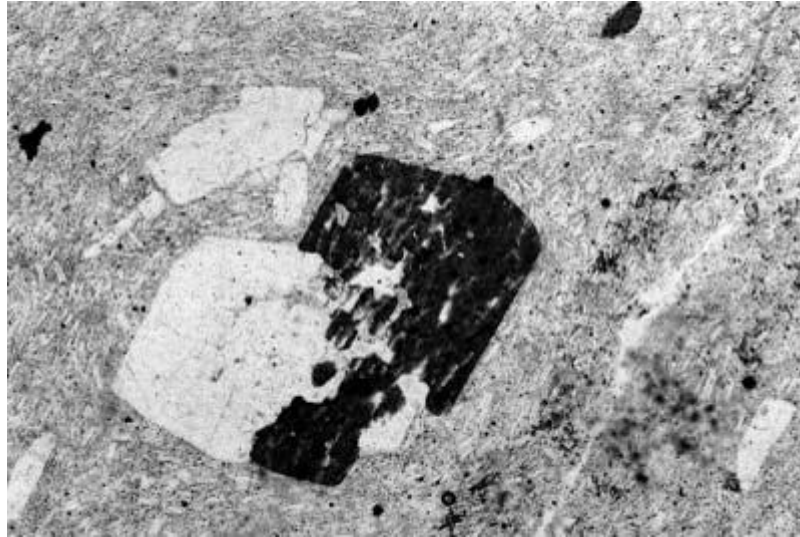


**Figure 4.4.3.1: an example of a phenocryst in location on groundmass. Plagioclase phenocrysts (white) and hornblende phenocryst (dark; intergrown with plagioclase) are set in a fine matrix of plagioclase laths that show flow structure (USGS, 2004).**

Once identified a Raman spectra of the microlites within the glass shards was recorded using the parameters described above. Once a spectrum of each glass shard within the square had been recorded the process was continued in each of the other squares in the 9 x 9 grid.

## **4.5- Results**

### **4.5.1- Hekla 1947**

A thorough analytical examination of the Hekla 1510 and Hekla 1947 samples via Raman spectroscopy revealed that it is possible to identify a range of mineral species. A dominant broad peak, within the spectra collected from the 1947 Hekla ash sample, at  $667\text{cm}^{-1}$  has been assigned to the  $A_{1g}$  species of  $\text{Fe}_3\text{O}_4$ , magnetite (fig 4.5.1.1) (Shebanova & Lazor, 2003; Muralha *et al*, 2011; Faria & Vena, 1997).

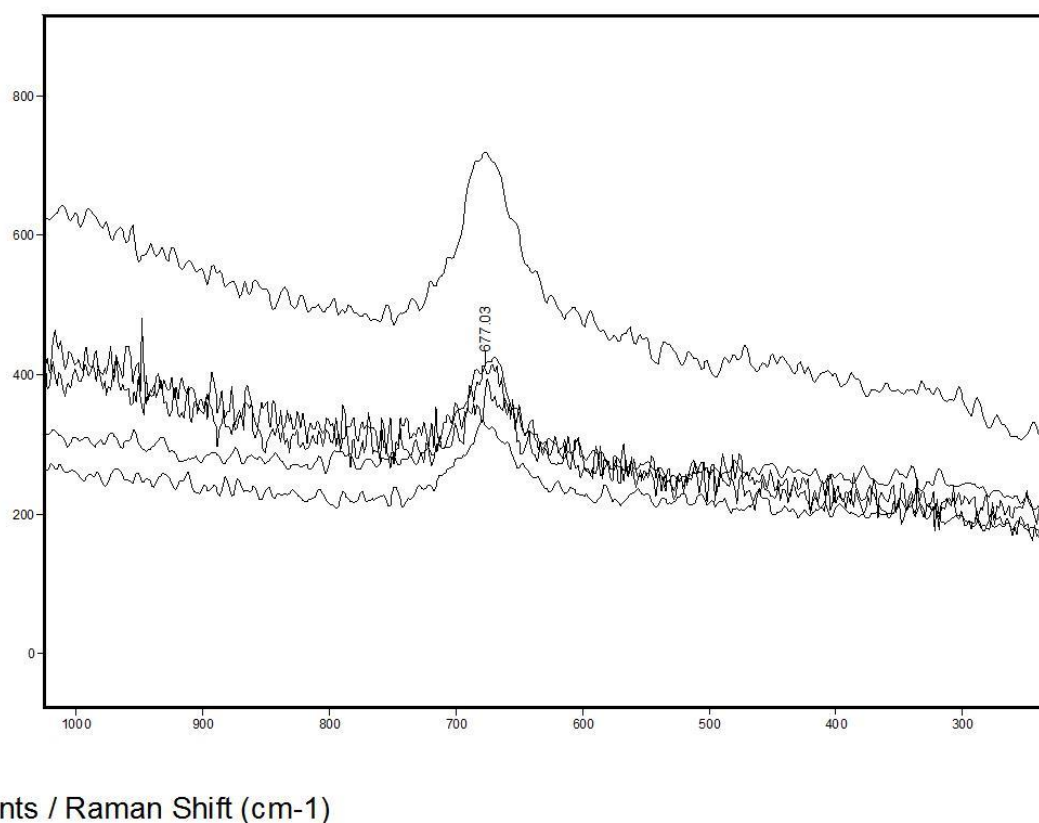


**Figure 4.5.1.1:** These spectra demonstrate the broad peak at  $677\text{cm}^{-1}$  relating to magnetite. Each of the spectra was collected from a different location within the sample.

Further spectral features observed in the spectra from the 1947 ash sample are observed at  $670$ ,  $460$ ,  $396$ ,  $324$ ,  $266$  and  $215\text{cm}^{-1}$ . The peak observed at  $324\text{cm}^{-1}$   $E_g$  (Fe–O sym. bend) have been assigned to magnetite. The peak

observed at  $460\text{ cm}^{-1}$  has been identified as alpha quartz (Krucnra & Hnvr, 1994). The additional peaks observed at 396 (Fe–O–Fe/OH sym. str), 324, 266 Eg (Fe–O sym. bend) and  $215\text{ cm}^{-1}$  A1g (Fe–O sym. str) have been assigned to haematite (fig 4.5.1.2) (Chourpa *et al.*, 2005; Legodi *et al.*, 2007).

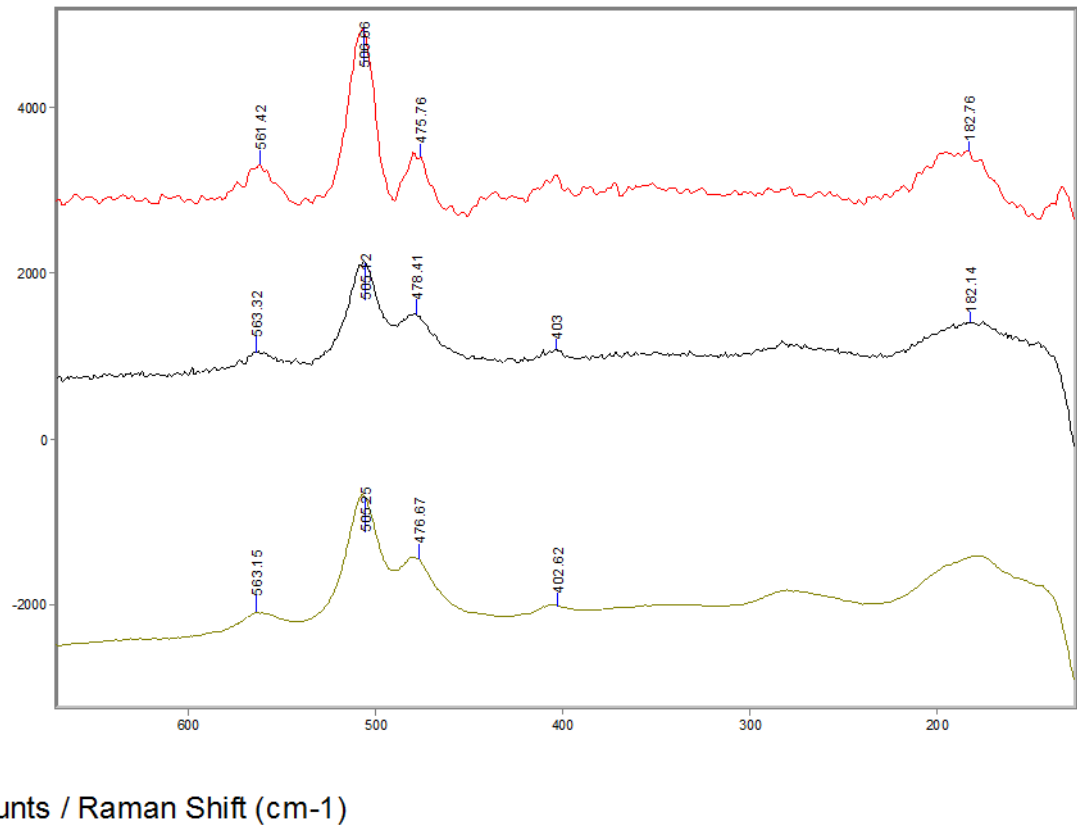


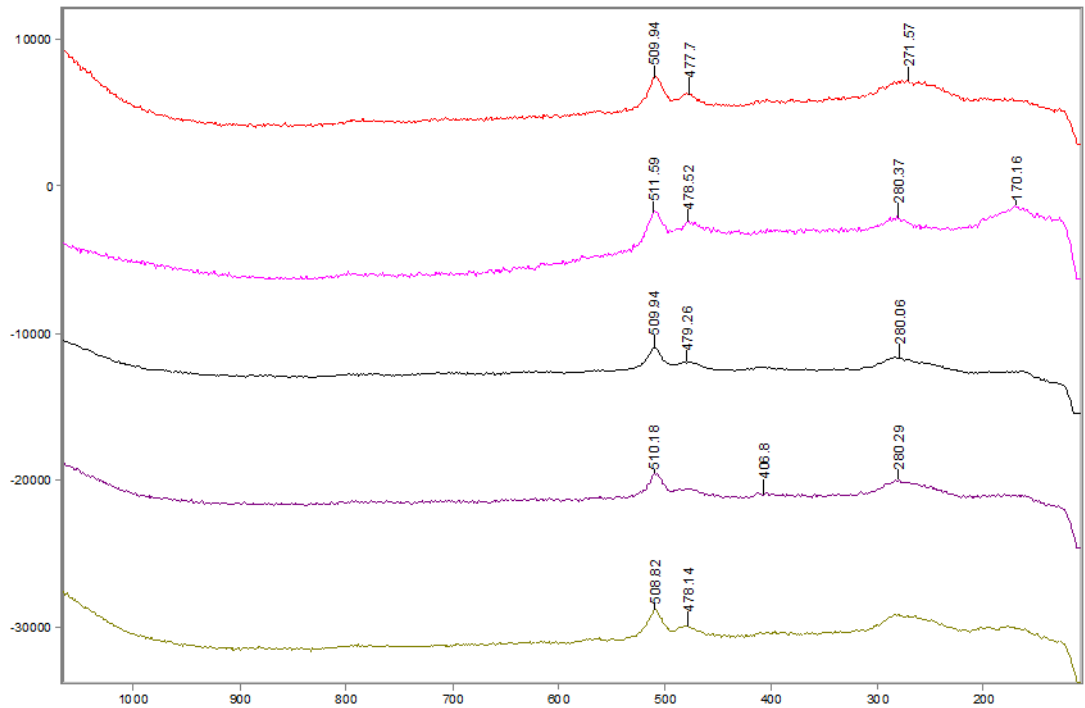
**Figure 4.5.1.2:** The majority of the spectral features observed in the 1947 sample have been attributed to magnetite (see fig 4.5.1.1). This figure displays further spectral features observed in sampling sites from the 1947 tephra.

#### 4.5.2- Hekla 1510

Raman analysis of the 1510 Hekla samples was found to be more difficult when compared to the 1947 samples due to issues with fluorescence. Fluorescence within Raman spectroscopy can occur for many reasons including sample colour, causing the excitation photon to not provide sufficient

energy to the molecule, or contamination possibly caused by hydrocarbons decomposed on the silica glass surface of the tephra grains (Egerton *et al.*, 1974). If the fluorescence is caused by hydrocarbon contamination it is possible to reduce the fluorescence with heat treatment although in this work heat treatment was intentionally avoided due to the risk of chemical changes in the iron oxide chemistry of the sample. Fluorescence does not change the nature of the Raman spectra due to it being an absorption process. Fluorescence can simply be overcome with a change in laser excitation or post-processing of the spectra.

The spectral features observed in the 1510 samples appeared at 512 (Fe–OH asym. str), 465 (Fe–OH asym. Str), 280 (Fe–OH sym. bend), 197 (Fe–O sym. str) (Legodi *et al.*, 2007). These peaks have been attributed to goethite. The two peaks located at 156 and 127  $\text{cm}^{-1}$  appear to be the E(LO+TOI) mode of  $\text{SiO}_2$  quartz stretch (Krucnra & Hnvrr, 1994). Two of the spectra also contained a large, broad peak at 680  $\text{cm}^{-1}$  which has been assigned as magnetite. The peaks observed at 464nm have been assigned to quartz  $V_1$ , indicative of the mineral coesite (Korsakov *et al.*, 2007) (figure 4.5.2.1).



Counts / Raman Shift (cm-1)

**Figure 4.5.2.1: Spectral features found within the tephra sample from the 1510 eruption of Hekla.**

In this study, pre-processing of the spectra was carried out to reduce inherent noise caused either by instrument or sample variability. The Savitsky-Golay smoothing filter was applied in order to smooth the curves of the spectra and thus reduce the noise (Tsai & Philpot, n.d.). This filter does not distort the overall spectra or the frequency position of the peaks. The standard normal variate (SNV) was performed which is a normalisation method that uses the spectrum itself for correction. SNV achieves this by firstly by calculating one mean and one standard deviation value for the entire spectrum. It then subtracts the mean value from each spectral point and then divides by the standard deviation. This has the effect of centring the mid-point of the spectrum at zero and standardising the entire spectrum to its overall variance, thus reducing differences in baseline and peak intensity between spectra.

## 4.6- Discussion

Analysis of small tephra shards and cryptotephra with Raman spectroscopy provides a considerable analytical challenge from a spectroscopic point of view. This is due to the fact that volcanic ashes are polyphase (containing both glasses and minerals). Minerals within the volcanic glass exist as phenocrysts and microlites (<0.3 mm). Volcanic ashes are complex and variable in composition (even within a single eruption) and are therefore difficult to analyse (Barletta, 2012).

The newly-collected data present some challenges. In the case of heterogeneous samples, the area of the sample illuminated by the laser spot may not be characteristic of the entire sample (White, 2009). In order to resolve this issue, a large amount of data needs to be collected from the sample to obtain a representative sample. Further challenges of laser Raman spectroscopy for mineral identification are laser-induced sample alteration and fluorescence. Although laser Raman spectroscopy is a non-destructive technique, samples can undergo localized heating and oxidation if the laser power is too high (what is considered “high” laser power depends on the individual sample). Considering our analytical area of 5  $\mu\text{m}$  and power at source of 50 mW, the sample was subjected to a power of  $4 \times 10^8 \text{ W per cm}^2$ . In this study, the parameter settings of the Raman spectrometer were carefully and systematically designed in order to prevent the sample from overheating which could lead to chemical alteration. This was carefully monitored with the spectra collection on pure iron oxide standards. This presented us with the need for a spectral “trade-off”. To maintain sample integrity, the signal to noise ratio was sacrificed resulting in the need for multiple sample measurements and

chemometric analysis (SNV processing) to amplify the differences between spectral data-sets. Principal Components Analysis (PCA) was applied here to identify groups within the data whilst removing any contribution from background noise.

The spectra were split into two datasets, one set for the 1510 data and one for the 1947 data. After pre-processing PCA was carried out on the data. This resulted in a number of scores (principle components PC) and loadings (spectral variables). The early scores were then plotted against each other to form a three-dimensional score plot with related samples clustering together.

PC axes were used and accounted for 98% of the variables within the data. As one can observe in figure 4.6.1, the combined and processed data-sets largely split into two data clusters- one representing the 1947 and the other 1510. In general, the data relating to the 1947 tephra sits on the left hand side of the axis whilst the data from 1510 sits on the right, although there is some overlap. Four of the spectra obtained from the 1510 data-set fall in the main cluster of data from the 1947 data. This cross-over of data can be observed in the individual spectra and has been associated with the presence of small amounts of magnetite within the 1510 data. The data collected through Raman spectroscopy offers better discrimination when compared with the data collected through EMPA alone (figure 4.6.2). However, at this time EMPA data is still required to identify the source volcano.

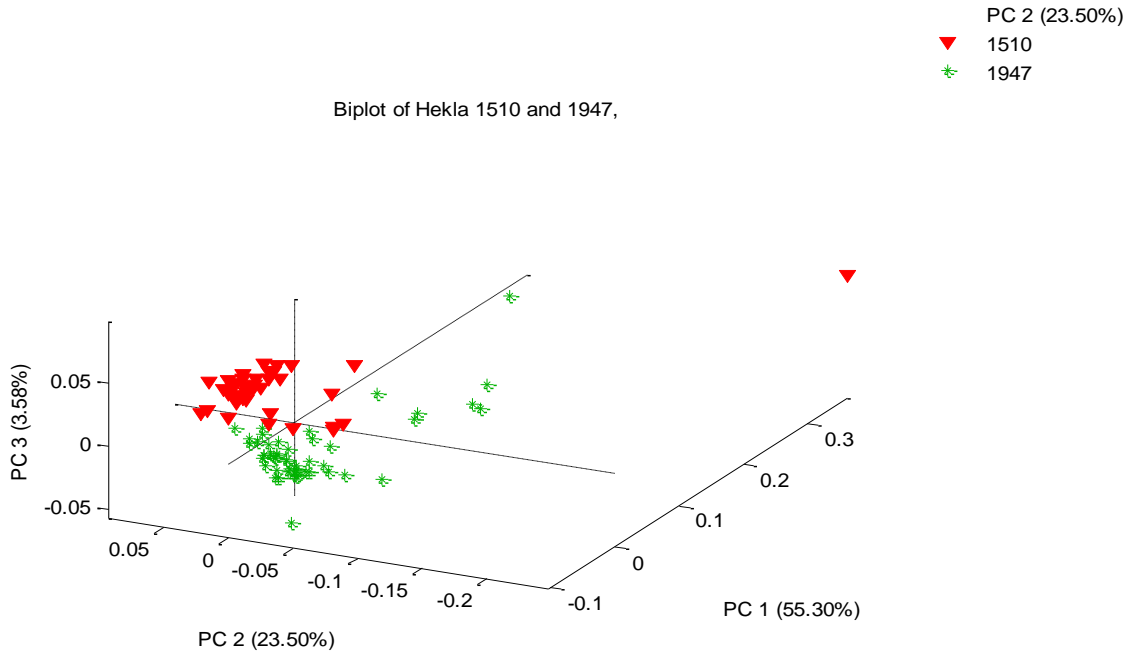


**Figure 4.6.1: Biplot of the datasets from the Hekla eruptions of 1510 and 1947.**

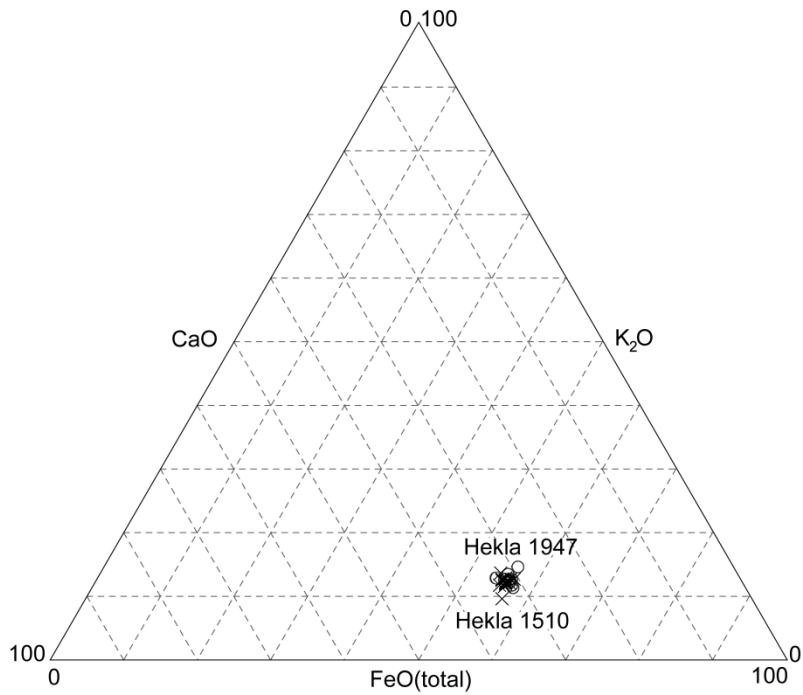


**Figure 4.6.2: Triplot of EMPA data from the Hekla eruptions of 1510 and 1947. (Rea *et al.*, 2012)**

One further interesting variation observed between the two samples was in the SiO<sub>2</sub> mineralogy observed in the Raman spectra. The spectra obtained from the 1947 sample show traces of  $\alpha$ -quartz indicated by the peaks at 460 cm<sup>-1</sup>. This mineralogy was not unexpected because of the high silica content of the samples shown in the EMPA data. However, this mineralogy is not observed in the 1510 sample, where coesite (Chopin, 1984), a commonly found mineral in rhyolite eruptions (Borisova *et al*, 2014), was observed instead. The presence of these mineral polymorphs provides further data to support the proposed Hekla 1947 and Hekla 1510 sample discrimination.

Geothite, Haematite and Magnetite were identified through the Raman spectra of both the tephra samples from the Hekla 1947 and Hekla 1510 eruptions. It is well documented that Geothite and Magnetite can convert to haematite through heating to approximately 250°C. Whilst we cannot comment on these conversions having occurred in nature we are certain that such conversions were not caused through the experimental procedure.

#### **4.7- Conclusions:**

Raman spectroscopy has a role to play in the analysis of tephra samples, especially when electron microprobe methods do not provide the level of discrimination required. In this study we demonstrate that Raman spectroscopy can be used for mineral species identification in tephra enabling the differentiation of glasses with similar chemical composition via the presence of various magmatic crystals contained within the glass. For example, current methods in tephra analysis have hitherto been unable to provide any discrimination between the tephra from the Hekla eruptions of AD 1510 and AD 1947. Here, we show that Raman spectroscopy can differentiate between

these tephtras, primarily through the identification of the species forming their iron oxide content, and secondly through the presence of their different SiO<sub>2</sub> polymorphs. This Raman method is not designed to be a replacement for current chemical analysis, rather as an additional technique to aid discrimination between compositionally similar tephtras. Principal components analysis (PCA) proves to be a good tool for separation of the tephtras based on data from Raman spectroscopy; however, a large amount of data is needed for an effective analysis.

## 4.8- References

- Alber, J.S., Volcanism of the Eifel, Germany Region. (2012)  
<http://academic.emporia.edu/aberjame/tectonic/eifel/eifel.htm>
- Barletta, R. E. (2012). Raman analysis of blue ice tephra: an approach to tephrochronological dating of ice cores. *Antarctic Science*, 24(02), 202–208. doi:10.1017/S0954102011000885
- Borisova, A. Y., Toutain, J., Dubessy, J., Pallister, J., & Zwick, A. (2014). RESEARCH ARTICLE H<sub>2</sub>O – CO<sub>2</sub> – S fluid triggering the 1991 Mount Pinatubo climactic eruption ( Philippines ), 1–9. doi:10.1007/s00445-014-0800-3
- Di Carlo, I., Rotolo, S. G., Scaillet, B., Buccheri, V., & Pichavant, M. (2010). Phase Equilibrium Constraints on Pre-eruptive Conditions of Recent Felsic Explosive Volcanism at Pantelleria Island, Italy. *Journal of Petrology*, 51(11), 2245–2276. doi:10.1093/petrology/egq055
- Dugmore, A, Newton, A & Larsen, G 1992, 'Geochemical stability of fine-grained silicic Holocene tephra in Iceland and Scotland.' *Journal of Quaternary Science*, vol 7, no. 2, pp. 173-183.
- Egerton, T. A., Hardin, A. H., Kozirovski, Y., & Sheppard, N. (1974). Reduction of Fluorescence from High-Area Oxides of the Silica , Types and Raman Spectra for a Series of Molecules Adsorbed on These Surfaces, 361, 343–361.
- Faria, D. L. a., & Lopes, F. N. (2007). Heated goethite and natural hematite: Can Raman spectroscopy be used to differentiate them? *Vibrational Spectroscopy*, 45(2), 117–121. doi:10.1016/j.vibspec.2007.07.003
- Faria, D. L. A. D., & Vena, S. (1997). Raman Microspectroscopy of Some Iron Oxides and Oxyhydroxides, 28(February), 873–878.
- Gehrels, George E.; Valencia, Victor A.; Ruiz, Joaquin (2008). Enhanced precision, accuracy, efficiency, and spatial resolution of U-Pb ages by laser ablation-multicollector-inductively coupled plasma-mass spectrometry. *Geochemistry, Geophysics, Geosystems* vol. 9 (3)
- González, G., Sagarzazu, A., & Villalba, R. (2000). Study of the mechano-chemical transformation of goethite to hematite by TEM and XRD. *Materials Research Bulletin*, 35(14-15), 2295–2308. doi:10.1016/S0025-5408(00)00434-7
- Hafliðason, H., Eiriksson, J., & Kreveld, S. V. (2000). The tephrochronology of Iceland and the North Atlantic region during the Middle and Late Quaternary: a review. *Journal of Quaternary Science*, 15(1), 3–22. doi:10.1002/(SICI)1099-1417(200001)15:1<3::AID-JQS530>3.0.CO;2-W

- Hall, V. A., & Pilcher, J. R. (2002). Late-Quaternary Icelandic tephra in Ireland and Great Britain : detection , characterization and usefulness, 2, 223–230.
- Higham, T., Brock, F., Peresani, M., Broglio, A., Wood, R., & Douka, K. (2009). Problems with radiocarbon dating the Middle to Upper Palaeolithic transition in Italy. *Quaternary Science Reviews*, 28(13-14), 1257–1267. doi:10.1016/j.quascirev.2008.12.018
- Hunt, J. B., & Hill, P. G. (1993). Tephra geochemistry: a discussion of some persistent analytical problems. *The Holocene*, 3(3), 271–278. doi:10.1177/095968369300300310
- Hogg, A. G., & McCraw, J. D. (1983). Late Quaternary tephra of Coromandel Peninsula, North Island, New Zealand: A mixed peralkaline and calcalkaline tephra sequence. *New Zealand Journal of Geology and Geophysics*. 04/1983; 26(2):163-187.
- Katsuta, N., Takano, M., Kawakami, S., Togami, H. Fukusawa, M. Kumazawa, Y. Yasuda (2007). Advanced micro-XRF method to separate sedimentary rhythms and event layers in sediments: its application to lacustrine sediment from Lake Suigetsu, Japan. *J. Paleolimnol.*, 37, pp. 259–271
- Korsakov, A. V., Hutsebaut, D., Theunissen, K., Vandenabeele, P., & Stepanov, A. S. (2007). Raman mapping of coesite inclusions in garnet from the Kokchetav Massif (Northern Kazakhstan). *Spectrochimica acta. Part A, Molecular and biomolecular spectroscopy*, 68(4), 1046–52. doi:10.1016/j.saa.2007.04.005
- Krucnra, J., & Hnvrr, J. (1994). Raman spectroscopic study of microcrystalline silica, 79, 269–273.
- Larsen, G. (1983). The Hekla Eruption 1980-1981, 46(August 1980).
- Larsen, G., Dugmore, a., & Newton, a. (1999). Geochemistry of historical-age silicic tephra in Iceland. *The Holocene*, 9(4), 463–471. doi:10.1191/095968399669624108
- Legodi, M. A., Waal, D. D., & Africa, S. (2007). The preparation of magnetite , goethite , hematite and maghemite of pigment quality from mill scale iron waste, (February).
- Lima, A. (2008). "Urban geo-chemical mapping in the Campania region (Italy)." *Geo-chemistry : Exploration, Environment, Analysis* 8: 19-29.
- Lowe, D.J. (1985), "Application of impulse radar to continuous profiling of tephra bearing lake sediments and peats: An initial evaluation." *New Zealand Journal of Geology and Geophysics* 28: 667-674.

- Lowe, D.J. (1988), "Stratigraphy, age, composition and correlation of late Quaternary tephras interbedded with organic sediments in Waikato lakes, North island, New Zealand." *New Zealand Journal of Geology and Geophysics* 31: 125-165.
- Marshall, M., Lamb, H., Davies, S., Nakagawa, T., Metcalfe, S., Jones, M., Boyle, J., 2010. High-resolution XRF and X-radiographic core scanning: a powerful tool in palaeolimnology, Abstracts, ITRAX 2010 Conference "Applications, Innovations and Future Developments", Lipari, Italy (12-14 April), p. 21.
- Muralha, V. S. F., Rehren, T., & Clark, R. J. H. (2011). Characterization of an iron smelting slag from Zimbabwe by Raman microscopy and electron beam analysis. *Journal of Raman Spectroscopy*, 42(12), 2077–2084. doi:10.1002/jrs.2961
- Pfeiffer, T., Hekla Volcano, Iceland (2003). Available from: <http://www.decadevolcano.net/volcanoes/iceland/hekla.htm>
- Rea, H. a., Swindles, G. T., & Roe, H. M. (2012). The Hekla 1947 tephra in the north of Ireland: regional distribution, concentration and geochemistry. *Journal of Quaternary Science*, 27, n/a–n/a. doi:10.1002/jqs.1566
- Révillon, S., Etoubleau, J., Dennielou, B., Berné, S., Hémond, C., 2010. Can we detect microtephra layers in marine sediment cores using XRF core scanner technology? Abstracts, ITRAX 2010, Applications, innovations and future developments, Lipari, Italy (12-14 April), p. 29-30.
- Shebanova, O. N., & Lazor, P. (2003). Raman spectroscopic study of magnetite (FeFe<sub>2</sub>O<sub>4</sub>): a new assignment for the vibrational spectrum. *Journal of Solid State Chemistry*, 174(2), 424–430. doi:10.1016/S0022-4596(03)00294-9
- Sverrisdottir, G. (2007). Hybrid magma generation preceding Plinian silicic eruptions at Hekla, Iceland: evidence from mineralogy and chemistry of two zoned deposits, *144*(May), 643–659. doi:10.1017/S0016756807003470
- Swindles, G. T., Vleeschouwer, F. D., & Plunkett, G. (2010). Dating peat profiles using tephra: stratigraphy, geochemistry and chronology, *7*, 1–9.
- Takemura, K., A. Hayashida, M. Okamura, H. Matsuoka, M. Ali, Y. Kuniko, and M. Torii, Stratigraphy of multiple piston-core sediments for the last 30,000 years from Lake Biwa, Japan, *J. Paleolimnol.*, **23**, 185–199, 2000.
- Thornalley, D. J. R., McCave, I. N., & Elderfield, H. (2011). Tephra in deglacial ocean sediments south of Iceland: Stratigraphy, geochemistry and oceanic reservoir ages. *Journal of Quaternary Science*, 26(2), 190–198. doi:10.1002/jqs.1442
- Tsai, F., & Philpot, W. (n.d.). Derivative Analysis of Hyperspectral Data, *4257*(98).

- Turner, M., Cronin, S., Bebbington, M., Platz, T., 2008a. Developing probabilistic eruption forecasts for dormant volcanoes: a case study from Mt Taranaki, New Zealand. *Bulletin of Volcanology* 70, 507-515.
- United States Geological Survey - Figure 4, Trip 4, *Geology of the National Capital Region—Field Trip Guidebook*, Circular 1264, (2004) Department of the Interior, U.S. Geological Survey  
<http://pubs.usgs.gov/circ/2004/1264/html/trip4/fig4.html>
- Vleeschouwer, F., van Vliët-Lanoé, B. & Fagel, N. (2008a) Long-term mobilisation of chemical elements in tephra-rich peat (NE Iceland). *Applied Geochemistry*, 23, 3819–3839.
- Vleeschouwer, F., van Vliët-Lanoé, B., Fagel, N., Richter, T. & Boës, X. (2008b). Development and application of high-resolution petrography on resin-impregnated Holocene peat columns to detect and analyse tephras, cryptotephras, and other materials. *Quaternary International*, 178, 54–67
- Vogel, T., Simonet, P., Jansson, J., Hirsch, P., Tiedje, J., van Elsas, J., Bailey, M., Nalin, R., Philippot, L., *Nat Rev Micro* **2009**, 7, 252.
- White, S. N. (2009). Laser Raman spectroscopy as a technique for identification of seafloor hydrothermal and cold seep minerals. *Chemical Geology*, 259(3-4), 240–252. doi:10.1016/j.chemgeo.2008.11.008

## Conclusions and further work

The overall aim of this work was to develop Raman spectroscopic techniques for use in the field of geo-chemistry. The aim of this work was to investigate its use in more general terms; as a tool for whole sample interrogation. Detailed conclusions for each of the areas of focus can be read at the end of chapters three and four. This section is designed to offer a general summary of the work and areas where it can be utilised and advanced.

Generally we found that one of the major issues of using Raman spectroscopy in geo-chemistry was fluorescence which swamped the Raman signals that would have allowed sample identification. Indeed, this has proved so much of an issue in the analysis of tephras that only one study had previously been attempted with very limited results (Barletta, 2012). We were able to reduce the fluorescence from the samples by utilising and adapting established digestion techniques to remove some of the organic debris which were causing some of the fluorescence. We illustrate that a stepwise oxidative treatment of soil samples with hydrogen peroxide can be used to overcome this issue. We also demonstrate an improved methodology for an acid digestion (concentrated Sulphuric acid 98% SLR and Nitric acid 68-72% SLR) in order to remove any organic materials but leave, unchanged, the inorganic matter (glass and crystals). Further to these digestion methods we demonstrate that the application of several Raman spectroscopic techniques to increase the signal to noise ratio within the samples and data processing to reduce background noise. Through application of Raman spectroscopic techniques and the developed digestion methods we have been able to reduce fluorescence sufficiently to identify the peaks relating to the materials that make up the samples.

We have successfully shown that Raman can be a valuable tool in the field of geo-chemistry. Identification of geo-chemical samples has always relied on a multi-proxy approach that is time consuming and introduces an increased chance of error at each stage. In this work we have shown that Raman spectroscopy is capable of identifying both the organic and the inorganic fractions of geo-chemical samples and with further method development and study may negate the need for multi-proxy techniques in sample identification. This is demonstrated by the successful application of Raman spectroscopy to soil samples from a small localised area along the route of the A65 road. This route overlays several distinct bedrock types and utilising Raman spectroscopy alone we were able to successfully attain Raman spectra of the soils at each location. We were further able to provide evidence to differentiate between some of the locations through the presence of soil contaminants such as nitrates and tin. Several techniques would normally be utilised to successfully discriminate between soil samples of this type including light microscopy, electron microscopy, PXRD and NMR.

Furthermore, we have demonstrated that Raman spectroscopy offers far greater sample discrimination than the current methods in use. The current multi-proxy methods used in tephra analysis have one large shortfall- they cannot be used to identify mineral species. Through this research we have demonstrated that Raman spectroscopy offers greater mineral species identification which can be used to offer greater discrimination between tephras of similar chemical composition.

This has been demonstrated by the discrimination of tephra samples from the Hekla eruptions of 1510 and 1947. Current analytical methods employed in

tephrochronology, particularly the use of EPMA, had never before been able to definitively separate these tephras (Rea *et al.*, 2012). Separation had previously been a subjective approach utilising microscopy. Using Raman spectroscopy and its ability to identify individual mineral species we have separated these tephras based on their individual mineral species. We have also demonstrated the use of PCA as a tool in order to visually separate the data. Utilising the 3-dimensional graphics that can be generated we are able to clearly see the separation of the two tephras.

One believes that the use of Raman spectroscopy in geo-chemical interrogation may find its greatest use in the field. There is a large body of work looking at soil contamination, soil typing, and forensic soil placement. The geological potential of an *in situ* field test that can identify full soil and tephra fractions is huge whether the purpose is forensically looking to place people at a scene, discover contaminants or as a geological surveyor looking to document or discover. Due to the increased amounts of free carbon in our atmosphere since the industrial revolution radio-carbon dating has become inaccurate and many experts are looking for new methodologies for dating. Tephrochronology is one such method that relies on tephra from known volcanic eruptions forming in distinct layers. Being able to identify which eruption these layers have come from provides a fast and accurate method of dating. Raman spectroscopy could play a major part in this by quickly and accurately identifying the mineralogical composition of these layers and hence providing a date for that temporal marker.

Field analysis would require the use of portable Raman spectroscopy, although this technique could be used in theory in practise it becomes very difficult due the issues of fluorescence. However, further development of the digestive

techniques for use in the field would allow the use of portable Raman spectroscopy for the *in-situ* analysis of soil and tephra samples in location. If it becomes possible for the *in-situ* analysis of these samples with portable Raman spectroscopy then a large body of experimentation will be necessary in order to develop a representative and reproducible protocol for the testing of the samples. It has been shown that this is difficult under laboratory conditions and this will make it more so in the field.

## Appendix

The appendix for this work has been provided as a separate file on a CD. On the CD is a file called Appendix. Within this file are several sub-files containing all the appendix data.

The sub-file names are:

Images Tephra\_Raman

- 65 images showing the sampling sites from the Hekla samples (chapter 4)

Iron oxides\_reference

- 66 Raman spectra of magnetite, goethite and haematite reference samples (chapter 3 and 4)

Paper\_Holocene\_Hekla

- All data relating to the paper accepted for publication in the Holocene

Paper\_JRS\_Soil

- All data relating to the paper published in 2010 in the JRS

PXRD Hekla

- 7 PXR diffractograms relating to chapter 4

PXRD Soil

- 65 PXR diffractograms relating to chapter 3

Raman Soil

- 330 Raman spectra relating to chapter 3

Raman Tephra

- 409 spectra relating to chapter 4

SEM Hekla 1510 & 1947

- 20 SEM images of tephra relating to chapter 4

TGA Soil

- 19 thermal traces relating to chapter 3

